

ELECTRONICS WORLD

THE ESSENTIAL ELECTRONICS ENGINEERING MAGAZINE

Volume 116 • Issue 1887

March 2010 • £4.60



www.electronicsworld.co.uk

SPECIAL REPORT:

- SIGNAL PROCESSING
- IDENTIFICATION AND ELIMINATION OF HUM IN AUDIO AMPS



SHRINKING BASESTATION DESIGNS

WITH AN INTEGRATED μ MODULE RECEIVER



TECHNOLOGY
EUROPEAN
COLLABORATION
IN GRAPHENE
BREAKTHROUGH



INSIGHT
LACK OF RF
INTEROPERABILITY
AFFECTS
INDUSTRIAL APPS



PRODUCTS
NEW ANALYZERS,
PROCESSOR BOARDS,
ROBOT BITS
AND COMPONENTS

ALSO IN THIS ISSUE: ON THE BUG HUNT • DESIGN • TIPS 'N' TRICKS

LeCroy

WaveAce Oscilloscopes 40 MHz – 300 MHz



FROM
£550*

The New Affordable Oscilloscopes
from the Manufacturer of the
Fastest Oscilloscopes in the World

- 40 MHz – 300 MHz Bandwidth
- 2- and 4-Channel Models
- Up to 2 GS/s Sample Rate
- Up to 20 kpts Memory
- 5.7" Colour Display in all models
- Class Leading Math and Measurements
- Advanced Trigger
- LAN/USB Connectivity
- 3 Years Warranty

www.lecroy.co.uk

Phone: 01235 - 536973

*Launch Special Offer valid until 31 March 2010

REGULARS

05 TREND

INTERNATIONAL CES 2010 GIVES A VERDICT

06 TECHNOLOGY

08 ON THE BUG HUNT

MUST-READS FOR SOFTWARE ENGINEERS

Bi-monthly column on helping identify and fix bugs in hardware and software designs

10 INSIGHT

WHY IS LACK OF INTEROPERABILITY IN WIRELESS A CONCERN IN INDUSTRIAL APPLICATIONS?

by **Syed Tauseef Ahmad**

12 THE TROUBLE WITH RF...

ANOTHER BORING LECTURE ABOUT THE RECESSION

by **Myk Dormer**

16 FOCUS

PRINTED ELECTRONICS USES MORE INORGANICS AND COMPOSITES

The selection of inorganics and composites materials used by printed electronics firms
by **Raghu Das**

44 DESIGN

47 PRODUCTS

50 LAST NOTE

Cover
supplied by
**Linear
Technology**
more on pages
14 & 15

Disclaimer: We work hard to ensure that the information presented in Electronics World is accurate. However, the publisher will not take responsibility for any injury or loss of earnings that may result from applying information presented in the magazine. It is your responsibility to familiarise yourself with the laws relating to dealing with your customers and suppliers, and with safety practices relating to working with electrical/electronic circuitry – particularly as regards electric shock, fire hazards and explosions.

Electronics World is published monthly by
Saint John Patrick Publishers Ltd,
6 Laurence Pountney Hill, London, EC4R 0BL.

2.25Vp-p or
1.5Vp-p
Analog
Input

LTC2209

16-Bits

LVDS
or
CMOS

160Msps

PGA

Dither

18

FEATURES

18 GETTING THE MOST OUT OF YOUR HIGH SPEED ADC

Derek Redmayne and **Alison Steer** look at practical ways of achieving full performance from an analogue-to-digital converter

22 EXTRACTING A CIRCLE AND ITS CENTRE IN A MOVING DUMMY MASS

A host of authors present this study on an extraction method of a circle outline and its centre in a moving dummy mass, with a view to developing a 3D system for parabolic flights in space R&D programmers

26 COBE AND WMAP: SIGNAL ANALYSIS BY FACT OR FICTION?

Stephen J. Crothers goes in depth of the experiments, results and pitfalls of COBE and WMAP

31 SECURITY AND MOBILITY – THE FUTURE IS NOW

Gernot Heiser says that to avoid the security morass of the desktop PCs, mobile software architecture must take a different path to OS approach with a minimalist microkernel technology being the perfect candidate

34 THE HUM FIGURE – RELOADED

Burkhard Vogel discusses measurement of the Hum Figure of hum-infected phono-amplifiers

41 PLC WITH PIC16F648A MICROCONTROLLER – PART 17

Dr Murat Uzam presents the seventeenth article in the series, describing decoder macros

01279

**Credit Card
Sales**

467799

Motor Drivers/Controllers

Here are just a few of our controller and driver modules for AC, DC, Unipolar/Bipolar stepper motors and servo motors. See website for full range and details.

Computer Controlled / Standalone Unipolar Stepper Motor Driver

Drives any 5-35Vdc 5, 6 or 8-lead unipolar stepper motor rated up to 6 Amps. Provides speed and direction control. Operates in stand-alone or PC-controlled mode for CNC use. Connect up to six 3179 driver boards to a single parallel port. Board supply: 9Vdc. PCB: 80x50mm. Kit Order Code: 3179KT - **£15.95**
Assembled Order Code: AS3179 - **£22.95**



Computer Controlled Bi-Polar Stepper Motor Driver

Drive any 5-50Vdc, 5 Amp bi-polar stepper motor using externally supplied 5V levels for STEP and DIRECTION control. Opto-isolated inputs make it ideal for CNC applications using a PC running suitable software. Board supply: 8-30Vdc. PCB: 75x85mm. Kit Order Code: 3158KT - **£23.95**
Assembled Order Code: AS3158 - **£33.95**



Bi-Directional DC Motor Controller (v2)

Controls the speed of most common DC motors (rated up to 32Vdc, 10A) in both the forward and reverse direction. The range of control is from fully OFF to fully ON in both directions. The direction and speed are controlled using a single potentiometer. Screw terminal block for connections. Kit Order Code: 3166v2KT - **£22.95**
Assembled Order Code: AS3166v2 - **£32.95**



DC Motor Speed Controller (100V/7.5A)

Control the speed of almost any common DC motor rated up to 100V/7.5A. Pulse width modulation output for maximum motor torque at all speeds. Supply: 5-15Vdc. Box supplied. Dimensions (mm): 60Wx100Lx60H. Kit Order Code: 3067KT - **£17.95**
Assembled Order Code: AS3067 - **£24.95**



Most items are available in kit form (KT suffix) or assembled and ready for use (AS prefix).

Controllers & Loggers

Here are just a few of the controller and data acquisition and control units we have. See website for full details. Suitable PSU for all units: Order Code PSU445 £7.95

8-Ch Serial Isolated I/O Relay Module

Computer controlled 8-channel relay board. 5A mains rated relay outputs. 4 isolated digital inputs. Useful in a variety of control and sensing applications. Controlled via serial port for programming (using our new Windows interface, terminal emulator or batch files). Includes plastic case 130x100x30mm. Power Supply: 12Vdc/500mA. Kit Order Code: 3108KT - **£64.95**
Assembled Order Code: AS3108 - **£79.95**



Computer Temperature Data Logger

4-channel temperature logger for serial port. °C or °F. Continuously logs up to 4 separate sensors located 200m+ from board. Wide range of free software applications for storing/using data. PCB just 45x45mm. Powered by PC. Includes one DS1820 sensor. Kit Order Code: 3145KT - **£19.95**
Assembled Order Code: AS3145 - **£26.95**
Additional DS1820 Sensors - **£3.95 each**



Rolling Code 4-Channel UHF Remote

State-of-the-Art. High security. 4 channels. Momentary or latching relay output. Range up to 40m. Up to 15 Tx's can be learnt by one Rx (kit includes one Tx but more available separately). 4 indicator LED's. Rx: PCB 77x85mm, 12Vdc/6mA (standby). Two and Ten channel versions also available. Kit Order Code: 3180KT - **£49.95**
Assembled Order Code: AS3180 - **£59.95**



DTMF Telephone Relay Switcher

Call your phone number using a DTMF phone from anywhere in the world and remotely turn on/off any of the 4 relays as desired. User settable Security Password, Anti-Tamper, Rings to Answer, Auto Hang-up and Lockout. Includes plastic case. Not BT approved. 130x110x30mm. Power: 12Vdc. Kit Order Code: 3140KT - **£74.95**
Assembled Order Code: AS3140 - **£89.95**



Infrared RC Relay Board

Individually control 12 on-board relays with included infrared remote control unit. Toggle or momentary. 15m+ range. 112x122mm. Supply: 12Vdc/0.5A. Kit Order Code: 3142KT - **£59.95**
Assembled Order Code: AS3142 - **£69.95**



New! 4-Channel Serial Port Temperature Monitor & Controller Relay Board

4 channel computer serial port temperature monitor and relay controller with four inputs for Dallas DS18S20 or DS18B20 digital thermometer sensors (£3.95 each). Four 5A rated relay channels provide output control. Relays are independent of sensor channels, allowing flexibility to setup the linkage in any way you choose. Commands for reading temperature and relay control sent via the RS232 interface using simple text strings. Control using a simple terminal / comms program (Windows HyperTerminal) or our free Windows application software. Kit Order Code: 3190KT - **£69.95**



PIC & ATMEL Programmers

We have a wide range of low cost PIC and ATMEL Programmers. Complete range and documentation available from our web site.

Programmer Accessories:

40-pin Wide ZIF socket (ZIF40W) £14.95
18Vdc Power supply (PSU120) £19.95
Leads: Serial (LDC441) £3.95 / USB (LDC644) £2.95

USB & Serial Port PIC Programmer

USB/Serial connection. Header cable for ICSP. Free Windows XP software. Wide range of supported PICs - see website for complete listing. ZIF Socket/USB lead not included. Supply: 16-18Vdc. Kit Order Code: 3149EKT - **£49.95**
Assembled Order Code: AS3149E - **£59.95**

USB 'All-Flash' PIC Programmer

USB PIC programmer for all 'Flash' devices. No external power supply making it truly portable. Supplied with box and Windows Software. ZIF Socket and USB lead not included. Assembled Order Code: AS3128 - **£49.95**



See website for full range of PIC & ATMEL Programmers and development tools.

INTERNATIONAL CES 2010 GIVES A VERDICT

What this piece says is that there are consumer trends emerging which will make work and play a lot easier and more fun.

The International Consumer Electronics Show (CES) opened the new decade with a glimpse of what the next ten years will bring. And if these four days in the desert of Las Vegas, US, are indicative of what lays before us, the next ten years could prove to be the most remarkable yet.

BY SHAWN DUBRAVAC

LEAPS IN
TECHNOLOGICAL
INNOVATION, SUCH
AS DUPLICATING
THE HUMAN BODY'S
FUNCTIONS FROM
WRITING TO SPEECH
AND MOVEMENT,
HAS ALWAYS BEEN
DEMANDING

First, the home entertainment experience is changing in two important ways: 3D is becoming a viable home entertainment technology and content richness is expanding by means of Internet-connected displays.

3D was ever-present at CES – from laptops to cameras, mobile devices, gaming platforms and Blu-ray players – but nowhere was it more prevalent than with televisions. Every major television manufacturer was showing close to retail-ready television displays. At CES, content providers like ESPN and DirectTV also made important announcements about bringing 3D programming into the home. The entire 3D ecosystem came together at CES in preparation of making 2010 the year of home 3D.

Like any nascent technology, the initial years of 3DTV adoption will be measured, but for the first time, consumers can finally bring 3D technology into their home in a meaningful way.

Beyond 3D, Internet connectivity is changing the home entertainment experience. This year a number of Internet-connectable television sets were launched at CES, enabling consumers to marry the traditional richness of full HD content with the access of a myriad of offerings available on the web. This will exponentially increase the availability of content but, perhaps more importantly, it will empower consumers with new services. For example, Skype announced HD video conferencing via Internet-connectable displays.

Moving beyond the television, displays continued to play an integral role in framing this year's International CES. Before 2009, there was largely a void of devices between five and fifteen inches. Then in 2009, two important devices in the e-reader and netbook began to see broad consumer adoption. Both device categories did well in the marketplace with momentum driving into CES. The one-time void became a battlefield at the show. This year dozens of new e-readers and netbooks were launched, content partnerships solidified and service offerings announced.

Beyond new models, an entirely new category in slate tablet computers was brought to fruition in the middle of the battlefield for 5 to 15-inch display devices. We've seen tablet computers in the past, but the offerings popping up at CES are aimed at providing a richer digital media experience – taking us well beyond the tablet computers we've seen previously.

These are all product classes ready for primetime and we'll see most of the viable offerings in the marketplace by the end of the year. CES also brought to surface the innovations driving us deep into the new decade. Perhaps one of the most exciting developments was the continued push into direct human interaction.

The Holy Grail of technology has always been the human body; nothing is more complex. Leaps in technological innovation, such as duplicating the human body's functions from writing to speech and movement, has always been demanding. At this year's CES we saw technologies getting tantalizingly closer. For example, Toshiba's Cell TV showed how consumers could navigate content literally with a flip of a wrist. Microsoft announced that it was bringing to market its Natal project, which will continue the push of human interaction.

The energy level at the 2010 CES was as high as it has ever been. With more new exhibitors than in any prior year of its 43-year history, the International CES showed that innovative companies are combating the global downturn of the last two years head on. This first year of the new decade will be an important one for technology and CES has set the tone for many more years of innovation.

Shawn DuBravac is chief economist at the CEA

EDITOR: Svetlana Josifovska
Email: svetlanaj@stjohnpatrick.com
PRODUCTION MANAGER: Tania King
Email: taniak@stjohnpatrick.com
DISPLAY SALES: John Steward
Tel: +44 (0) 20 7933 8974
Email: johns@stjohnpatrick.com
PUBLISHING DIRECTOR: Chris Cooke

PUBLISHER: John Owen
SUBSCRIPTIONS:
Saint John Patrick Publishers
PO Box 6009, Thatcham,
Berkshire, RG19 4QB
Tel: 01635 879361
Fax: 01635 868594
Email: electronicsworld@cirdata.com

SUBSCRIPTION RATES:
1 year: £46 (UK); £67.50 (worldwide)
MISSING ISSUES:
Email: electronicsworld@cirdata.com
NEWSTRADE:
Distributed by Seymour Distribution Ltd,
2 East Poultry Avenue, London, EC1A 9PT
Tel: +44 (0) 20 7429 4000

PRINTER: William Gibbons Ltd
ISSN: 1365-4675

St John Patrick Publishers

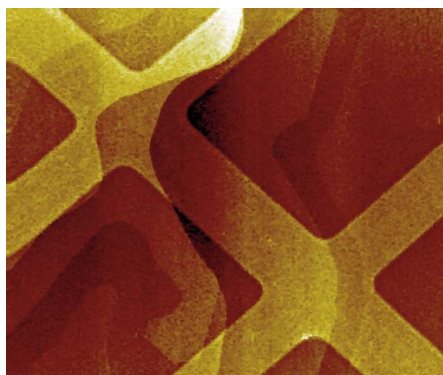
European Collaboration Makes Breakthrough in Developing Super-Material Graphene

A collaborative research project has brought the world a step closer to producing a new material on which future nanotechnology could be based.

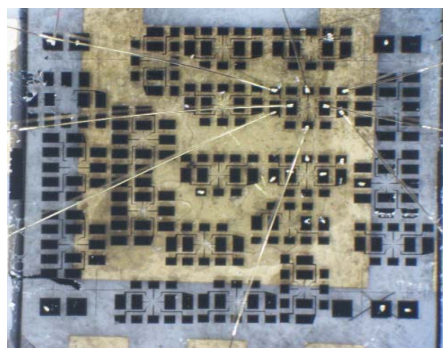
Researchers across Europe, including the UK's National Physical Laboratory (NPL), have demonstrated how graphene could hold the key to the future of high-speed electronics, including semiconductors, microchips and touchscreen technology.

Graphene is a form of carbon made up of a single layer of atoms arranged in a honeycomb shaped lattice. Despite being one atom thick and chemically simple, graphene is extremely strong and highly conductive, making it ideal for high-speed electronics and photonics among others. Graphene is a strong candidate to replace semiconductor materials, as this type of transistor can potentially run at faster speeds and cope with higher temperatures.

However graphene has previously only been produced on a very small scale,



Graphene device



Whole graphene chip

limiting how well it could be measured, understood and developed. This project saw researchers for the first time produce and successfully operate a large number of electronic devices from a sizable area of graphene layers (approximately 50mm²).

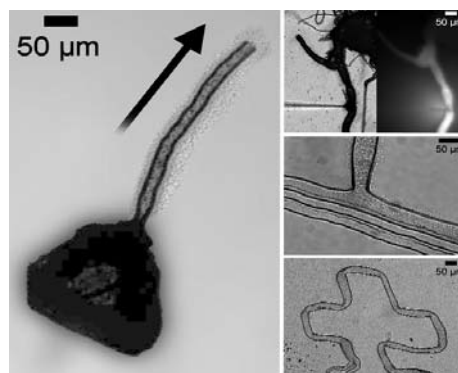
The graphene sample was produced epitaxially – a process of growing one crystal layer on another – on silicon carbide. Prof Alexander Tzalenchuk from NPL's Quantum Detection Group said: "It is truly sensational that a large area of epitaxial graphene demonstrated not only structural continuity, but also the degree of perfection required for precise electrical measurements on par with conventional semiconductors with a much longer development history."

The second key breakthrough of the project was measuring graphene's electrical characteristics with unprecedented precision. For products such as transistors, manufacturers must be able to make such measurements with incredible accuracy against an agreed international standard.

The international standard for electrical resistance is provided by the Quantum Hall Effect, a phenomenon whereby electrical properties in 2D materials can be determined, based only on fundamental constants of nature.

Graphene shows the Quantum Hall Effect at much higher temperatures. This means the graphene resistance standard could be used much more widely as more labs can achieve the conditions required for its use. In addition to its advantages of operating speed and durability, this would also speed the production and reduce costs of future electronics technology based on this material.

The research was a joint project carried by the National Physical Laboratory; Chalmers University of Technology, Göteborg, Sweden; Politecnico di Milano, Italy; Linköping University, Sweden and Lancaster University, UK. Measurement was carried out by the Quantum Detection Group at the UK's at the National Physical Laboratory, Teddington, UK.



Scientists 'photograph' nano-particle self-assembly

Scientists 'Photograph' Nano-Particle Self-Assembly

Scientists at the University of Glasgow have photographed the self-assembly of nano-particles, unveiling the blueprint for building molecular machines atom by atom.

The researchers, along with colleagues from the University of Bielefeld, Germany, devised an experiment which enabled them to observe molecules being constructed around a transient template cluster. During the experiment, they observed the self-assembly of molybdenum oxide wheel molecules around an intermediate structure in the centre of the wheel, which they found to be the 'template' or scaffold used to construct the larger molecule. Following completion of the molybdenum oxide wheel molecule, which is just 3.6nm in diameter, the template was ejected, freeing it to repeat the process. The researchers were able to 'photograph' this process and the template using X-ray crystallography.

Professor Leroy Cronin from the Department of Chemistry, who devised and led the study, said: "This advance is very important since in the construction of molecular nano-objects we must rely on 'self-assembly' where the nano-scale object builds itself – a process which is almost impossible to understand or control using current step-wise chemical synthesis approaches."

The discovery could lead to 'designed' assembly of a whole range of precisely defined nano-particles with applications in electronics and medicine, but also help create intelligent nano-sensors and nano-functional machines.

"This result is massively interesting, not only do we get to 'image' self-assembly for the first time, this discovery will allow us to devise new types of blueprint that could allow the assembly of a whole new class of designer nano-particles," said Cronin.

ELECTROMAGNETIC SIMULATOR SUPPORTS DESIGN OF MAGNET FOR CANCER TREATMENT

The Opera electromagnetic simulator has played an important role in the design of the particle beam steering magnet currently being commissioned at Italy's new hadron therapy centre in Milan – the Centro Nazionale di Adroterapia Oncologica (CNAO).

Weighing in at 70 tonnes, the 1.81 Tesla dipole magnet is believed to be the largest ever produced for medical applications, and is positioned at the end of a particle acceleration line. It turns the particle beam through 90 degrees to direct it down onto a patient treatment table.

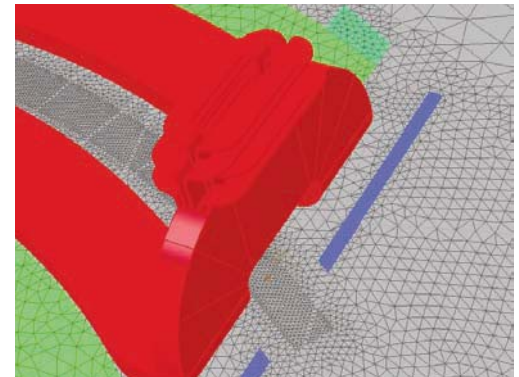
The magnet has been produced by the high performance magnet supplier, Sigmaphi, which specializes in custom magnetic systems and beam transport lines for particle accelerators. This particular specification called for a very large magnetic field region of 20 x 20cm, combined with exceptional field homogeneity.

Sigmaphi's chosen electromagnetic simulator for this design task is the Opera finite element analysis tool from Cobham Technical Services. This simulator is the world

standard for this scientific application because of its accuracy and execution speed. Fast simulation is very important in complex applications like this, and in this case the speed of simulation was aided by Opera's ability to use Biot-Savart calculations for computing coil fields, greatly reducing the need for complex finite element meshing of the model – with its impact on computation time.

"We spent around six months designing and optimising this magnet before we put it into production," said Frédéric Forest, Engineering Director at Sigmaphi. "Even though the design model was complex, the 3D Opera simulations took only seven or eight hours on a standard PC, a speed that helped us to investigate a large number of design variations."

The Opera simulator used in this application – known as Tosca – employs a discrete finite element model in order to solve the partial differential equations governing the behaviour of static



A view of one end of the model for the magnet coil with its busbar cooling structure, showing the different mesh densities

electromagnetic fields. It computes the total magnetic scalar potential in the magnetic material and the reduced magnetic scalar potential in the regions where source currents in coils are specified.

The reduced potential represents only that portion of the field produced by magnetization, the remainder of the field being computed directly from source currents, yielding very high accuracies.

Recom Engineers Crack the 10kV Barrier for DIP 24 DC/DC Converters

US-based Recom has designed a DC/DC converter in a DIP24 case that breaks the 10kV barrier.

At the heart of this new development is a new transformer concept, based on its "Re³inforced" technology, for which patents have already been applied. The Re³inforced DC/DC converters offer up to 10kVDC isolation.

DC/DC converters typically offer galvanic input to output isolation. Depending on the converter, the isolation voltage can be as low as 1kVDC or as high as 10kVDC. The isolation rating is functional isolation. However, UL

defines three classes of isolation quality: functional, basic and reinforced.

Sophisticated applications in medical or power electronics often require "reinforced" isolation for isolation strengths higher than 6kVDC.

Although 1kVDC sounds impressive, the transformer construction is very simple. A typical low-power DC/DC converter will use an internal toroidal or bobbin-type transformer, consisting of primary and secondary windings of magnet-wire wound upon a ferrite core. Even if the insulation on one winding fails, the insulation on the other winding can still withstand the full 1kVDC test voltage. This means that the input and output windings can be wound directly on top of one another without compromising the electrical isolation. This class of isolation is called 'operational' or 'functional' isolation.

Considering that an industry standard low-power DC/DC converter is in a DIP24 case with outside dimensions of around 32mm x

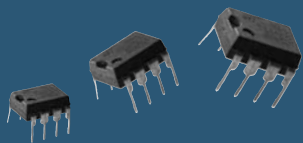
20mm x 10mm, a transformer with a creepage separation of over 4.6mm as required by UL.

Previous attempts to build a compact transformer with reinforced isolation have been largely unsuccessful; the main reason being that the efficiency of the transformer decreases if the electric and magnetic fields within the transformer are not closely coupled together. However, in order to meet the clearance requirements for reinforced isolation, there has to be gaps and physical barriers between the input and output windings.

Recom engineers have finally developed a DIP24 sized DC/DC converter that meets all of the requirements for Re³inforced isolation. Not only has the size been significantly reduced, the winding capacity has also been reduced by a factor three down to 20pF. This feature ensures extremely low leakages as are required in medical applications, where the electronic circuit is in contact with the patient.



Recom's DIP24 DC/DC converter



MUST-READS FOR SOFTWARE ENGINEERS

Vicky Larmour from Cambridge Consultants gives an overview of some of the on-line sites that might help with the job or just lighten up the daily load

LOOKING FOR HELP with a specific programming or design issue? *Dr Dobbs Journal* contains code and design tutorials, well supported with accompanying code examples available for download and accompanied by blogs, reader polls and forums.

Experts Exchange is a forum for asking computing-related questions, everything from "How do I revert to older USB drivers?" to "Why doesn't this C program give me the output I expect?". It gives a powerful search capabilities but the downside is that you need to register (which is not free) to view solutions.

StackOverflow was created by Joel Spolsky (of *Joel on Software*) and Jeff Atwood (of *Coding Horror*). It's similar to *Experts Exchange* but is completely free. A flexible tagging system makes it easy to find out if your question has already been asked or answered.

Competitions and Puzzles

If you're learning a new language, or want to stretch yourself to learn new features in a language you already know, there's no better way than to try out some coding puzzles.

CodeKata and *Project Euler* are both well structured problem sets designed to help you learn new programming languages or techniques. *CodeKata* has a wiki and mailing list for discussion of the problems, and submitting a solution to a Project Euler problems grants access to a forum specific to that problem where the solution and any issues can be discussed. The Project Euler problems are also often discussed on *StackOverflow*.

Google Code Jam is an annual programming challenge hosted by Google. It incorporates multiple rounds and you

can use the language/platform of your choice to solve the problems.

CodeGolf presents programming problems with the challenge being to provide a solution using the fewest characters possible. The official challenges at the site are for Perl, PHP, Python and Ruby, but you can always give the problems a go in your preferred language if it's not listed. The site includes a forum for discussion of each problem.

The International Obfuscated C Coding Contest, or *IOCCC*, is an annual challenge where the goal is to write the most non-obvious or complicated C code to solve the given problem. It's definitely not a good way for a beginner to learn C, but for those of you who already know C, why not have a go at your own solutions to the various challenges, or peruse the winning solutions to pick up some new tricks or information about how C really works internally?

Unfortunately, the annual competition finished in 2006 and there appear to be no plans to re-open it, but the website includes full source code and explanations for the archived competitions right back to 1984.

Humour

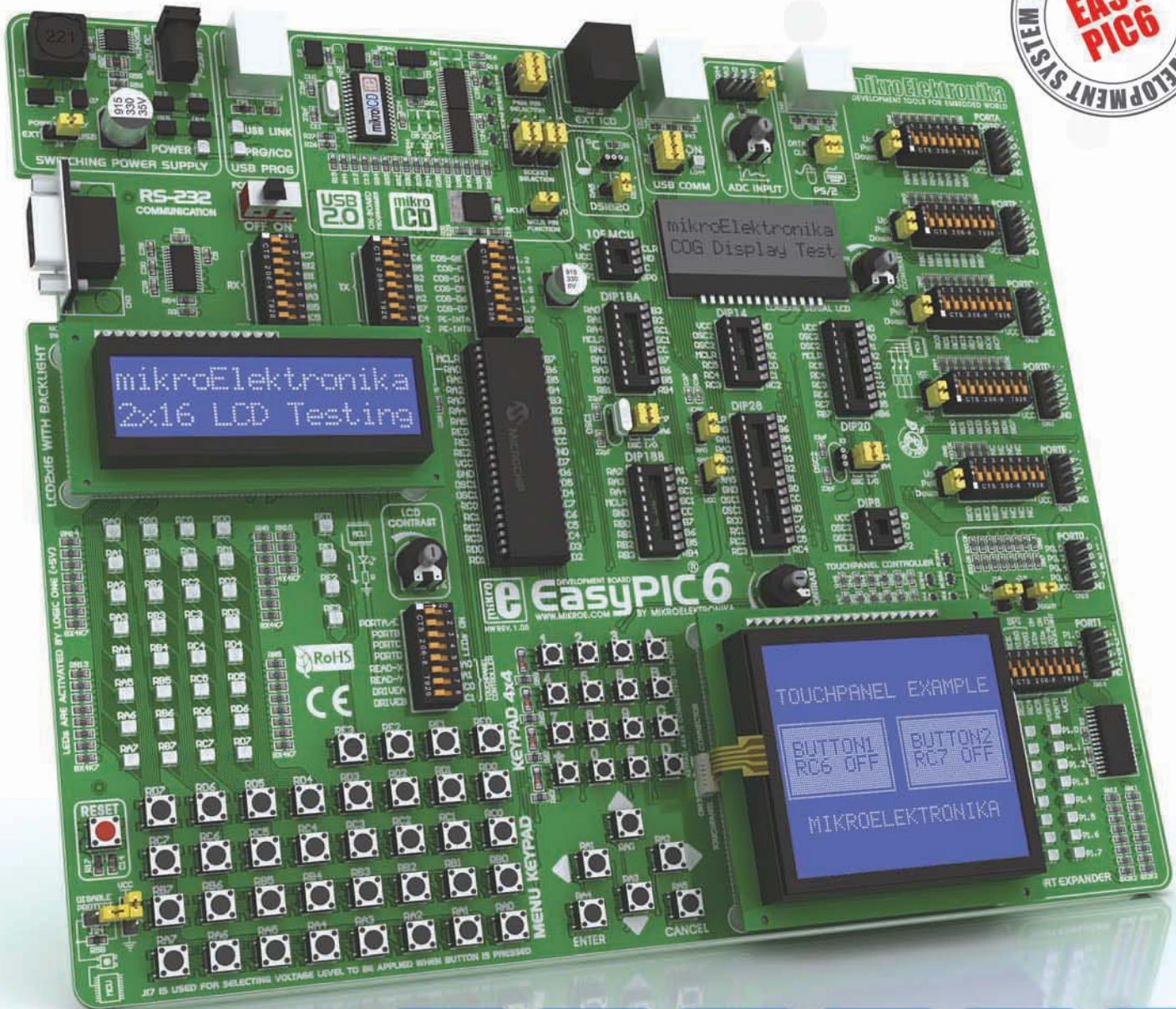
For a good dose of how not to program, check out Jeff Atwood's *CodingHorror* and Alex Papadimoulis' *DailyWTF*.

The best webcomic for geeks is Randall Munroe's *xkcd*, updated three times a week with a new strip. And don't forget Scott Adam's classic, *Dilbert*, for anyone who has ever been frustrated in an engineering job.

Finally, to treat yourself to some geek toys or attire, have a browse around the *ThinkGeek* shop.

Cambridge Consultants is a technology and innovation company, renowned for its ability to solve technical problems and provide creative, practical solutions to business issues.
www.cambridgeconsultants.com

PICK UP YOUR **PIC** AND GO



EasyPIC6 development system is a full-featured system for 8-, 14-, 18-, 20-, 28- and 40-pin PIC microcontroller applications development and testing. The mikroICD (Hardware In-Circuit Debugger) enables very efficient step by step debugging. Examples in C, BASIC and PASCAL are provided with the board.

Experience the ease of creating your own electronic device **EasyPIC 6**

WHY IS LACK OF INTEROPERABILITY IN WIRELESS A CONCERN IN INDUSTRIAL APPLICATIONS?



WHILE THE AVAILABLE potential for wireless deployment in factory automation is high, the adoption of wireless is plagued by various concerns surrounding the wireless technology, one of which is lack of interoperability.

In the recent past, interoperability was not as major concern as it is currently. Companies predominantly used to build their own systems or purchased them from a single supplier. Increasing plant automation has spurred the demand for wireless devices and systems for numerous applications, like monitoring, alarm and telemetry, with a large number of suppliers offering these systems or solutions. They are often customized on proprietary protocols but not based on a common standard or architecture.

As a result, these devices offered from multiple suppliers are not often compatible with one another. So even though the options have increased, the end users have become more concerned about the compatibility of the devices.

End users are wary of becoming locked into a proprietary system that may hinder their future advancement, as they may not be able to adopt any new technology. Integration issues with existing infrastructure results in time and effort to be spent by end users, while they prefer plug-and-play devices. End users are also extremely cautious of investing in wireless when they are not confident about the benefits that wireless has to offer.

Given that the end users will not be very keen to replace the existing Fieldbus installation, suppliers should look to integrate wireless devices to existing wired Fieldbus. Currently, plant IT network assumes significance over automation network. Hence, clear boundaries and smooth integration of wireless is required with the wireless devices' existing network. The existence of several open and proprietary communication protocols results in

confusion among the wireless devices' end-users who are ready to wait until a uniform standard is established.

Around 83% of the end users across process and factory automation rated interoperability as a medium to high concern. However, the level of concern varies depending on different parameters such as end-user environment, types of wireless devices being used, the application area and the experiences of the end user with wireless devices.

For example, the refining and pharmaceutical industries express a greater concern over interoperability among end users. They believe that integration with the existing network is important and the presence of numerous controls, Fieldbus and automation devices implies that the wireless devices need to integrate seamlessly into the existing network. Similarly, in the oil and gas, and the water and waste water industries wherein one of the preferred application areas for wireless devices is telemetry, end users are convinced that the wireless devices must be compatible with each other in order to ensure that there is a smooth flow of data.

Attainment of true interoperability would require an open architecture such as software-based systems, in which various standards could be applied.

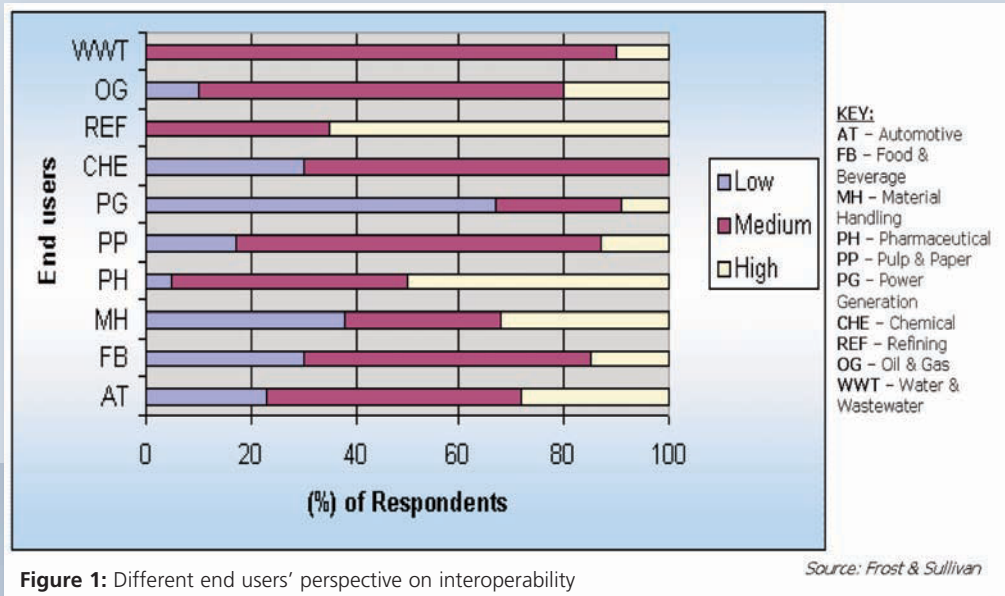
Software such as National Instruments's

Laboratory Virtual Instrumentation Engineering Workbench (NI LabVIEW) is capable of communicating with both standards-based and proprietary wireless networks. End users also believe that the lack of universal standard is another major concern. The need of the hour is to have common standards that offer interoperability from both the supplier and the end-user perspective.

In order to increase the level of adoption of wireless in the discrete and the process environment, suppliers must come up with wireless devices that are compatible with each other. Moreover, there is a need for a uniform standard and open architecture to enable the

“END USERS ARE WARY OF BECOMING LOCKED INTO A PROPRIETARY SYSTEM THAT MAY HINDER THEIR FUTURE ADVANCEMENT, AS THEY MAY NOT BE ABLE TO ADOPT ANY NEW TECHNOLOGY”

Syed Tauseef Ahmad,
Research Analyst for
Industrial Automation
and Process Control
Europe at Frost & Sullivan,
discusses the need for
standardisation of
wireless systems in various
industrial applications



seamless integration of wireless devices with existing plant infrastructure such as Fieldbus or other control systems. End users must also be convinced about interoperability through product trials or demos suppliers should offer.

Nevertheless, the future for wireless devices in automation looks promising. Although the end-user concern is expected to hamper the

adoption of wireless in the near future, the upcoming standards like SP100.11a and wireless HART are going to address this issue. In addition, numerous suppliers are supporting the initiatives that aim to establish a common standard. The increasing success stories of smooth wireless integration and functioning are likely to reduce end-user conservatism and raise the level of adoption of wireless devices.

EXTENSIVE FREQUENCY CONTROL RANGE

Euroquartz high quality frequency control products for aerospace, medical, wireless, communications and telecom applications.

- Quartz crystals
- Oscillators
- VCXOs, TCXOs & OCXOs
- Crystal, SAW & custom filters
- Resonators

On-site production, quick turnaround, custom design, prototypes, up-to-date production and test methods, engineering design and support, 100% product validation. ISO 9001:2000 certified.

EUROQUARTZ

Euroquartz, Blacknell Lane
Industrial Estate, Crewkerne,
Somerset, TA18 7HE.
Tel: +44 (0) 1460 230000,
Fax: +44 (0) 1460 230001,
email: sales@euroquartz.co.uk

Website: www.euroquartz.co.uk

4most

FCT Waterproof "D" Connectors*
Four Sprung Duck Technique

(*Made in Germany)

- ▶ Waterproof Plastic + Metalised Hoods
- ▶ Waterproof "D" Connectors IP67 + IP69K
- ▶ High Density + Mixed Layout "D"
- ▶ Specialised "D" Connectors

www.4most.co.uk T: 01371 811171

Another Boring Lecture About the **RECESSION**



Myk Dormer

UNLESS YOU LIVE in a cave in Siberia, or keep a dark felt bag tightly fastened over your head at all times, it cannot have escaped your notice that something isn't quite right in the economy, in our industry, or in your bank accounts.

The global recession – or to give it the favorite, loathsome, tabloid name “Credit Crunch” – has become an undeniable fact and, as such, it has had (and continues to have) a definite effect on the low power wireless market.

Initial influences on companies and users in this area were minimal. The generally weak linkage between this industry area and the financial/consumer sectors provided a degree of insulation. Suppliers in the alarm/security subsector may even have seen marginal upturn in orders, in response to generalized feelings of unease and insecurity.

With time, however, certain effects and trends have become apparent: General activity in the sector has reduced. While the market for low power wireless devices has not completely collapsed, order levels are down and scheduled or repeat orders are being postponed, delayed or canceled.

This, in turn, has reduced the immediate income of what are in this industry area generally small-to-medium sized manufacturers, forcing economies in both staffing and capital investment. So:

- Enquiry response times and technical support are degraded;
- Component purchase dependant lead-times are increased;
- New products are being delayed or shelved;
- Invoice payment terms become less favourable.

In those instances where the supplier has been forced to seek financial help from investors or banks, the effects are far more pronounced, as the banks (despite being basically responsible for the entire crisis originally) are imposing punitive conditions on these small companies seeking loans, without actually having any

understanding of their business area at all.

Consequently, ignorant financial executives are forcing changes based entirely on maximizing very short term returns (the removal of important technical staff, the cancelation of entire future design programs and preventing the purchase of replacement test and production equipment and basic component stock).

While the current depressed state seems fairly stable, as the market begins to re-inflate and order levels rise, there are a few effects that must be watched. Initially, the level of enquiries will

seem to be out of proportion to the level of orders, resulting in an apparently excessive demand on technical support/engineering effort.

To the customer this will appear as a further slowing-down of the response times of these now understaffed departments. As orders begin to arrive, cash-starved companies will reflexively concentrate on the largest orders first (even if a raft of smaller orders would bring more profit). This will result in a degree of randomization in lead times, as some smaller orders will be initially overlooked.

Finally, with continuing overall increase in market activity and order volumes, the long-term damage caused by the short-term decisions made under the duress of the recent crisis will appear:

- Understocking of critical parts during the ‘lean’ period will now impact production, and the delivery of some (but not all) product lines will stall, pending delivery of out-of-stock parts, limited by component supplier lead-times.
- Lack of staff in critical areas will further slow production/test processes, while engineering support to solve ongoing production issues will be insufficient, resulting in even more delay.
- Impatient customers will cancel recently placed, but now delayed, orders.

The result is a brief, apparent recovery, followed by an

**"CUSTOMERS: ANTICIPATE
LONGER LEAD-TIMES; ORDER
EARLIER; TALK TO YOUR
SUPPLIER; BUT MOST
IMPORTANTLY, DON'T PANIC
AND DON'T GIVE UP "**

irreversible collapse of the company concerned.

So what can be done? It seems, relatively little.

Suppliers: Minimise the long term damage caused by external conditions and directives, by using part-time working or sabbatical schemes instead of wholesale redundancies. Keep especially careful track of strategic parts stock levels.

If necessary, consider introducing interim designs to bypass long-lead time parts or use up available stock.

Customers: Anticipate longer than usual lead-times. Order earlier, even if this means placing a sequence of smaller scheduled purchases. Talk to your supplier(s) and, if necessary, consider adopting a near-equivalent product, to avoid specific part lead time hold-ups. But most importantly, don't panic and don't give up. A good design has an inner merit of its own, and with time and effort will find its place.

As with other turbulent times, the current problems will pass.

Myk Dormer is Senior RF Design Engineer at Radiometrix Ltd
www.radiometrix.com

THE ORIGINAL SINCE 1994
PCB-POOL[®]
 Beta LAYOUT
 Specialising in Prototype PCBs

NEW! Free Laser Stencil with all Prototype PCB orders

NEW! 1 WD prototype service

NEW! Chemical Tin Finish (no extra cost)

Free Phone
 UK 0800 389 8560

@ Simply send your layout files and order ONLINE
PCB-POOL.COM • sales@pcb-pool.com

Beta LAYOUT

Food 2000 • Designer • EDA • iDesign • Gerber • RS-274-X • Easy-PC • PULSONIX

RADIO MODULES FOR WIRELESS DATALINKS

Radiometrix continues to be recognised as the leading manufacturer of wireless datalinks for a wide variety of applications: it brings to market high-quality yet cost effective VHF & UHF low power radio modules that cater for the needs of OEMs manufacturing for international wireless data transmission industries.

Products available include:

- Narrow Band and Wide Band FM Transmitters, Receivers and Transceivers
- Single Channel and Multi-channel operation
- UHF and VHF ISM bands
- Custom design service
- Encoders and Decoders for RF remote control
- Radio Packet Modems
- Radio Packet Controllers
- Evaluation Kits

Applications include:

- Security & Alarm
- Telecommand or Remote Control
- Telemetry
- Industrial and Commercial
- Data Logging
- Automatic Meter Reading (AMR)
- Tracking



Radiometrix Ltd
 Hartcran House
 231 Kenton Lane
 Harrow, Middlesex
 HA3 8RP UK

Tel: +44 20 8909 9595
 Fax: +44 20 8909 2233
sales@radiometrix.com

www.radiometrix.com

RADIOMETRIX
 20 YEARS OF INNOVATION FROM THE PIONEERS IN WIRELESS

Integrated μ Module Receiver Shrinks Diversity Base Station Designs

Todd Nelson, Signal Chain Module Development Manager, Mixed Signal Products,
Linear Technology Corporation

The majority of full-size cellular basestation transceivers rely on an Intermediate Frequency (IF) sampling architecture with receiver chains for main and diversity antennae. A common configuration uses 14-bit Analogue to Digital Converters (ADCs) sampling at 122.88MSPs at an IF of 140MHz. The ADC driver includes some gain to recover the insertion loss of the Surface Acoustic Wave (SAW) filter. Given this basic configuration with two channels, it is challenging to reduce board space via integration due to process technology incompatibility between the ADC, its driver and all the ancillary passive components. However, the use of System in Package (SiP) technology provides a compelling alternative to traditional silicon integration.

The LTM9002 dual-channel, IF/baseband receiver harnesses years of applications design experience and squeezes it into an easy-to-use 11.25mm \times 15mm μ Module[®] package, see Figure 1. Inside the package is a high performance dual 14-bit ADC sampling up to 125MSPs, anti-aliasing filters, two fixed gain differential ADC drivers and a dual auxiliary DAC. By combining these components, the LTM9002 eliminates the burden of input impedance matching, filter design, gain/phase matching, isolation between channels and high frequency layout, dramatically reducing board space and improving time to market. Even in this small package, the LTM9002 guarantees high performance that will enhance many communications and communication test applications.

Extensive hands-on applications experience is a prerequisite for any designer hoping to take full advantage of an ADC's capabilities when sampling high dynamic range signals in IF-sampling, diversity receivers. An intimate knowledge of the amplifier output stage and ADC front end is required to match the impedances, while careful attention to layout is required to minimize coupling of the digital outputs into the sensitive analog inputs. Good layout is paramount for maintaining ADC performance, yet demanding market requirements complicate layout, with demands for compact design and high channel density. These design requirements can challenge even the most seasoned engineers if their expertise lies in the RF or digital worlds.

DIVERSITY ADC APPLICATIONS

Multichannel applications such as diversity receivers add channel matching requirements to the list of performance criteria. Like I/Q receivers, diversity receivers require excellent isolation between channels because crosstalk appears as noise corruption and can be more difficult to suppress with digital filtering. Clearly, channel matching and

channel isolation of the ADC and driver circuits directly impact system-level performance. For many applications, these errors cannot be corrected in the digital domain.

The LTM9002 achieves 66dB Signal to Noise Ratio (SNR) and 76dB Spurious Free Dynamic Range (SFDR) at 140MHz input frequency. Figure 2 shows the FFT under these conditions. SNR is a function of the ADC and amplifier performance as well as the amplifier gain and filter bandwidth. The inherent amplifier noise is proportional to the voltage gain; therefore, the 26dB amplification increases the amplifier noise by 20 times, whereas 8dB amplification would only increase the noise by 2.5 times. Likewise, the amplifier noise (in nV/ $\sqrt{\text{Hz}}$) increases with the square of the filter bandwidth. It is important to remember these relationships when assessing the entire signal chain.

As mentioned above, channel-to-channel matching and isolation are important considerations. The LTM9002 achieves 90dB isolation at 140MHz input frequency despite the small form factor. The overall gain is typically 26dB on the default span setting and varies just 0.1dB between the two channels. The 12-bit auxiliary DAC can be configured to adjust the span by 61 μ V per step.

For printed circuit board (PCB) area efficiency, the LTM9002 excels. The LTM9002 requires no external components — no supply bypass capacitors, no passive filtering, no impedance matching or translating components. In many IF-sampling applications, gain can be obtained through transformers, but they are often large and difficult for automated assembly equipment to mount. In DC-coupled applications, amplifiers are required as ADC drivers, along with their associated anti-alias filter network. It is not uncommon for the entire IF/baseband receiver system to consume two square inches of board area (approximately 25mm \times 50mm). None of this external circuitry is

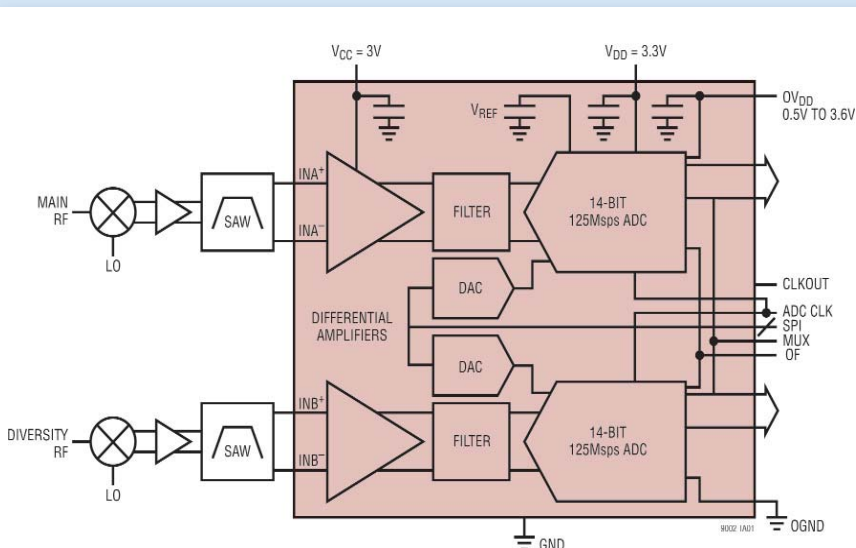
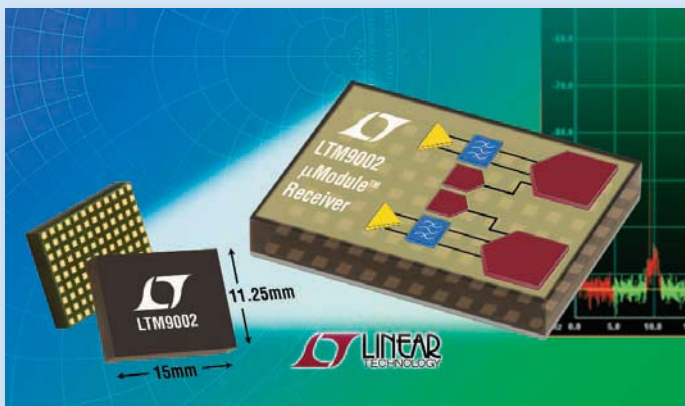


Figure 1: LTM9002 used for a Main/Diversity receiver



required with the LTM9002, so it requires only about one-quarter of a square inch (11.25mm × 15mm), better by a factor of eight.

ATTRIBUTES AND CONFIGURATIONS

The μModule construction allows the LTM9002 to mix standard ADC and amplifier components regardless of process technology and match them with passive components for a particular application. The μModule receiver consists of wire-bonded die, packaged components and passives mounted on a high performance, four-layer, Bismaleimide-Triazine (BT) substrate. BT is similar to other laminate substrates such as FR4, but BT has superior stiffness and a lower coefficient of thermal expansion.

The LTM9002-AA utilizes a dual, 14-bit, 125Msps ADC, two 26dB fixed-gain amplifiers and also includes a 12-bit dual DAC configured for full-scale span adjustment, as shown in Figure 1. Internal anti-alias filters limit the input frequency to less than 170MHz, perfect for 140MHz IF with wide signal bandwidth. Other configurations are possible and easy to implement. The amplifiers present a 50Ω differential input impedance and an input range of ±50mV, or -16dBm. This default span is set by connecting the SENSE pin to VDD, and can be adjusted in three ways. For a -3dBm lower span, the SENSE pin can be connected to 1.5V. By connecting SENSE to VDD or 1.5V, the internal reference is used. An external reference can be used by applying 0.5V–1.0V to the SENSE pin. The auxiliary DAC offers a final option for selecting the range. Alternately, fine adjustments to the span, such as balancing the gain of the two channels, can be made with external references or the auxiliary DAC.

Multiple power saving modes include independently disabling either amplifier or the ADC. The ADC has two shutdown states: NAP and SLEEP modes. In NAP mode, the internal reference remains biased so that conversions can resume within 100 clock cycles upon startup. In SLEEP mode the reference is shut down and start-up takes milliseconds. A clock duty cycle stabilizer feature is available and an output clock signal is provided for accurately latching the output data. The two channels can be output on separate parallel busses or multiplexed onto a single parallel bus to save processor pins.

INTERFACING TO THE ANALOG INPUTS

The analog inputs of the LTM9002 present a differential 50Ω resistive input impedance, which in most cases exactly matches the signal path. The input common mode level should be approximately VCC/2. Traditionally, the input of an ADC requires considerable care in terms of drive current, settling time and response to the nonlinear characteristics of sample-and-hold switching. For lowest distortion performance, the common mode level at the ADC inputs must be optimized for the particular ADC front-end; for best signal-to-noise (SNR) performance, the signal swing must utilize the maximize ADC input range. All this is taken care of by the LTM9002.

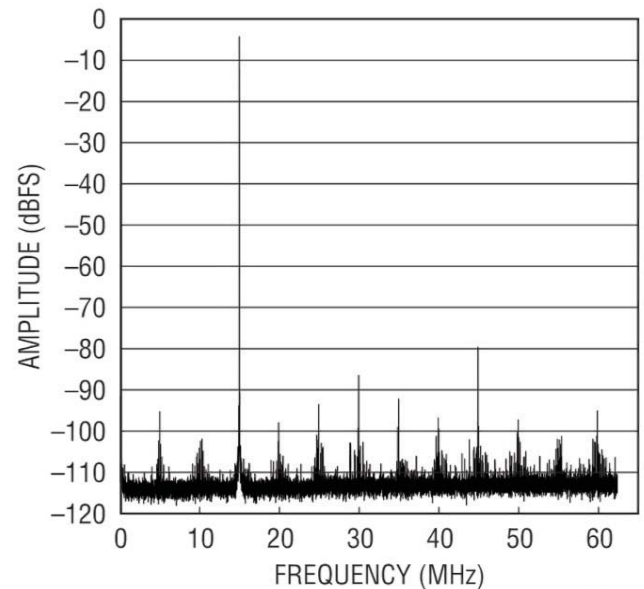


Figure 2: Figure 2. FFT showing LTM9002 AC performance with 140 MHz input frequency

9002 G08

INTERFACING TO THE DIGITAL OUTPUTS

The LTM9002 uses standard CMOS output buffers that switch from OVDD to OGND. OVDD can range from 0.5V to 3.6V, accommodating many different logic families and OGND can be as high as 1V. Because the LTM9002 supplies are internally bypassed, no local supply bypass capacitors are required. The power supply for the digital output buffers should be tied to the same supply that powers the logic being driven. For example, if the converter drives a DSP powered by a 1.8V supply, then OVDD should be tied to that same 1.8V supply. Lower OVDD voltages also help reduce interference from the digital outputs to the analog or clock circuitry. OVDD and OGND are isolated from the ADC power and ground. An internal resistor in series with the output makes the output appear as 50Ω to external circuitry and may eliminate the need for external damping resistors.

POWER SUPPLIES AND BYPASSING

The LTM9002 requires a 3.0V supply. To optimize performance for each block within the LTM9002, multiple supply pins are used. Internally, each supply is bypassed to ground very close to the die to minimize coupled noise. A common problem with traditional ADC board layouts is long traces from the bypass capacitors to the ADC degrade system performance. The bare die construction with internal bypass capacitors in the LTM9002 provides the closest possible decoupling and eliminates the need for external bypass capacitors.

CONCLUSION

Diversity basestation applications need good ADC channel-to-channel matching and isolation without consuming valuable board space. Driving high performance ADCs is challenging enough without the matching, isolation and board space constraints. The LTM9002 integrated dual IF/baseband receiver subsystem addresses all of these requirements while eliminating the design task of mating an ADC and its driver. By integrating the passive filtering and supply bypassing, the overall size is dramatically smaller than otherwise possible with discrete implementations. The LTM9002's μModule packaging is itself developed to maximize the performance of the integrated components. ■

PRINTED ELECTRONICS USES MORE INORGANICS AND COMPOSITES

By Raghu Das, CEO of market research organization IDTechEx

PRINTED ELECTRONICS is using more inorganics and composites in the quest for higher performance, lower costs, finer feature size, stretchability and creation of radically new components such as memristors, supercapacitors and metamaterials. Here is what 26 developers and suppliers have been up to in 2009.

Copper Indium Gallium Diselenide

Ascent Solar Technologies, a developer of flexible thin-film photovoltaic modules, recently announced success manufacturing monolithically interconnected 5-meter long, flexible, light-weight modules on a polyimide substrate using Copper Indium Gallium Diselenide (CIGS).

That means such modules can be hand-carried and installed without roof strengthening, as opposed to glass modules that have to be hoisted with a crane across rooftops. It can produce 123 watts under standard test conditions with an aperture area efficiency of 9.1%. CIGS promises to be more efficient, have lower cost of ownership and longer life than amorphous silicon flexible alternatives for open air use.

Titanium Dioxide

Electronic memory chips may soon gain the ability to bend and twist as a result of work by engineers at the National Institute of Standards and Technology (NIST) who have found a way to build a flexible "memristor" memory component out of inexpensive, readily available materials. A memristor is a resistor that changes its resistance depending on the amount of current that is sent through it and retains this resistance even after the power is turned off.

The new device is promising because of its potential applications in medicine and other fields. The memristor is a fundamentally new component for electronic circuits developed in 2008. By low cost sol-gel process, the researchers depositing a thin film of titanium dioxide on polymer sheet. By adding metal contacts, the team created a flexible memory switch that operates on less than 10 volts, maintains its memory when power is lost

and still functions after being flexed more than 4,000 times.

New Silicon Inks

The manufacturing costs for high-efficiency 50-micron crystalline solar cells will now be significantly lower thanks to a high-throughput industrial silicon-ink inkjet printing system, according to developers OTB Solar in partnership with Innovalight. They use inkjet printing of silicon ink to halve the number of costly manufacturing processes required to produce highly efficient solar cells.

NanoGram silicon inks for printed electronics are based on its proprietary laser pyrolysis process. NanoGram has developed processes to make large area, thin layers of silicon cheaply through the additive process

WITH IMPROVED
CONDUCTIVITY AND
STRETCHABILITY, IT IS
NOW POSSIBLE TO FOLD
THE DISPLAY IN HALF
OR EVEN CRUMPLE IT
UP WITHOUT DAMAGE,
AND TO STRETCH IT UP
TO 50% OF THE
ORIGINAL SHAPE

of printing nano-Si based inks and, like Kivio, which also prints its own specially developed silicon inks and focuses on transistor circuits, it intends to make complete devices, both solar cells and transistors being in its sights.

Key to silicon ink manufacture is to achieve the appropriate particle sizes and size distributions, which enable low temperature processing when the ink is used to create devices. The particle sizes in a given

measure need to be within a controlled distribution, and the particles need to be non-agglomerated, which was previously a considerable problem. In addition, particle oxidation needs to be avoided in order to achieve high performance in printed electronic devices. Stable inks must also be formulated from these particles to be compatible with standard printing techniques such as ink jet printing and wide area coating.

NanoGram has also developed techniques for doping the silicon particles during the reaction in highly controllable doping levels.

Another of NanoGram's focus is on transistors, and one application is display backplanes. Within a few months of development, the company has passed the mobility of amorphous silicon and believes that mobility in the range of $> 100\text{cm}^2/\text{Vs}$ is achievable, although for display backplanes that is not needed.

While the sintering temperature of the deposited transistors is confidential, IDTechEx notes that Teijin, the plastic substrate supplier, is a partner of NanoGram involved in a joint development agreement to develop silicon inks for flexible electronic applications. In addition, NanoGram investors include a wide range of companies with a number from Japan, given that one of the largest applications will be display backplanes.

Indium Zinc Oxide, Zinc Oxide, Hafnium Oxide

Zinc-oxide-based semiconductors hugely outperform organic alternatives in conventional transistor electrical parameters, although organics have a place by sometimes being ambipolar, light emitting and potentially lower cost. Indium zinc oxide with up to $50\text{cm}^2/\text{Vs}$ mobility is the favoured formulation at developers Hewlett Packard (process licensed to two companies already), Oregon State University, Tokyo Institute of Technology, Toppan Printing, Cambridge University CAPE and various Portuguese and German institutions, such as the University of Karlsruhe for example. The more troublesome P types have now been produced so CMOS circuits are feasible.

Now add Samsung, which exhibited a printed oxide TFT array for an LCD display this year. The display was 4 inches, 100 pixels per inch (ppi) and the mobility achieved was $0.6\text{cm}^2/\text{Vs}$.

Lead Zirconate Titanate

Lead Zirconate Titanate PZT is the archetypal piezoelectric used for energy harvesting and sensors. Using sol-gel processes, it is now routinely printed to reduce cost and improve performance, work proceeding at Virginia Tech, Southampton University in the UK and elsewhere.

Printable Copper

In 2009, printable copper ink has been announced by NovaCentrix, Hitachi Chemical and others for antennas, interconnects, electrodes and other parts. It is argued that, in the form of the new inks, it does not have the traditional problem of an insulating oxide forming and it is not a biocide (when in nano form) subject to the severe price hikes suffered by silver.

New Silver Inks

Creative Materials's Medical Grade Electrically Conductive Ink is now used in a range of medical electrode applications, including ECG and TENS electrode applications, transdermal drug delivery, defibrillation and monitoring systems. These products feature excellent adhesion to a wide variety of surfaces, including polyester, polyimide and glass. With a high percentage silver filler, they are often used in defibrillator electrodes and to make disposable ECG electrodes.

Cima nanotech CEO Jon Brodd reports his company is sampling its flexible transparent conductive film made with silver nanoparticles in emulsion that self align into a connected netting-like pattern upon drying, rather like irregular chicken wire. The random openings allow 80% transparency, about the same as some ITO, while the silver lines reportedly provide sheet resistance of 5 ohms/square, as good as or better than ITO.

Sintering Metal Inks on Low-Cost Substrates

Novacentrix is introducing a scalable solution to processing high temperature semiconductor materials on low temperature substrates like paper and plastic, with a new generation Pulseforge tool with 10-20 times the power of the previous production models, which are aimed at drying or sintering metallic inks.

Carbon Nanotube – Graphene and CNT Nanocomposites

The Paper Battery Co first reported on its carbon-nanotube-based paper battery a couple of years ago. It has now closed an initial round of seed funding and targets a roll-to-roll printed supercapacitor by next year, having decided that this is the better route to market for these composites.

Instead of having to press together the usual electrode, electrolyte and separator layers needed for batteries and supercapacitors, and seal them in a can, the company has a process to make them all in one nanocomposite sheet of cellulose polymer matrix that binds together carbon nanotubes and other carbon materials for the electrodes, and also soaks up the ionic liquid electrolyte.

The resulting black paper-like sheets can be shaped into the skin of a device, or even wrapped in to the casing of a battery to extend its performance. Initial product target energy density is 10-20Wh/kg, for a launch next year.

Meanwhile UK start-up Nanotecture has announced that it will be sampling its supercabatteries that combine the electrochemistry of both supercapacitors and batteries. Some versions are less than one millimeter thick and they employ inorganic nanomaterials. The company refers to them as microbatteries, although it sees potential for replacing supercapacitors rather than batteries with this technology.

Researchers at UCLA have developed a new method for producing a hybrid graphene-carbon nanotube, or G-CNT, for potential use as a transparent conductor in

solar cells and consumer electronic devices. Indeed, the earlier invented flexible CNT-based conductor is now used to connect organic light-emitting diodes (OLEDs) with the organic transistors addressing each OLED pixel. With improved conductivity and stretchability, it is now possible to fold the display in half or even crumple it up without damage, and to stretch it up to 50% of the original shape.

Using a rubbery CNT-based conductor developed a few months ago, researchers at the University of Tokyo have now made a stretchable display. With the advantage of being printable, this brings us closer to cheap flexible and conformal displays.

Nano-Feature-Size Printing

The UK Government's leading funding agency for research and training in engineering and the physical sciences, the Engineering and Physical Sciences Research Council (EPSRC), has announced a new £6m, six-year program on nanostructured metal photonic metamaterials, to be established at the University of Southampton.

Metamaterials are artificial electromagnetic media with unusual and useful functionalities achieved by structuring on a sub-wavelength scale. They employ the finest printing, such as flexography and dip-pen nanolithography, because the feature size is less than the wavelength of light. They have this in common with the nanoantennas that are alternatives to photovoltaics and are being developed by Idaho National Laboratory. Ballistic diodes for the rectification side are being printed by Manchester University in the UK.

The aim of the Southampton metamaterials project is to develop a new generation of revolutionary switchable and active nanostructured photonic media, thus providing groundbreaking solutions for telecoms, energy, light generation, imaging, lithography, data storage, sensing, and security and defence applications. The project runs from July 2009 to the end of 2015. ■

Getting the Most Out of Your HIGH SPEED ADC

Derek Redmayne, Applications Engineer, and **Alison Steer**, Product Marketing Manager, both at Linear Technology's Mixed Signal Product group, look at practical ways of achieving full performance from an analogue-to-digital converter

This is a two-part article, continuing in the next issue

ACHIEVING FULL performance from an analogue-to-digital converter (ADC) with 100dB SFDR, GHz input bandwidth and SNR in the neighbourhood of 80dB can be a challenge. Board level designers need to be equipped with an intimate understanding of the clock and sampling mechanism.

This two-part article looks at the most common ways in which the ADC performance can be compromised. There are a number of issues that we see reoccur and which can render a design unusable:

- Believing the term "low jitter".
- Thinking the clock is a digital signal.
- Thinking that differential signalling provides noise margin.
- Copying the demo board.
- Squaring up the clock signal.
- Not thinking about GHz frequencies when designing for baseband.
- Isolating analogue and digital ground planes.

Not all of these are necessarily always bad but each requires careful consideration. Please follow the following words of caution to avoid the same traps of your predecessors.

Caution 1: Believing the Term "Low Jitter"

Many clock sources, synthesizers, repeaters, zero delay buffers and so on are designed for high speed serial communications, not sampling. Although datasheets for these devices may mention the term "low jitter", the term is relative. For de-serialization, low jitter may be 30-50ps. For a DLL in an FPGA to maintain lock 30-50ps is on the order of what is required. However, for IF undersampling, with high dynamic range ADCs, low jitter means somewhere below 1ps (see **Figure 1**).

The encode clock of a high performance ADC is much like the local oscillator of a radio receiver. As in radio, noise, in the form of phase noise and thermal noise in the clock, will limit the sensitivity of the ADC if there is a strong signal present.

Much like the mixer in a super-heterodyne radio, the ADC mixes the clock with the analogue input. Indeed, this similarity in behaviour extends to producing mixing products on the input port, again like the LO RF feed-through of a true mixer. In the case of the highest speed ADCs, those with high input bandwidth and the highest performance, like Linear's 16-bit, 185Msps LTC2209 family,

there are mixing products that extend out to GHz frequencies. This issue will be discussed in further detail in Part 2 of this article.

In fact, the sensitivity of the ADC to jitter, or phase noise is greater than that of a mixer as the bandwidth of the subsequent outputs is greater. In the case of the ADC, the output bandwidth is really not limited, even though it all folds down into a band from DC to half the sample frequency ($f_s/2$).

In the case of a mixer as used in radio design, the output of the mixer is typically band limited by a filter, generally selecting only the difference frequencies of interest; not the sum and difference products of the input, nor all the harmonics of the clock bandwidth extending out to approximately 1GHz on the analogue input and 2-3GHz on the clock. In addition, most radio design

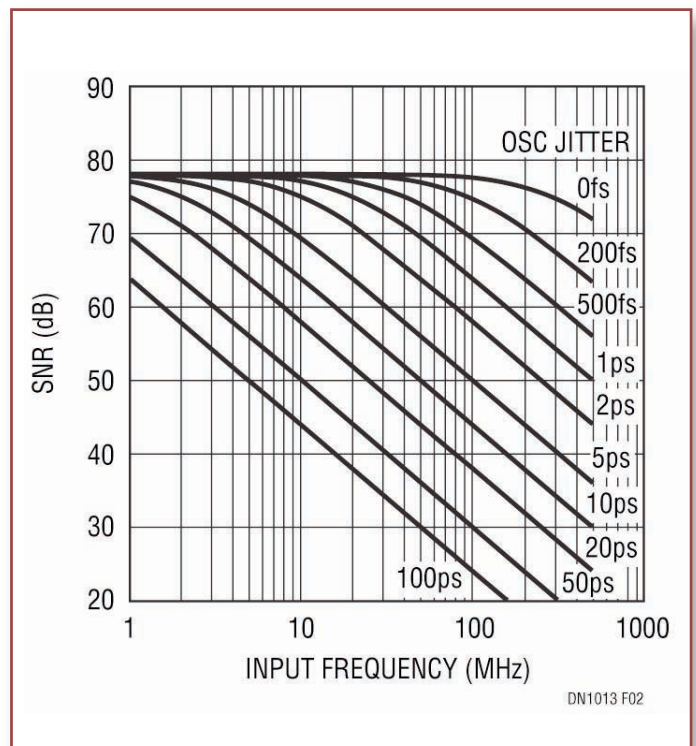


Figure 1: Jitter degradation of SNR as a function of input frequency



does not involve undersampling, except in the case of harmonic mixers; and undersampling, often used with ADCs, exaggerates the effect of jitter by $10\log_{10}(f_{in}/f_s)$.

To relate this back to radio design, this is the reason that the super-heterodyne is generally chosen in receiver design, as the LO being higher than the RF mitigates the effect of jitter.

The term "low jitter" has become meaningless and should not be taken at face value. There are a considerable number of clock generator devices on the market that range from rather poor monolithic devices with internal VCOs, loop filters and poorly grounded packaging, to fairly expensive multi-loop modules with either external VCOs or VCXOs.

We do not want to endorse or condemn clock generator products from other manufacturers, but must warn that you have to evaluate these early in your design process and that this may be the greatest value in getting a demoboard for the ADC, as it (and a facsimile of your signalling) is the best way to evaluate the effect of potential clock sources. We see a great deal of effort spent, trying to confirm the datasheet performance of an ADC, when the usual outcome, after coming face to face with the limitations of signal generators, is that yes, the parts do perform as specified.

All lab bench generators require filters to produce data sheet SNR, or SFDR. Some PCB mount clock generators may have specs that at first glance may seem attractive, but may have jitter integrated over a frequency range that opportunistically avoids spurs produced by the architecture and which may be difficult to eliminate. The common 12kHz to 20MHz integration for jitter may be meaningless if there is a 25MHz spur just outside those limits. Note that single chip clock generators are likely to be poor unless they use a very high frequency internal VCO at more than just a few GHz.

Caution 2: Thinking the Clock Is a Digital Signal

Now, assuming that a low phase noise oscillator or synthesizer of some type is adopted and incorporated into the system, effort must then be expended to ensure that this is preserved until it reaches the ADC. There are many ways in which a clean clock source can subsequently be compromised. The most popular are:

- Passing the clock through an FPGA.
- Routing through an internal layer of the PCB alongside digital data lines.

- Routing across a back plane.
- Routing through clock fan-out devices that have features such as zero delay, programmable skew etc.

These could all be lumped under the banner of considering the encode clock to be a digital signal.

Even relatively good clock management devices intended for ADC use can be made marginal by compromises in layout in their immediate surroundings; ignoring the effects of lead inductance, trace inductance, via inductance in bypass, poor or absent isolation barriers between neighbouring traces in the layout.

If you route a clock output from a device equipped with programmable dividers alongside an output at a different frequency than that intended for the ADC, you will see some manifestation of the other clock frequency. For example, routing lines producing $\frac{1}{2} f_s$ right next to the encode clock will produce image frequencies mirrored around $\frac{1}{2}$ Nyquist. This is due to phase modulation of the clock that produces aliasing of products as if they were sampled at $\frac{1}{2} f_s$. The unwanted images may be 70dB down from the originator, but that can be a show stopper in many applications. What works for OFDM or WCDMA, both fairly tolerant of images and jitter, will not necessarily work for general purpose software defined radio.

Many clock management devices will have some limits in terms of the isolation that they can maintain between outputs. Make sure that you test with all outputs enabled, at different frequencies if that is an eventuality, and make sure that any digital signals, such as other optional ADCs are active. Testing a multiple ADC design, without all the ADCs operational is a big mistake.

The performance of clock management devices can be made worse by introducing heavy loading, creating asymmetry in the loading, and reflections from loads, and of course routing lines alongside each other. Not following recommendations in placement of bypass, placement of ground vias can have a very negative effect. Routing clock lines, even at the same frequency, alongside each other is not recommended. We have seen cases where serpentine routing has placed these in close proximity at different points in time, and this can cause waveform distortion.

One last note: digital signals are often daisy chained. Do not do this with encode clocks; the earlier devices will see a compromised edge, often producing a dwell in the threshold region.

Caution 3: Thinking That Differential Signalling Provides Noise Margin

On the subject of routing clock lines, even differential signalling such as PECL or CML will couple into neighbours if they are too close. If you have had, or are having problems along these lines, there are experiments that can be performed on your board to determine how effectively neighbouring lines are isolated from each other.

Take a bare board and a network analyzer, and introduce the stimulus into one line that is in close proximity to your clock line; examine S12, or the power transferred into your clock line, sensed at the ADC. You may need to use a high frequency Guanella type balun such as the M/A-COM ETC1-1-13 to translate the single ended stimulus to differential and back again for the analyzer, emulating the differential input of the ADC. You will need to add source and end termination to your board on those traces involved, or partially populate and power select devices to get realistic measurements. If you have intervening traces, or neighbouring traces, they may need to be terminated in realistic fashion to get an accurate reading of how much crosstalk you will see.

One of the pitfalls we have observed is the use of signal integrity software that gives yes and no answers and is intended to be used to predict crosstalk in digital signalling, being used to validate the clock layout.

The encode clock of an ADC has no noise margin. The acceptable amount of crosstalk into the clock from digital lines carrying 3V logic is in the neighbourhood of -100dB or more.

If you make the mistake of thinking of the encode clock as a digital signal and run it alongside the data bus, you will allow digital feedback to phase modulate the clock. One line running at minimal separation from another, with power passing in opposite directions is very much how a directional coupler is constructed.

The fact that one of these lines is part of a differential pair has little impact on the signal that is induced in the nearest member of the pair. If sandwiched between closely spaced ground planes, the rejection of near channel interference may be less than 30dB. The nearer member will have a stronger signal induced, so rejection is minimal. If the clock source were located close to the FPGA (and this is not recommended), the clock line should be isolated from any digital lines, even those with low repetition rates by a layer of solid copper, or at least an uninterrupted line of vias between grounded copper, above and below the clock. This should be regarded as a coaxial cable buried in the board. Similar issues will be found on the surface.

One feature that we often see in clock distribution is some attention to signals in the same layer, but an apparent lack of diligence in ensuring that there is nothing offensive in those layers above and below the clock lines. This seems like stating the obvious, but it occurs very frequently that it must be a kind of blind spot in common CAD practices.

There must be no lines paralleling the clock lines in layers above or below the clock lines; this also means power planes. Making a sandwich of power planes, ground planes and clock lines can be

an expensive mistake. There is some conventional wisdom that causes some grief with clock distribution. A large collection of lines that cross perpendicular in an adjacent layer, common in digital signalling, can still electro-statically couple into the clock line. If the clock lines are differential, this would be a common mode signal, but there are limitations to common mode rejection in a clock receiver. It is unrealistic to expect more than about 30-40dB common mode rejection at high frequency, and that can be further compromised by asymmetry in the clock path to the ADC.

If a clock originates at some distance from the ADC, the odds of picking up digital noise en route to the ADC increases dramatically. If a single ADC, or a small group of ADCs, is involved in a design, the clock source should be located as close as possible to the ADC. Of course this should be done without compromising the layout of either the ADC, or the clock synthesizer, or compromising thermal design. If however, there is a master clock at the encode rate, that is centrally located and must be distributed to multiple boards, you must consider either a filter where that clock is received from the back plane or via a coaxial connector, or you must use a jitter cleaner PLL.

A jitter cleaner is effectively a very narrow band filter. It cannot improve the jitter within the loop BW, but will reject wideband noise and distant spurs. The bandwidth of the PLL as a filter is essentially 2x the bandwidth of the loop filter. If the passage of a clock through a backplane only acquires far-out-of-band interferers, it may be practical to filter it with an LC filter before it is presented to the ADC or to any kind of clock fan-out device.

The use of a low-pass filter to filter out noise acquired when passing through an area of digital circuitry may be unwise, as low repetition rates or low frequency content in a digital data bus may get into the clock trace. A band-pass filter is better in this case. A frequent justification for routing the clock among digital signals is that they are low repetition rate or static. If these originate in an FPGA, DSP or microcontroller, there will be problematic noise present. Any low rate signal that passes through RF or clock generation circuitry should be band limited and low pass filtered. ■

FURTHER READING

Further information on Linear's High Speed ADC portfolio can be found at <http://www.linear.com/ad/highspeedADC.jsp>, which includes the new 1.8V lowest power, LTC2261 ADC family that consumes just 127mW at 125Msps.

Linear offers complete ADC evaluation systems comprised of clock source, signal source and ADC demo boards for use with the free Quick-Eval software tool. These systems are available through local Linear sales representatives.

SUBSCRIBE TO ELECTRONICS WORLD

AND SAVE

13%

...AND receive a **FREE** one year subscription to the digital publication – delivered to your inbox (**WORTH £36.50**)

One year subscription for only **£40 (UK)** and **£60 (Overseas)**

- **FREE DELIVERY** to your door
- **SAVE 19%** on the Shop Price
- **NEVER MISS** an Issue
- Solutions & Case studies for the professional engineer
- Fresh ideas, tips and tricks
- Analysis of what's coming next in technology
- Features on a wide range of markets from automotive to medical
- In-depth technical articles
- International coverage around the globe

CALL OUR HOTLINE:

UK: 0870 428 1426

International: +44 1635 879361

SUBSCRIBE ONLINE:

www.electronicsworld.co.uk



Jin Tao, Jia Hongzhi and Hou Wenmei from the University of Shanghai, **Yamamoto Ryo, Nagai Norihiro, Fujii Yusaku, Maru Koichi and Ohta Naoya** from Gunma University in Japan, and **Shimada Kazuhito** from the Japan Aerospace Exploration Agency (JAXA) in Houston, the US, present this study on an extraction method of a circle outline and its centre in a moving dummy mass with a view to develop a 3D system for parabolic flights in space R&D programmes

Extracting a Circle and its Centre in a MOVING DUMMY MASS

A METHOD OF extraction of a circle outline and its centre in a moving object in zero gravity is presented in this article. The final goal of the study is to develop a 3D position-and-attitude (rotation) estimation system using CCD cameras for use in parabolic flight experiments, which are of benefit to the space research-and-programme development projects.

To extract the characteristics of a moving object is one of the key techniques for computer vision in the application of movement detection, vision measurement, 3D reconstruction etc. To detect a circle is important and in demand because of its high frequency appearance in the natural world.

Circle detection methods include statistics based on the least square, linear solution, Hough Transform etc. The Hough Transform, firstly proposed by Hough in 1962, was applied extensively due to its effective identification of different shapes, including circles. It offers the following advantages in identifying circles:

- It can eliminate the noise in the image, as it is not sensitive to it;
- It can detect even discontinuous circles, as it does not account for the points of distribution on the circle.

However, its disadvantages include:

- The number of calculations is large;
- It needs large memory;

The extraction parameters are limited by quantized intervals in the parameter space.

Randomized Hough Transform (RHT), firstly proposed by Xu et al, uses three random non-collinear points in an image space to map the parameter space. This can decrease the number of performed calculations and does not require large memory. RHT is effective for simple backgrounds, but it will detect many false circles in complex backgrounds.

Zero Gravity Experimentation

In this article, the circle outline of a moving object and its centre, under a zero-gravity condition, was extracted by a combination of moving track estimations, RHT and grey value accumulation.

The zero gravity experiment was conducted by a parabolic flight using a jet airplane. The experiment was for evaluating the efficiency of a prototype of the astronaut's mass measuring device called "Space Scale" for use in the International Space Station (ISS). In the experiment, a dummy mass is used and its mass evaluated using the prototype of the Space Scale.

In order to increase the detection efficiency, the track of the moving dummy mass in the video stream was firstly estimated by a combination of background subtraction and a consecutive-frame-difference algorithm. This



Figure 1: One of a frame in a video stream. Pointed by the white arrow is the object circle

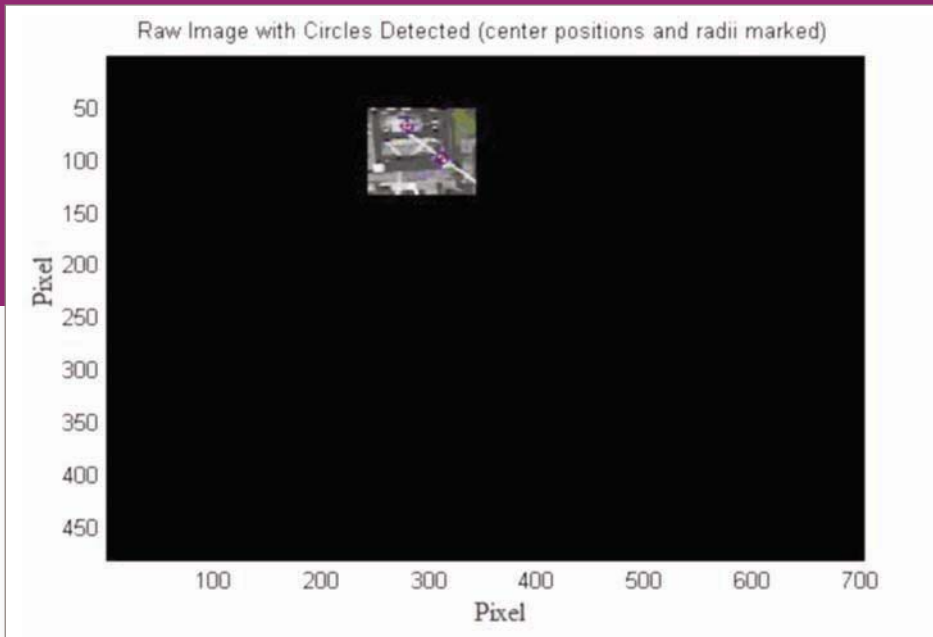


Figure 2: Detected result for one frame

algorithm is simple and can track the changing information in the video stream very effectively.

The search range and the step of the RHT can be decreased by estimating the detection area according to the parameter of moving track estimation. Then the grey values are added together (because the circle we want to detect is white, in order to distinguish the object and the other circles, the grey values of the pixels in the circle are accumulated). The circle can then be determined by the total of the grey values. The results show that the method discussed here can 'extract' the object circle in the moving dummy mass rather effectively.

Movement Estimation

Movement estimation refers to detecting the moving object in a video stream, based on any one of these methods: optical flow, frame difference, invariable characteristic matrix detection and so on.

In this case we used the frame difference method to estimate the moving track. It includes background difference and consecutive frame difference. Background difference subtracts a fixed reference frame from the other frames in the video stream. Consecutive frame difference subtracts the current frame from the next frame. The deciding condition of the moving detection is as follows:

$$I_d = |I_c - I_r| \quad (1)$$

Here, I_d is the output image after frame

difference, I_c is the subtrahend frame and I_r is the reference frame. For the background difference, I_c is the other frame and I_r is the background frame. For the consecutive frame difference, I_c is the frame to be detected and I_r is the current frame.

If (x_i, y_i) and (x_i, y_i) are the pixel position of the image frame I_c and image frame I_r respectively, then the movement relationship between these two image frames is as follows:

$$x'_i = f_1(W, x_i, y_i) \quad (2)$$

$$y'_i = f_2(W, x_i, y_i) \quad (3)$$

Here, W is the parameter set of the movement, f_1 and f_2 are the parameter set expressions and i is the corresponding subscript. Then the brightness residual error set W can be expressed as :

$$W = \arg \min \sum_{(x_i, y_i)} (I_c(x_i, y_i) - I_r(x'_i, y'_i))^2 \quad (4)$$

Here $I_c(x_i, y_i)$ represents the grey value of corresponding point in the subtrahend frame (I_c) and $I_r(x_i, y_i)$ represents the grey value of corresponding point the reference frame (I_r).

Randomized Hough Transform (RHT)

RHT calculates the circle parameter by three random non-collinear points in the image. This can decrease the occupancy rate of the memory.

The basic algorithm thought is to firstly use the edge function in Matlab to extract all the borderlines in the image and set them as M . The candidate circle parameter P can be calculated from the random three non-collinear points in M . By accumulating the number of the points N in the boundary set D , which satisfied the candidate circle parameter P , the candidate circle is a true circle if N is larger than the number of points that must be required from a circle. Then all points in this circle will be deleted from the boundary set D .

The next circle will be detected when the number of points meets the next circle requirement. The maximum detection time for the number of circles detected is set as K , in order to prevent the algorithm running continuously.

The specific steps of this algorithm are as follows:

1. Construct the set of border points M , initialize sample number $k = 0$.
2. Randomly select three points from M .
3. Calculate the circle parameter P according to these three points. If the solution can be found, go to step 4; otherwise go to step 5.
4. If the number of points N on the candidate circle whose parameter is P are larger than N_{min} , go to step 6, otherwise the circle is false, go to step 5.
5. $k = k + 1$, if $k > K$, go to end; otherwise go to step 2.
6. Detect the true circle whose parameter is P , then judge whether the number of detected circles is equal to the expected number, of how many circles need to be detected. If it is equal, go to end; otherwise

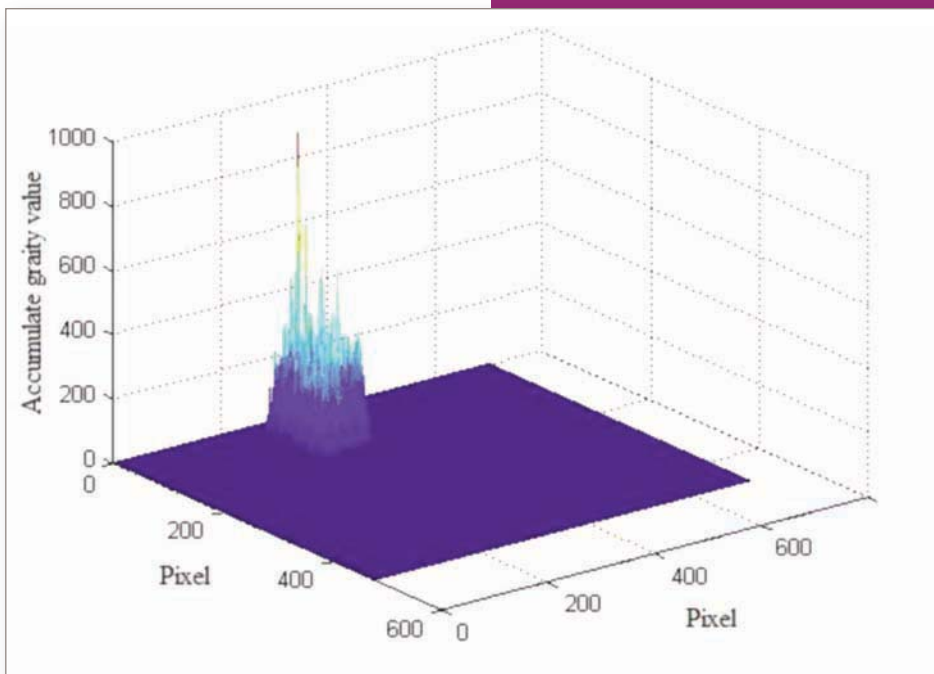


Figure 3: Grey value accumulation results for the circle detected in Figure 2

delete all the points on the circle whose parameter is P from M , reset $k = 0$, go to step 2.

The Algorithm

Based on RHT, a movement estimation can reduce the detection range greatly. This is effective in detecting the circle in movement.

The movement to be detected lasts only a few seconds, but the brightness changes dramatically.

Although the background difference can show the movement information overall, it is very easy to make a wrong decision due to its weak anti-interference ability. In consecutive frame differences it is very hard to catch small changes.

In this paper, the combination of these two methods is used to extract the movement information. The steps of detection are as follows:

1. Extract the first frame as the background frame 1.
2. Subtract the background frame from the next five frames, and then add the total magnitude of change W . If W is larger than the threshold T setting beforehand, the consecutive frame difference should be used to detect the movement, as the movement during this period is rather obvious. Set the last frame as the new background frame and then on to detect the next five frames. The threshold value T was of empirical value here.
3. If W is smaller than T , the movement change is very small during this period. A background frame difference should be

used to detect the movement. Set the last frame as the new background frame and then detect the next five frames.

4. Repeat steps 2 and 3 until all frames are detected.

Renewing the background frame can improve the detection effect of the consecutive frame difference and reduce the noise for the next image fragment. Extracting the movement information and estimating the moving track in the video stream by movement estimation can decrease the difficulty of extracting the feature point in the image greatly.

Realization of RHT

The detection range of RHT decreased greatly after movement estimation. Because of the complex background, there were also many invalid circles in the detection range. Because the circle we want to detect is white, in order to distinguish the object circle from the other detected circles, by accumulating the grey value of all points in the circle, the circle with maximum grey value was selected as the object circle according to our experimental condition. Then the centre pixel coordinates of the object circle can be obtained.

The parameter of movement estimation was used to determine the suitable range of object area in the next frame. The method mentioned above was used to detect the centre pixel coordinate of the object circle in the next frame until all frames (I_{\max}) were detected. The algorithm realization is as follows:

1. Calculate the image position of the object area in the present frame i .
2. Construct the set of edge points M , initialize the sample number $k = 0$.
3. Select three points d_1, d_2, d_3 from M randomly.
4. Calculate the circle parameter determined by these three points. If the solution exists, go to step 5, otherwise go to step 6.
5. If the number of the points N on the circle with the parameter P is larger than N_{\min} setting beforehand, go to step 7; otherwise the circle is a false circle, go to step 6.
6. Set $k = k + 1$, if k is bigger than K setting before, the present frame detection finishes, go to step 1 and set $K = 0$; otherwise go to step 3.
7. Accumulate the grey value of the pixels in the detected circle with parameter P as G_i . Judge whether the number of the detected circles reaches the expected number. If yes, go to end; otherwise delete all the points on the circle with parameter P from M .
8. Calculate the centre of the true circle. Reset $k = k + 1$, go to step 3.
9. If $I > I_{\max}$, count the circle centre track where G_i is maximum in each frame.

Experimental Results

The zero gravity experiment was conducted by the parabolic flight using a jet airplane for evaluating the efficiency of the prototype of the "Space Scale". Each experiment run was completed during 0-G state about 20 seconds long. Before a measurement run, an experimenter holds the test object on the holding stage manually. The rubber cord was extended from its natural length to its extended length before the experimenter releases the object.

The signs to be detected in our experiment are the circles on the back of a moving dummy mass under microgravity. Two CCD cameras were used to collect the video stream. The controller of the CCD cameras is CC421 and the lenses of CCD cameras are T1675F, both manufactured by Elmo.

The cameras are set to shutter speed (auto),

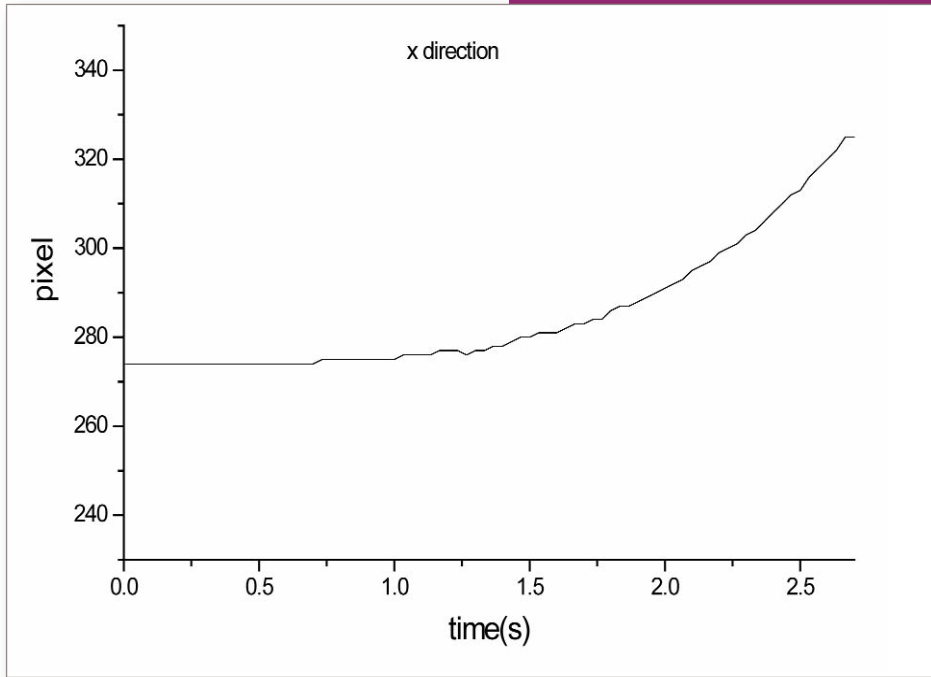


Figure 4: The orientation moving tracks of the object circle centre in the whole video stream

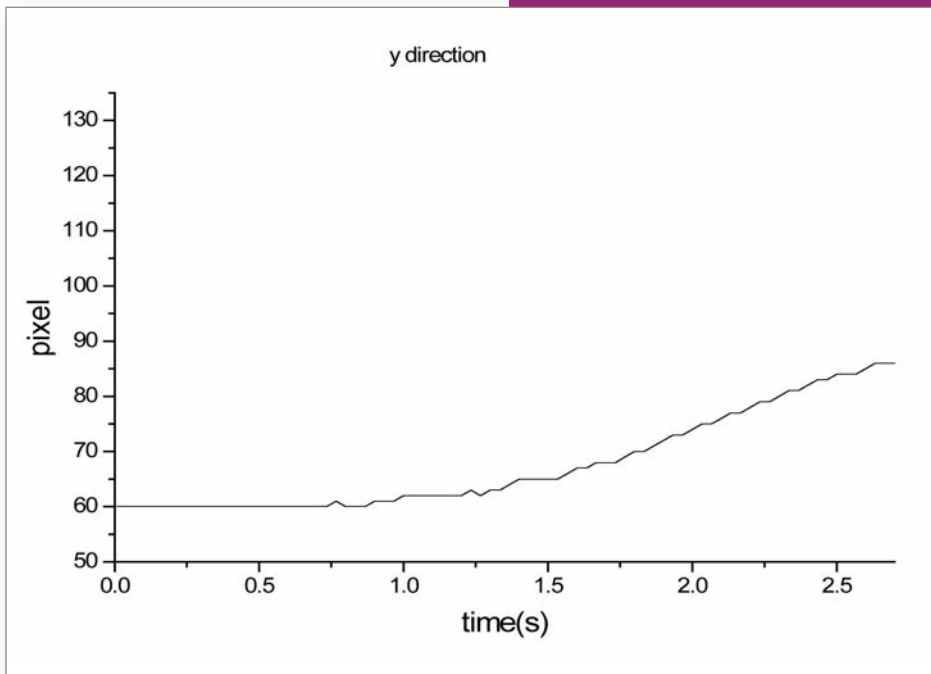


Figure 5: The longitudinal moving tracks of the object circle centre in the whole video stream

auto-gain (off), white balance (auto). **Figure 1** is a frame in the video stream.

As we were only interested in the dummy mass movement, a small area containing the whole dummy mass was extracted in the image. The white circle was the object circle we want to detect. **Figure 2** is the detection results. From there we can see that the detection area decreased greatly by movement estimation. This reduced the interference for the next RHT. But we can also find many false circles.

Because the circle we want to detect is white, in order to distinguish the object and

the other circles, the grey values of the pixels in the circle were accumulated, as shown in **Figure 3**. From Figure 3, we can see that the circle with the maximum grey value is the object circle. Then we can calculate the pixel coordinates of this circle's centre.

Figure 4 is the transverse moving tracks of the object circle centre in the whole video stream. **Figure 5** is the longitudinal moving tracks of the object circle centre in the whole video stream. These two figures showed the object circle movement in the video. In the experiment, the velocity of the dummy mass gradually increased because the dummy mass

was tensioned by a rubber cord. The results shown in Figures 4 and 5 agree with this actual behaviour of the dummy mass.

An Effective Method

The method discussed in this article detected the moving track of an object circle in the moving dummy mass effectively. Estimating the moving track of the dummy mass reduced the object area for RHT and reduced the probability of false and ineffective circles. This improved the efficiency of the RHT algorithm.

By adding all the grey values, the object circle can be identified effectively. The experimental results showed that the method mentioned in this article could obtain the moving track of the dummy mass in the video.

The weakness of this method is that it cannot perform the detection in real time.

The parabolic flight experiment was conducted as part of the "Ground-based Research Announcement for Space Utilization" promoted by the Japan Space Forum (JSF) with the cooperation of Diamond Air Service, Inc (DAS). This work was supported by the Innovation Fund Project For Graduate Student of Shanghai (JWCXSL0902) and partly supported by the Shanghai Leading Academic Discipline Project and a program the from Shanghai Committee of Science & Technology. ■

COBE and WMAP: Signal Analysis by Fact or Fiction?

Stephen J. Crothers goes in depth of the experiments, results and pitfalls of COBE and WMAP

PIERRE-MARIE ROBITAILLE, a Professor of Radiology at Ohio State University, is an expert when it comes to instrumentation and signal analysis. It was Robitaille who conceived and directed the construction of the world's first 8 Tesla Magnetic Resonance Imaging (MRI) scanner. In doing so, he nearly doubled the maximum field strength in MRI and gave birth to Ultra High Field Magnetic Resonance Imaging (UHfMRI).

Robitaille's scanner immediately revealed anatomical structures within the human brain that were previously never seen on human scans. In recent years, Robitaille has applied his skills to astrophysics and his findings are very significant.

Great Triumphs?

COBE (The Cosmic Background Explorer, also referred to as Explorer 66, a satellite dedicated to cosmology) and WMAP (The Wilkinson Microwave Anisotropy Probe, also known as the Microwave Anisotropy Probe [MAP] and Explorer 80, is a spacecraft which measures Cosmic Microwave Background Radiation) have been hailed by the astrophysical scientists as great triumphs in science, measuring the temperature of the Universe, the ~ 3K Cosmic Microwave Background (CMB) remnant of the Big Bang; a signal first detected by Penzias and Wilson from the ground, in 1965. Stephen Hawking has dubbed this "the scientific discovery of the century, if not of all time".

However, upon closer examination, the claim does not stand up; in fact, it has no valid basis in science, as Robitaille has revealed. According to Robitaille, COBE and WMAP have produced almost nothing of any scientific value. Moreover, Robitaille concludes that the CMB is not cosmic, but a signal produced by the oceans of the Earth: "Throughout the detection history of the microwave background, it remained puzzling that the Earth itself never provided interference with the measurements. Water, after all, acts as a powerful absorber of microwave radiation. This is well understood, both at sea aboard submarines, and at home within microwave ovens". "...If the Earth's oceans cannot interfere with these measurements, it is precisely because they are the primary source of the signal."

The COBE and WMAP teams model the Earth as a blackbody source of emission at ~ 280K. But Robitaille points out that "since the oceans are not enclosed" they do not satisfy the requirements for application of Kirchhoff's Law of thermal emission, and so the emission profiles of the oceans "do not necessarily correspond to their true temperatures". By means of scattering in steady-state conditions,

Robitaille argues: "Consequently, a mechanism for creating isotropy from an anisotropic ocean signal is indeed present for the oceanic ~ 3K Earth Microwave Background".

Misapplication of Kirchhoff's Law of thermal emission is far from the only major problem with both COBE and WMAP. Robitaille has shown that both projects are plagued by very serious problems with the performance of satellite onboard instruments and methods of signal processing. Aboard COBE is the Far Infrared Absolute Spectrophotometer (FIRAS) (Figure 1), operating from ~ 30 to ~ 3,000GHz.

"FIRAS was designed to function as a differential radiometer, wherein the sky signal could be nulled by the reference horn 1cal". Signal from the sky horn is compared to a signal provided by the reference horn. The FIRAS team reported a null point at 2.759K, which is 34mK above the reported sky temperature, $2.725 \pm 0.001K$.

Null should ideally occur at the sky temperature. Owing to 18mK error in the thermometers, ~ 3mK temperature drift, 5mK error in the sky horn Xcal and 4mK error in 1cal, Robitaille determines an overall error bar of ~ 64mK in the microwave background. Yet the

Figure 1: Salient components of FIRAS: Sky horn, reference horn, 1cal (2 thermometers) and Xcal (3 thermometers) (1cal = Internal calibrator, Xcal = External calibrator)

[Courtesy of NASA and the COBE Science Working Group. Reproduced by permission of the AAS]

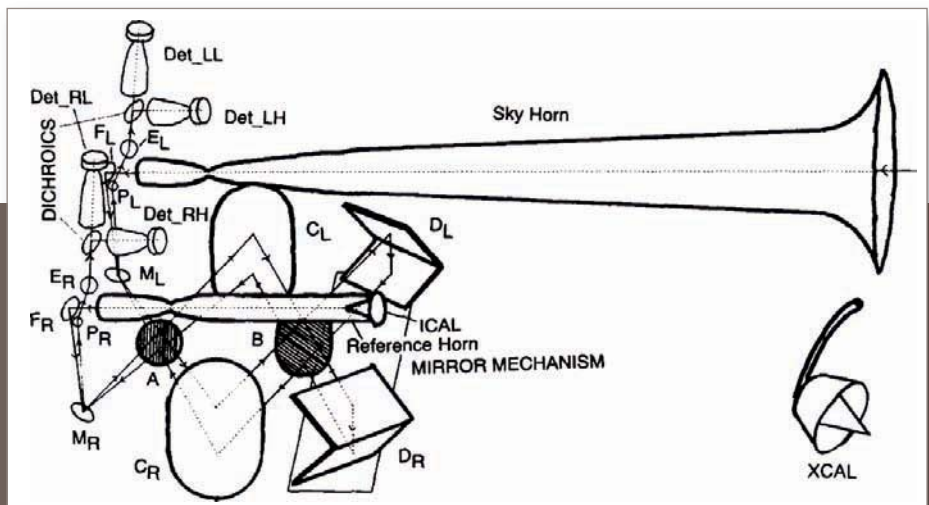
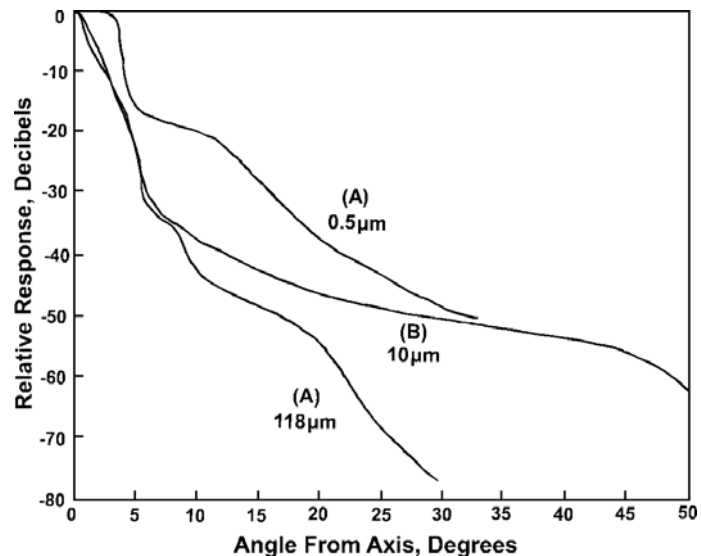


Figure 2: Side-lobe response of FIRAS horn without the RF shield.

Mather J.C., Toral M., Hemmati H., Heat trap with flare as multipole antenna, *Appl. Optics*, 1986 v. 25(16), 2826-2830. [Reproduced from with permission of *Appl. Optics*]



FIRAS team reports only ~ 1mK. Errors were evidently dumped into the calibration files. And as Robitaille observes: "a 1mK error does not properly reflect the experimental state of the spectrometer". The FIRAS team's calibration procedures produced calculated Ical emissivities great than 1.3 at the higher frequencies; but the theoretical maximum for emissivity is 1.

In their initial reports the FIRAS team included data for the frequency range 30 to 60GHz, but these frequencies disappeared from later reports. According to Robitaille, diffraction of atmospheric photons over the FIRAS shield, which the FIRAS team never adequately tested on the ground, would increase microwave power at lower frequencies, and comparatively reduce microwave power at higher frequencies; bearing in mind that the frequencies of interest for the microwave background are < 600GHz.

Misgivings were expressed by a member of the FIRAS team: "Dave Wilkinson, the FIRAS team sceptic, argued effectively at numerous meetings that he did not believe that Ned" (Wright) "and Al" (Kogurt) "had proven that every systematic error in the data was negligible. Dave's worry was that emissions from the earth might be shining over and around the spacecraft's protective shield". Even so, Wilkinson never contemplated that the entire ~ 3K signal has its origin in the oceans.

Validity of Tests

On the balance of the evidence pre-flight testing of COBE's instruments was seriously compromised. Owing to the Challenger disaster, COBE could not be launched by space shuttle and so the satellite underwent a major late stage redesign. John Mather, a principle investigator on FIRAS, reported: "Every pound was crucial as the engineers struggled to cut the spacecraft's weight from 10,594 pounds to at most 5,025 pounds and its launch diameter from 15 feet to 8 feet. Getting COBE into orbit

was now Goddard's No.1 priority and one of NASA's top priorities in the absence of shuttle flights. In early 1987 NASA administrator Jim Fletcher visited Goddard and looked over the COBE hardware, then issued a press release stating that COBE was the centerpiece of the agency's recovery".

The FIRAS team did not examine "the interaction of the COBE shield with the FIRAS horn"; and the effects of earthshine were not "measured in preflight tests, only estimated from crude (by today's standards) calculations". Nor did the team conduct sufficient tests of FIRAS in the flight dewar, and testing of the assembled instrument was curtailed. No RF tests have been reported for side-lobe performance, sensitivity or diffraction on the ground for the fully assembled instrument. Some side-lobe testing was conducted on FIRAS whilst on the ground, at 118μm, 10μm and 0.5μm, but without its RF shield (Figure 2). Some frequencies below 100GHz were tested. However, only the 118μm in Figure 2 "is within the usable bandwidth of the instrument". But without the shield, this data is of little relevance.

Since the FIRAS team had little useful side-lobe performance data, they attempted to obtain it in flight, using the Moon assumed as a lambertian emitter at 1,500GHz (Figure 3). From this, Fixen et al. concluded a maximum side-lobe response of "less -38dB beyond 15° from the center of the beam" at 1,500GHz. But the FIRAS team then compared this with data at ~ 90GHz obtained on the ground without the RF shield. Furthermore, in-flight data for the lower frequencies where diffraction effects would be strongest are not reported, and no ground data seems to have been obtained at 1,500GHz, with or without the RF shield in place.

Over a period of 13 years the FIRAS team reported a reduction of error in the measured temperature of the microwave background, by almost two orders of magnitude, despite the existence of significant systematic errors (Table 1).

Concerning the blackbody spectrum, Fixen and Mather remark: "It is sometimes stated that this is the most perfect blackbody spectrum ever measured, but the measurement is actually the difference between the sky and the calibrator." Robitaille expresses the relationship thus:

$$(Sky - Ical) - (Xcal - Ical) = (Sky - Xcal)$$

Obtaining Nulls

It is clear from this that the effects of Ical and instrumental factors should be negligible: but that is not what the FIRAS team found. It is also clear that if Xcal matches the sky a null will result. Xcal is assumed an ideal blackbody spectrum and so the sky would also be an ideal blackbody spectrum in the event of a null.

The FIRAS team assumed from the outset that the sky is as an ideal blackbody. Note that if the calibration obtained with Xcal in place is dominated by leakage of sky signal into the horn, then a perfect blackbody spectrum would result because the sky would then be compared with itself. Robitaille has shown that it is most likely that there is significant sky leakage into the horn during calibration with Xcal.

Robitaille relates most significantly that, in actual fact, FIRAS was unable to obtain proper nulls, despite the FIRAS team's reports that they obtained "the most perfect blackbody spectrum ever measured". Unable to obtain a proper null, the FIRAS team blames instrument problems and the calibrations, but never entertains the possibility that the sky, owing to diffraction over the RF shield of emissions

REFERENCE	TEMPERATURE	ERROR (MK)*	FREQUENCY (CM-1)
Mather et al., ApJ, 1990, v.354, L37-40	2.735§	±60	1-20#
Mather et al., ApJ, 1994, v.420, 439 -444	2.726§	±10	2-20#
Fixen et al., ApJ, 1996, v.473, 576 -587	2.730§	±1	2-21t
Fixen et al., ApJ, 1996, v.473, 576 -587	2.725¶	±0.09	2-21t
Fixen et al., ApJ, 1996, v.473, 576-587	2.717¥	±7	2-21t
Fixen et al., ApJ, 1996, v.473, 576 -587	2.728**	±4	2-21t
Mather et al., ApJ, 1999, v.512, 511-520	2.725§	±5	2-20‡
Mather et al., ApJ, 1999, v.512, 511-520	2.725¶	±0.085	2-21t
Mather et al., ApJ, 1999, v.512, 511-520	2.722¥	±12	2-20‡
Mather et al., ApJ, 1999, v.512, 511-520	2.725**	±2	2-20‡
Fixen & Mather, ApJ, 2002, v.581, 817-822	2.725	±0.65	2-20‡
Fixen & Mather, ApJ, 2002, v.581, 817-822	2.725	±1	2-20‡

* 95% confidence intervals

§ Measurement using FIRAS microwave background lineshape. Calibration sensitive to the thermometers of the external calibrator, Xcal.

¶ Measurement using FIRAS microwave frequency. Calibration relies on CO and C+ lines at 7.69, 11.53, 15.38, and 16.42 cm⁻¹.

¥ Measurement using a fit of the dipole spectrum to the 1st derivative of a Planck function describing the microwave background with T_{cmb} set to 2.728 K.

** Composite value obtained from analysis of three previous entries.

Frequency range used is formally stated.

t Frequency range used is not formally stated but appears to be 2-21cm⁻¹.

‡ Frequency range used is not formally stated but appears to be 2-20cm⁻¹.

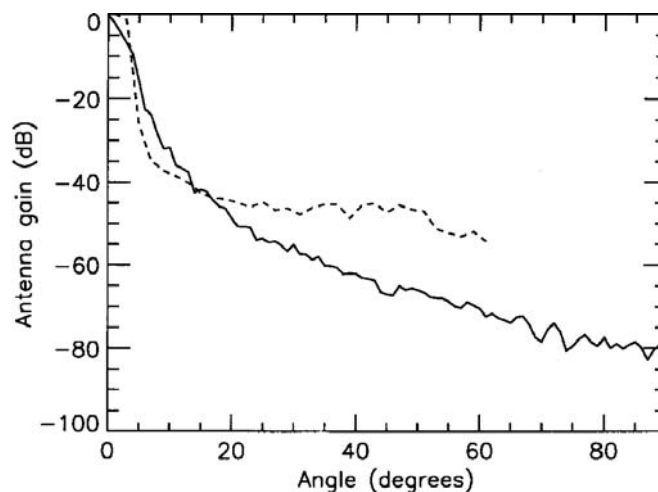
Table 1: Microwave background temperatures obtained by the COBE FIRAS team

[Courtesy of Pierre-Marie Robitaille and Progress in Physics]

originating from the Earth, is not behaving as a blackbody as they assume.

The FIRAS team published interferograms for a final temperature of $2.725 \pm 0.001\text{K}$ with lcal set at 2.759K. The published interferograms consists of three traces (**Figure 4**). The top and bottom traces are not drawn to the same vertical scale as the middle trace: "A correction factor of 3-5 should be applied to place the upper and lower interferograms on scale with the center one". Furthermore, noise power analysis with this data reveals that "the FIRAS team is not maintaining a constant vertical amplification". In order to attempt to account for the data, the FIRAS team applies, ad hoc, a 4% reflectance to lcal.

Figure 3: Side-lobe response for FIRAS shield on ground at 3cm⁻¹ (solid line) and in-flight with lunar source at 50cm⁻¹ (broken line)
[Courtesy of NASA and the COBE Science Working Group. Reproduced by permission of the AAS]



deviations are reported as less than 0.01%; and in 2002 the deviations become "50 parts per million (PMM, rms) of the peak brightness of the CMBR spectrum, within the uncertainty of the measurement". But Robitaille observes that: "Using technology established in the 1970s, the FIRAS team reported a spectral precision well beyond that commonly achievable today in the best radiometry laboratories in the world".

Robitaille also remarks that the blackbody trace published by the FIRAS team "is unusually drawn, as the frequency axis is offset. This makes it less apparent that data is not being shown below 2cm⁻¹". After 1994, all data below 2cm⁻¹ was omitted in FIRAS reports. Fixen et al make the remark: "However, the measured emission is higher than predicted, particularly at the lowest frequencies"; at the very frequencies at which diffraction of photons from Earth would be a maximum over the RF shield. In addition, all data when the Earth illuminated the instrument are rejected outright, thereby removing any effect of earthshine that might well assign the microwave

background to the oceans. Furthermore, "In the end, the FIRAS team transfers the error from the spectrum of interest into the calibration file" ... "Using this approach it would be possible, in principle, to attain no deviations whatever from the perfect theoretical blackbody. Given enough degrees of freedom and computing power, errors begin to lose physical meaning. The

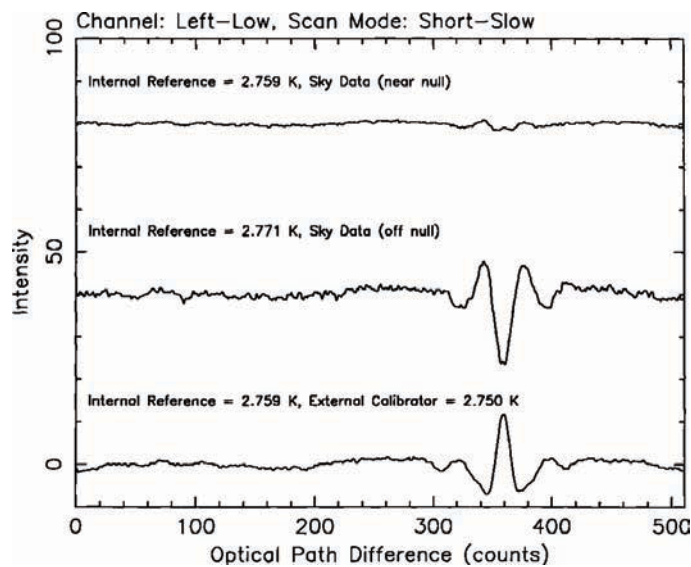


Figure 4: Interferograms obtained in flight with FIRAS

[Courtesy of NASA and the COBE Science Working Group. Reproduced by permission of the AAS]

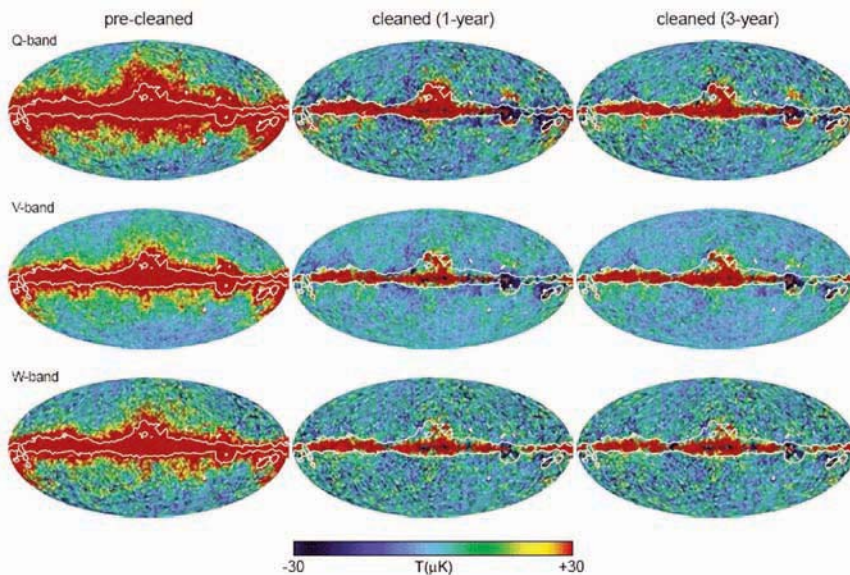


Figure 5: Comparative images

[Courtesy of NASA and the WMAP Science Team. Reproduced by permission of the AAS]

calibration file became a repository for everything that did not work for FIRAS".

Focusing on the Data Processing

Both COBE and WMAP must deal with the presence of a microwave dipole and a galactic foreground that is ~ 1000 times stronger than the signal sought. This is a dynamic range problem. As Robitaille advises, laboratory experience in medicine demonstrates that it is impossible to extract a signal ~ 1000 times smaller than the background without being able to affect the signal at its sources or without a priori knowledge of the source; neither of which are available to WMAP or COBE.

George Smoot, the principal investigator for the COBE Differential Microwave Radiometers

(DMR), relates that to extract the weak multipoles by data processing, which Smoot calls "*wrinkles in the fabric of time*", required first the removal of the dipole, galactic foreground and the quadrupole signals. Smoot puzzled over why the multipoles did not appear until the quadrupole was finally removed by data processing methods, since the raw data contained no systematic signal variations. Robitaille's answer is simple: "*when Smoot and his colleagues imposed a systematic removal of signal, they produced a systematic remnant. In essence, the act of removing the quadrupole created the multipoles and the associated systematic anisotropies*".

Smoot's "*wrinkles in the fabric of time*" are nothing more than consistent residual ghost

signals produced by his data processing. The appearance of such systematic ghost signals throughout an image when processing large contaminating signals is very well known in medical radiology. Robitaille advises that "*Apparent anisotropy must not be generated by processing*".

The foregoing far from exhausts the list of major problems with COBE. Robitaille gives detailed analyses of significant shortcomings in COBE's bolometer performance, grid polarizer performance, emissivities of Xcal and Ical, signal leakage around Xcal, design of the FIRAS horn, antenna gain, determination of error bars on data and the optical transfer function applied.

Concerning the latter, Robitaille makes the following points: (a) there is an unexplained and significant oscillation below $\sim 20\text{cm}^{-1}$; (b) FIRAS detects only 1 photon in 10; (c) FIRAS is non-linear in operation; (d) when applied to data beyond $\sim 30\text{cm}^{-1}$ there is a pronounced amplification of spectral noise, indicating that in this frequency range FIRAS is sub-optimal.

WMAP

WMAP does not measure absolute intensity of any microwave signal, but operates by measuring the difference between antennae. All data is therefore difference data. According to

Robitaille: "WMAP images do not meet accepted standards in medical imaging research". WMAP samples at five frequencies: K = 23GHz, Ka = 33GHz, Q = 41GHz, V = 61GHz, W = 94GHz. Claiming that the large galactic foreground signal can be removed, despite absence of access to signal source and a priori knowledge of it, the WMAP team produces Integrated Linear Combination (ILC) images, effectively assuming, without any scientific basis, that the foreground signal is frequency dependent and the sought after underlying anisotropy frequency independent.

WMAP anisotropy maps are composites of 12 sectional images, 11 thereof in the galactic plane. Robitaille notes: "The WMAP team invokes completely different linear combinations of data to process adjacent regions of the galactic plane". Numerical coefficients used by the WMAP team to process each section of their final image, vary by as much as 100%. Robitaille objects that "the sole driving force for altering the weight of these coefficients lies in the need to zero the foreground. The selection of individual coefficients is without scientific basis, with the only apparent goal being the attainment of a null point". Furthermore, the

WMAP team arbitrarily weights the V-band.

There is no scientific reason for preferring the V-band over any other band. To any chosen band there corresponds a particular set of ILC maps and so different sets of cosmological constants would result depending upon the band emphasised; as products of data processing. Robitaille considers this clear evidence that "the requirement that the signals of interest are frequency independent cannot be met and has certainly never been proven" and "there is no single map of the anisotropy, since all maps are equally valid, provided coefficients sum to 1" (which is precisely the condition set by the WMAP team). Consequently: "There is no unique solution and therefore each map is indistinguishable from noise. There are no findings relative to anisotropy, since there are no features in the maps which could guide astrophysics relative to the true solution".

The most important determinant of image quality is signal to noise. High signal to noise can permit some signal sacrifice to enhance contrast and resolution. Without high signal to noise, contrast and resolution will be poor. WMAP images have a maximum signal to noise

that barely exceeds 1, and so "WMAP is unable to confirm that the 'anisotropic signal' observed at any given point is not noise. The act of attributing signal characteristics to noise does not in itself create signal".

In the absence of high signal to noise, the only indicative feature of images is reproducibility. However, as Robitaille points out, WMAP images cannot evidently be reproduced, since the WMAP team not only selectively weights the V-band, but varies all ILC coefficients from year to year, for the central region of its images, and also averages images for a 3-year data image which differs significantly from the first year image, and did not publish any images for years two and three.

Moreover, the WMAP team's difference images are between year one and the averaged three years, not between images year-to-year. Figure 5 depicts comparative images, wherein Robitaille draws attention to the fact that "the difference images are shown with reduced resolution contrary to established practices in imaging science".

That WMAP and COBE have measured the temperature of the Universe is not substantiated by the facts. ■

www.stewart-of-reading.co.uk

CHECK OUT OUR WEBSITE, 1,000's of items currently in stock

 <p>HP53131A UNIVERSAL COUNTER WITH OPT 001 (oven) Unused Boxed 3GHZ £850 Unused Boxed 225MHZ £595 Used 225MHZ £495</p>	<p>AGILENT E4402B Spectrum Analyser 100HZ - 3GHZ with Option 1DN Tracking Gen; 1 DR Narrow Res; A4H GPIB, UKB £5800 HP 8591E Spectrum Analyser 9KHZ - 1.8GHZ with Tracking Gen No Moudlings, No Handle £1500 HP 35670A FFT Dynamic Signal Analyser 2 Channel. Unused in original box £1250 AGILENT 83752B Synthesised Sweeper 0.01-20GHZ £2500 HP83731B Synthesised 1-20GHZ with Opts IEI Attenuator, IE5 High Performance Mod Gen, IE5 High Stab TB £7000 HP83711B Synthesised 1-20GHZ with Opt IEI Attenuator £4500 AGILENT/HP E4431B Signal Generator 250KHZ-2GHZ Digital Modulation £5000 MARCONI 2024 Signal Generator 9KHZ-2.4GHZ Opt 04/11 HP1B £2750 MARCONI/IFR 2030 Signal Generator 10KHZ-1.35 GHZ £1250 MARCONI 2032 Signal Generator 10KHZ-5.4GHZ £995 MARCONI 2022E Synthesised AM/FM Signal Generator 10KHZ-1.01GHZ Special price £- HP3580A Spectrum Analyser 5HZ-50KHZ £325 Unused £500 HP8566A Spectrum Analyser 100HZ-22GHZ £1950</p>	<p>HP8568A Spectrum Analyser 100HZ-1500MHZ £1250 AVCOM PSA-37D Spectrum Analyser 1MHZ-4.2GHZ £- IFR 1200S Service Communication Monitor £2000 HP6624A Power Supply 0-20V 0-2A Twice, 0-7V 0-5A; 0-50V 0.8A Special price £350 AVO/MEGGAR FT6/12 AC/DC breakdown tester £- MARCONI/IFR/AEROFLEX 2025 Signal Gen 9KHZ-2.51GHZ Opt 04 High Stab Opt 11 High Power etc As New £2500 SOLARTRON 1250 Frequency Response Analyser 10uHZ-20MHZ £- HP3324A Synthesised Function Generator 21MHZ £500 TEKTRONIX AM503B with A6302 Probe and TM502A £750 HP41800A Active Probe 5HZ-500MHZ £750</p>	
 <p>HP33120A FUNCTION GENERATOR 100 MicroHZ - 15MHZ Unused Boxed £595</p>			
 <p>ANRITSU MS2601A SPECTRUM ANALYSER 10KHZ - 2.2 GHZ 50ohm £750</p>			
<p>STEWART of READING 17A King Street, Mortimer, Near Reading RG7 3RS T: (0118) 933 1111 • F: (0118) 933 2375 9am - 5pm Monday - Friday</p>	<p>Used Equipment - GUARANTEED Most Manuals Supplied Prices plus carriage and VAT Please check availability before ordering or CALLING IN.</p>	<p>EXTRA SPECIAL OFFER</p>  <p>MARCONI 2945 RADIO COMMUNICATIONS TEST SET with.... Opt 01 - 600 ohm Matching Unit - Opt 03 - High Stability OCXO - Opt 06 - Memory Card Drive with Real Time Clock - Opt 08 - SSB Demodulator - Opt 21 Demodulation Filters - Opt 22 POCSAG Decode Complete with Carrying Bag Only £2,500</p>	

Security and Mobility – the **FUTURE** Is Now

In this article, **Gernot Heiser**, cofounder and chief technology officer of Open Kernel Labs (OK Labs), explains that to avoid the security morass of the desktop PCs, mobile software architecture must take a different path to OS approach with a minimalist microkernel technology being the perfect candidate

This is the second article in a two-part series on micro-kernels and virtualization that started in the last issue

PERSONAL COMPUTERS present an irresistible magnet for “black hats” and the malware they create. When they least expect it, computer users and IT professionals face viruses, passwords stolen by keystroke loggers, hacked networks, machines hijacked for denial-of-service attacks, pilfering of individual identities and grand theft of entire databases of sensitive data. Notwithstanding this litany of larceny, government and industry forge ahead in deploying applications to conduct ever-increasing amounts of security-critical transactions on these infested information systems.

Now, consider mobile devices like smartphones and MID. Using mobile devices is also on the rise for financial and other secure transactions and will likely replace PCs for access to most web services. These devices in many respects already resemble PCs in functionality, albeit in a different form-factor. Will they be equally vulnerable to security exploits? Are we heading towards full-scale security disaster from relying on mobile web services to check bank balances, pay bills, trade securities and even more critical operations?

Enter Mobile Virtualization

The good news is that the technology that can protect us from these and

other emerging threats already exists.

The technology is not new – virtualization is a mature capability, re-factored and optimized for mobile devices. Originating in the mainframe world of the 1960s, virtualization recently caused a revolution in the data centre. Virtualization partitions physical servers into multiple virtual machines (VMs); each VM appears to software like distinct “real” hardware. This partitioning allows IT managers to consolidate multiple (logical) servers onto a single computer, reducing hardware costs and bringing down power bills, without compromising the security previously conferred by dedicated hardware.

Superficially, this data centre scenario does not appear to have much in common with mobile computing. However, both data centre and mobile computing benefit from a fundamental property of virtualization: isolation. Because virtualization partitions a single computing platform into multiple isolated logical VMs, it implicitly provides secure firewalls between them. The hypervisor (or virtual machine monitor) erects these firewalls, which appear to “guest” software running in each VM to be part of the hardware.

Imagine a PC used to access online services, except that whenever users must enter a PIN or password, that code is not entered via the PC keyboard, but rather through a physically separate device. As long as the remote server can ascertain that the entry comes directly from the separate device (e.g., via a secure network link), and that device is itself tamper-proof, the transaction can be secured, even if the PC itself is infected with malware and viruses and other PC pestilence.

Think of virtualization as a means to simulate this detached PIN-entry device and other security mechanisms by segregating operations like authentication into separate VMs. Normal phone software runs in its own VM (or more likely several). The hypervisor ensures that the security-critical functionality is completely protected from potentially compromised software running in other virtual machines.

Hypervisor Security

The above scenario begs the question “What about securing the hypervisor itself?” With enterprise-style virtualization, large complex hypervisors themselves present targets for compromise and exploits. These big systems include security-critical management components consisting of hundreds of thousands or even millions of lines of code

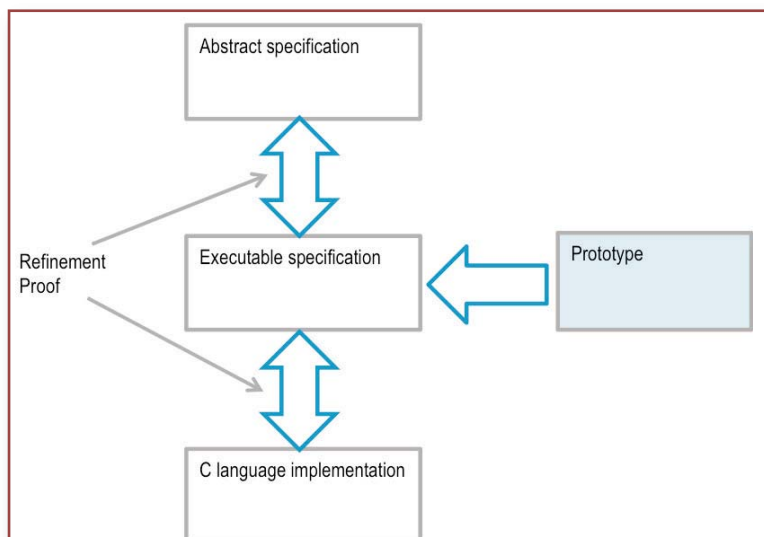


Figure 1: Verification

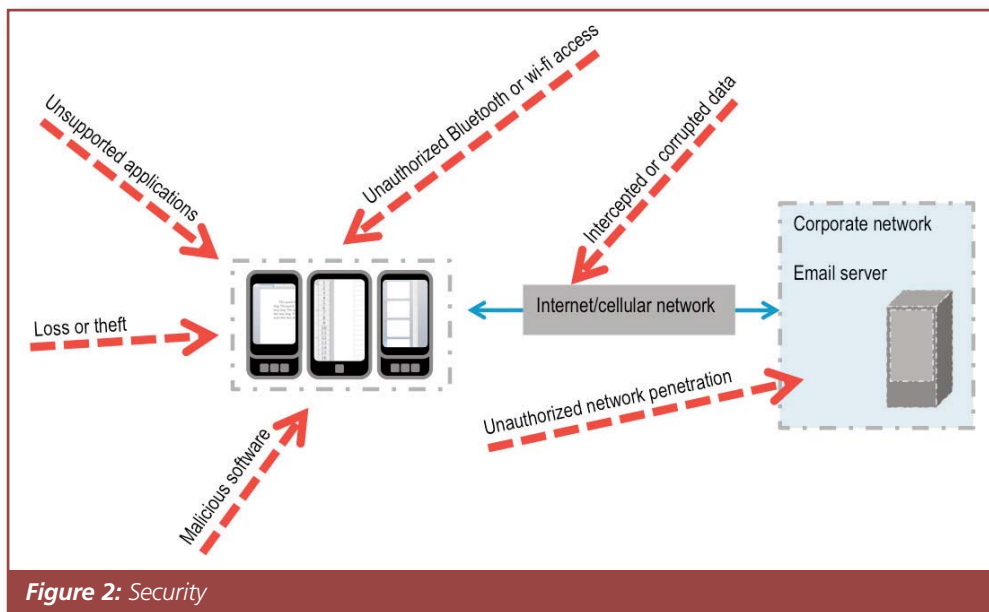


Figure 2: Security

(some include the entire Linux kernel). Recognized metrics indicate that even well-engineered software averages several bugs per thousand lines of code, meaning that these hypervisors can be expected to contain thousands of bugs. Bugs present opportunities for security exploits, open vulnerabilities to mischief by the same “black hats” that plague servers’ PC cousins.

Computer security, like its human cloak-and-dagger counterpart, is conducted on a need-to-know basis. The fewer people in the know, the better; comparably, the less code entrusted with ensuring security, the more secure is the total body of software involved.

With computer security, size matters. The goal in all security regimes, from mobile to desktop to servers to super-computers, is to minimize this trusted computing base (TCB). Indeed, a well-designed hypervisor for mobile use must be very small. The design of OK Labs’s OKL4 platform observes the following principles: start by adapting virtualization technology to create a hypervisor to meet the specific requirements of mobile systems (and similar requirements of other consumer electronics devices). Next, focus on careful design and implementation to provide just the minimum required set of primitives. Stir briskly and you will arrive at a hypervisor with a source code footprint of about 10,000 lines of code, with a minimalist design inherited from OS microkernels. We call this small hypervisor a microvisor.

Even with traditional software engineering methods, the number of bugs in such a small code-base can be reduced to a mere statistical handful. Hopefully, by applying good practices, none of these bugs will facilitate security exploits. But is such rigour sufficient to guarantee a hypervisor that is impervious to today’s security threats?

Enter Formal Verification

In fact, the answer is ‘no’. Traditional software engineering methods are by nature subject to “blind spots” and concomitant security vulnerabilities.

A landmark research project by NICTA – Australia’s National Centre of Excellence for ICT research – took a different approach: formal design followed by formal verification. Earlier in 2009, NICTA researchers announced the successful formal verification of the seL4 (Secure L4) microkernel, a kernel that shares its lineage and design principles with OKL4, OK Labs’s microvisor.

“Formal Verification” refers to establishing properties of systems with mathematical methods and rigour. The methods used by NICTA are not unique, but they do represent a quantitative and qualitative leap ahead of current practices.

For example, engineers frequently employ static analysis tools to detect

bugs in programs. The more sophisticated ones utilize formal methods to determine salient properties of code under inspection. The formal methods behind these tools fall into a category called model checking. While model checking can help eliminate bugs in programs, including very large ones, the scope of the approach is inherently limited to checking relatively simple and well-defined properties. As such model checking is limited to identifying a narrow class of bugs.

By contrast, the formal verification by NICTA is a refinement proof and shows, in a very strict sense, the correspondence between high-level and low-level representations of a system. An example of a high-level representation could entail functional description of the kernel (the APIs)

formulated in a mathematical language. A low-level representation would then involve the actual kernel implementation. Ultimately, such a refinement proof asserts and proves (with mathematical rigour) that all the possible behaviours of the low-level representation are completely captured in and permitted by the high-level representation.

Refinement proofs have been performed on some (very small) operating-system kernels before.

Verification of seL4

There are two facts that are new and exciting about the verification of seL4.

The low-level representation is the actual source code of seL4 (written in C). Past verification projects stopped at modelling a kernel (albeit at a low-level). Such models still require an informal (non-rigorous) step of arguing the correspondence between the model and the actual code.

seL4 is a general-purpose platform, allowing developers to construct systems above it as needed. For example, seL4 can also serve as a hypervisor, and in fact, is able to run Linux in a virtual machine with commercial-grade performance (comparable to OKL4). So, seL4 is not a toy or a mere academic exercise; it is suitable for use in the real world.

Together these attributes make seL4 the world’s first general-purpose operating-system kernel (or hypervisor) to be formally verified down to the actual source code.

The Implications of Formal Verification

The NICTA project and the resulting seL4 constitute a rock-solid foundation for building secure systems. A formally-verified hypervisor can truly act as an extension of the hardware – it is as reliable and secure as the underlying mobile chipset. seL4 and platforms built with the same rigour, then, can isolate virtual machines as securely as if they were each executing on distinct, isolated hardware – exactly the remedy for emerging challenges to mobile security.

Mobile devices are already evolving to take over functionality from PCs. To avoid the security morass that is today the rule on the desktop, mobile software architecture must take a different path from the bottom-up monolithic OS approach that accompanied desktop computing. A solid foundation built on minimalist microkernel technology delivers small, more maintainable code with a greatly reduced trusted computing base. And only a microkernel-based mobile hypervisor built on such a foundation can meet the challenges of today and tomorrow’s mobile world. ■



Printed
Electronics
EUROPE 2010

Co-located with



PHOTOVOLTAICS
EUROPE 2010

Electronics World readers

save 25%

by quoting PEE10EW

13-14 April, 2010, Dresden, Germany

MARITIM Hotel & International Congress Center

Creating the Focal Point for the Industry



All the applications. All the technologies.

Hear the latest technology progress including:

Radical New Printed Electronics Products

Healthcare & Bionic Man

Energy Harvesting

Thin/Flexible Batteries

Displays & Lighting

E-readers

Photovoltaics

Stretchable Electronics for Clothing

Carbon Nanotubes

Sensors & Actuators

Speakers Include:



Register at

www.IDTechEx.com/Dresden

IDTechEx

The Hum Figure – RELOADED

Burkhard Vogel discusses measurement of the Hum Figure of hum-infected phono-amplifiers

THERE ARE MANY reasons why it is worth insisting on the identification and elimination of hum in audio equipment. It can be demonstrated simply in **Figures 1** and **2**.

Figure 1 shows the hum and noise (H&N) output situation of a brand new Italian 2 x 200W/4R solid-state 2100 EUR audio product. It was published in March 2009 by the German magazine stereoplay. Not only it demonstrated this PA's hum infection but it also showed its influence on distortion, produced by a 125Hz 0dB tone into two different loads (red and green).

What they did not mention is the fact that, in conjunction with the 50Hz and 100Hz basic hum signals, the graphically suppressed 125Hz signal produces rather strong sidebands at 25Hz, 75Hz, 150Hz, 175Hz and 200Hz. All sidebands at frequencies > 200Hz disappear in the distortion artefacts of the 125Hz signal. Perhaps, because of their low amplitudes, all these hum signals may be inaudible when listening to loudspeakers of medium sensitivity. However, it must be taken into account that these hum-generated signals are all 100% correlated and they will sum up to a significant level.

Figure 2 was published in July 2007 by stereoplay too. It demonstrates the distortion of a 1kHz 0dB signal (graphically suppressed). The graph shows all 50Hz generated hum artefacts of this British/Chinese valve driven 1500 EUR audio product as well. Astonishing enough, there are nearly no 100Hz artefacts.

I would not say anything against hum infected low-cost equipment; it

may be the price to pay. However, there are many audio products on the market – including very expensive ones – that do not suffer from hum. Nevertheless, these two examples represent a broad range of very expensive hum-infected products. Many of them are from the valve or semi-valve world and much more expensive; for example, Thorens TEP3800, 15,000 EUR, FFT diagram in stereoplay 5-2008 or even mastering products at the beginning of the production chain like Dangerous Music's Monitor, MQ and Monitor, a total of 12,500 EUR, FFT diagrams in professional audio 4-2009.

I guess, it is not forbidden to sell products like these, but as a customer, from a certain price level on, I can expect to get precise information on H&N specs based on comprehensible measurement methods. Unfortunately, they do not exist to catch the hum precisely. Fortunately, there are many methods to suppress hum, but it is a heavy, expensive and rather long-lasting task to go through them all in the pursuit of good design results.

Hum Figure Measurement Details

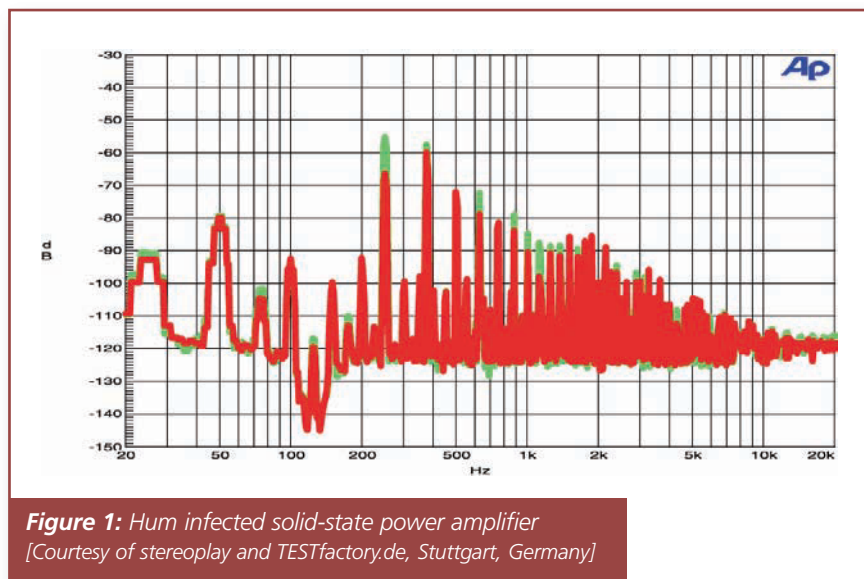
To understand better the complete mathematical and measurement approach behind the following descriptions on how to measure the hum of a hum-infected phono-amp, I strongly recommend reading The Hum Figure article that was published in the March 2009 issue of Electronics World magazine. This will help!

All the given measurement equipment (**Figure 3** shows the whole measurement set-up) and mathematical hints will enable the user to measure and calculate on an rms basis only. Results in **Table 1** are based on

it as well, including the A-weighting figures according to ANSI/NAB specs. I refrain from going through the European CCIR 468 or ITU-T J.16 quasi-peak non-weighted or A-weighted measurement approaches. The signal-to-noise ratio (SN) results will look very different.

As an example, they will differ as follows: a $-75\text{dBV}_{\text{rms}}$ white noise level in the rms world equals approximately -72dB_{qs} in the quasi-peak world. A-weighting in the rms world looks $\sim 10\dots 11\text{dB}$ better than in the quasi-peak world: a $-77\text{dBV}_{\text{rms}}$ (A) level equals approx -66dB_{qs} , but the hum figure values will become equivalent to the ones achieved by rms measurement methods ("q" stands for quasi-peak, "p" stands for the French word pondéré = weighted, "s" indicates the standard bandwidth of 22.4Hz...22.4kHz).

The mathematical relationship keeps the same as shown for power amps in the March article. To get the Hum Figure HF_e of phono-amps we need to find the phono-amp's non-equalized (ne) white noise (wn) based



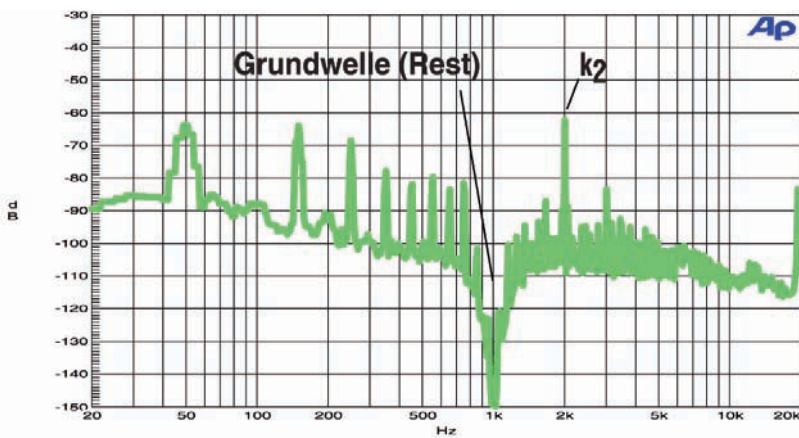


Figure 2: Heavy hum infection of a valve driven MC phono-amp
[Courtesy of stereoplay and TESTfactory.de, Stuttgart, Germany]

signal-to-noise ratio $SN_{ne,wn}$, as well as the phono-amp's non-equalized signal-to-noise-ratio SN_{ne} . The latter is the SN of the phono-amp without RIAA equalization but with the same gain of the RIAA equalized phono-amp at 1kHz. Hence, the basic equation looks as follows:

$$HF_e = SN_{ne} - SN_{ne,wn} \quad (1)$$

Nevertheless, how do we get these SNs? The value of the phono-amp's non-weighted SN SN_{riaa} is the result of a simple noise measurement in B_{20k} (= 20Hz...20kHz). To get SN_{ne} and $SN_{ne,wn}$ several precise steps have to be taken. I will go through the whole process using the example phono-amp of **Figure 4**. It consists of two OP27 op-amps with a very exact R2, R3, C3, R4, C4, R5 network (see my book 'The Sound of Silence', Chapter 8) to generate the RIAA transfer with a maximum deviation of less than $\pm 0.25dB$ from the exact RIAA transfer function between 1kHz and 20kHz.

In Search of SN_{ne}

The example phono-amp's hum-free, equivalent, voltage noise density is shown in **Figure 5**, lower half. Throughout this article, measurement and calculation results will be referenced to $0dBV = 1V_{rms}$. **Figure 6** demonstrates the mathematical sequence that has to be turned into a measurement approach.

The phono-amp's input is loaded with a 1k resistor. We can take the 1kHz o/p level from the FFT measurement chart of Figure 5 (remember: for an FFT analysis like this in B_{20k} , the division of the FFT size by the sample rate should be $\leq 1Hz$! Because of Nyquist the sample rate must be $> 2 \cdot 20kHz$). The picked-out level value becomes -118.8dBV (to be guessed between all the noise spikes around 1kHz, the respective calculated value becomes

-119.4dBV). Thus, Figure 6's black plot represents the hum-free (or hum-infected) RIAA transfer in B_{20k} .

This transfer is amplified by the gain $GM = +66dB$ of the measurement instrument. With that, the plot was shifted to the red curve position of -52.8dBV/-53.4dBV at 1kHz. This must be done to get the noise level of the phono-amp free of the noise level of the measurement instrument itself. Multiplication by the inverse RIAA

transfer function ARIA (Anti-RIAA) creates the flat blue white noise line at -52.8dBV/-53.4dBV.

To get the non-equalized SN_{ne} the logarithmic value equivalent of B_{20k} (= $43dB = 20 \cdot \log[\text{root}(20kHz-20Hz)]$) has to be summed up with the 1kHz value of the blue plot. Additionally, the measurement amp's gain GM has to be subtracted, hence SN_{ne} measured (calculated) becomes:

$$\begin{aligned} SN_{ne} &= \text{blue line level (1kHz)} - G_M + B_{20k} \text{ equivalent} \\ &= -52.8dBV (-53.4dBV) - 66dB + 43dB \\ &= -75.8dBV (-76.4dBV) \end{aligned} \quad (2)$$

From **Figure 7** it can be studied that, after this manoeuvre, a hum-infected phono-amp will not lose its hum artefacts nor will they be shrunken like after the application of ANSI/NAB A-weighting (see Figure 1 of the March 09 article). Instead, they will all be in place unchanged and, principally, they can be measured the way it was described in my first article on the hum figure.

In Search of $SN_{ne,wn}$

In Figure 7 the yellow curve represents the white-noise loaded frequency response of a "new" designed measurement bp. The "old" 10kHz hp that was used in the March 2009 article does not work exact enough here. The reason can be found in the fact that – especially $> 1kHz$ – any deviation from the exact RIAA transfer of the phono-amp under test will lead to wrong HF results. Growing deviation automatically leads to measurement results with growing errors.

The only "clean" portion of white noise can be found in a hum-free region $> 2kHz$ that ensures a very low amount of deviation from the exact

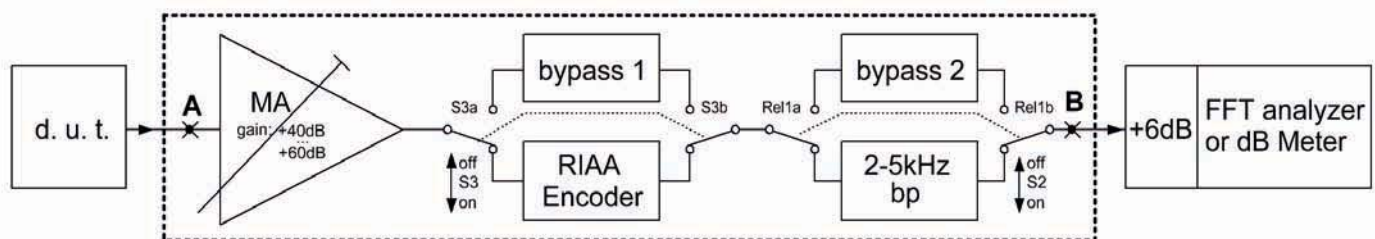


Figure 3: Measurement set-up

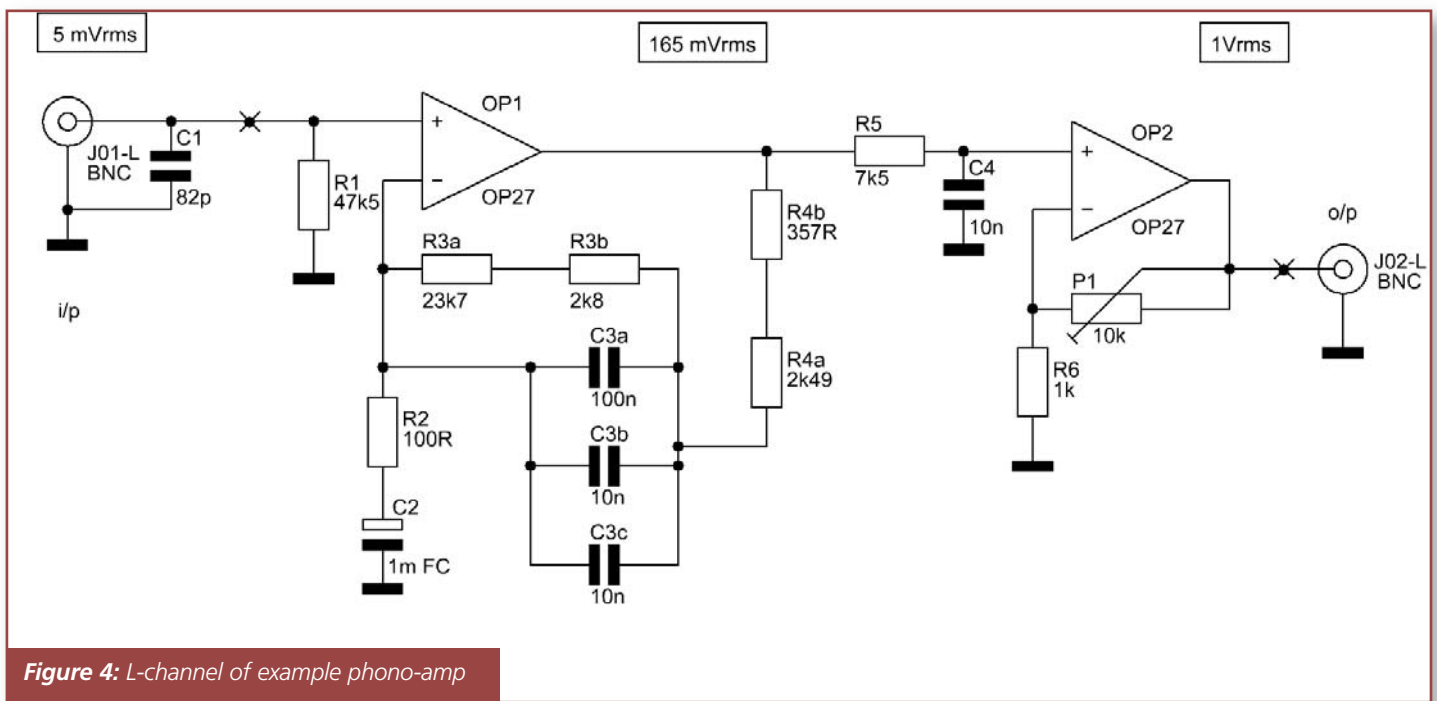


Figure 4: L-channel of example phono-amp

RIAA transfer. The graphs in **Figures 8** and **9** show the mathematically generated situation.

In Figure 8 the green RIAA transfer plot shows -3dB deviations from the red (exact) RIAA transfer at 20Hz and 20kHz. These deviations are transferred by multiplication with the ARIAA transfer function into the blue and the cyan white noise lines at -53.3dBV. The right magenta hp represents the old hp, the left black band-pass filter between 2.5kHz and 5.1kHz represents the new method to filter out a region of hum-free and low-deviation white noise.

The linear plots in Figure 9 give more details on the deviation disturbing level on the phono-amp's exact RIAA transfer.

The "old" measurement method is confronted with, what I call, a rather big deviation area. It is located between the magenta filter slope on the left, the red and green lines of the two different RIAA transfers on top and bottom and the vertical boundary on the diagram's right side set by the 20kHz line, which, in fact, is built-up by the sharp slope of the analyzer's anti-aliasing lp filter.

Multiplication with the ARIAA transfer function transfers this area into the one between the magenta hp filter slope at 11kHz and the blue/magenta and cyan plots between 11kHz and the 20kHz vertical boundary. The physical space of this rather big area can be taken as an equivalent for the deviation tolerance of the hp filter approach with phono-amp RIAA transfer

functions that differ up to $\pm 3\text{dB}$ from the exact one. Consequently, this effect will lead to wrong HF measurement results of up to a calculated +2.3dB additionally.

In contrast to these findings, in Figure 9, the "new" version's tiny area between the top of the bp filter (2.5kHz...4kHz), the blue and the cyan plots show significant less dependency on RIAA transfer function deviations of phono-amps. In this case, the maximum HF result error became a calculated +0.7dB at $\pm 3\text{dB}$ and a +0.2dB error at $\pm 1\text{dB}$ RIAA transfer function deviations at the upper end of B_{20k} . No similar problems could be detected at the lower end of B_{20k} .

Deviations from the exact RIAA transfer as well as $1/f$ noise effects in the region $< 1\text{kHz}$ do not play a significant role at all, because this frequency region is simply too small to influence the white noise and HF measurement in a countable way. A phono-amp's RIAA transfer change of $\pm 60\text{Hz}$ (or $\pm 0.5\text{dB}$) at 1kHz will lead to an additional HF error of +0.22dB.

All these findings make clear why a band filter that picks-out the most white noise region is as important as to develop a very exact solution for

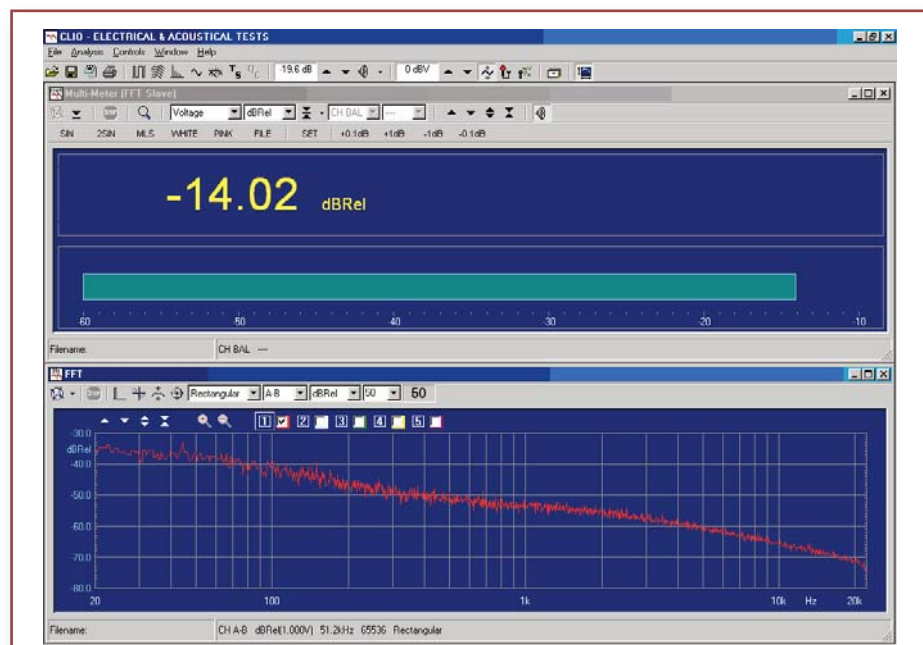


Figure 5: Equivalent voltage noise density of the example phono-amp's R-channel (lower part) with 1kHz at -52.8dBV, 0dBRel = -66dBV, hence, $SN_{riaa} = -80.0\text{dBV}$ (upper part)

the measurement instrument's ARIAA transfer function (see Figure 9 plus **Figures 10, 11**). I recommend that the deviation of this transfer function should not exceed a $\pm 0.05\text{dB}$ borderline.

The band filter circuitry around op-amps OP5, 6, 10, 7 is given in Figure 11. It consists of a 5th order 0.1dB Chebyshev 2.5kHz hp followed by a 3rd order 0.1dB Chebyshev 5.1kHz lp. Both together form the "new" bp filter.

It is assumed that no hum artefact will jump over the 1.5kHz mark. I've never been confronted with such a case. If this would happen and by accepting a less revealed tolerance range, one must choose a bp of higher centre frequency. OP7 serves to amplify the pure white noise "caught" by the bp – from the yellow to the black position in Figure 10.

Normally, it is an unusual situation that a phono-amp under test can be switched between a hum-free and a hum-infected state. It is hum-infected or not. However, only a hum-free phono-amp à la Figure 4 is switchable in a certain way: I forced the hum-free example phono-amp to catch hum interferences on several different hum producing locations inside my lab (loc 1...loc 4).

Table 1 lists the respective measured HF results in column I and in lines 4...8. The table should be self-explanatory. Due to the phone-amp's low noise, as well as in order to get it noise-free from the noise of the measurement instrument itself, I had to set the measurement gain to +66dB (column F). It is logical that the measured non-equalized white noise based $\text{SN}_{\text{ne.wn}}$ (column H) comes up with the same value in all lines. All values are rounded to one

Table 1: R-channel RMS measurement results of the bp measurement approach, based on the fact that there was only a 0.2dB maximum deviation from the phono-amp's ideal RIAA transfer function. (A means A-weighting according to ANSI/NAB specs, V means Vrms, quasi-peak and A-weighting measurements according to CCIR 468 or ITU-T J.16 will lead to the same HF results)

1/A	B	C	D	E	F	G	H	I	J
2	placement of phono-amp	SN_{riaa} (S2 off, S3 off)	SN_{ariaa} (S2 off, S3 off)	Delta C-D	MA gain	SN_{ne} (S2 off, S3 on)	$\text{SN}_{\text{ne.wn}}$ (S2 on, S3 on)	HF_e (G-H)	measured
3		dBV	dBV(A)	dB	dB	dBV	dBV	dB	calculated
4	hum-free	-80.0	-84.5	4.5	66.0	-75.8	-75.8	0.0	meas.
5	loc. 1	-75.1	-82.3	7.2	66.0	-74.4	-75.8	1.4	meas.
6	loc. 2	-71.6	-80.4	8.8	66.0	-73.1	-75.8	2.7	meas.
7	loc. 3	-60.7	-80.0	19.3	66.0	-72.7	-75.8	3.1	meas.
8	loc. 4	-52.6	-72.6	20.0	66.0	-66.5	-75.8	9.3	meas.
9	calculated	-80.1	-84.4	4.3	0.0	-76.4	-76.4	0.0	calc.

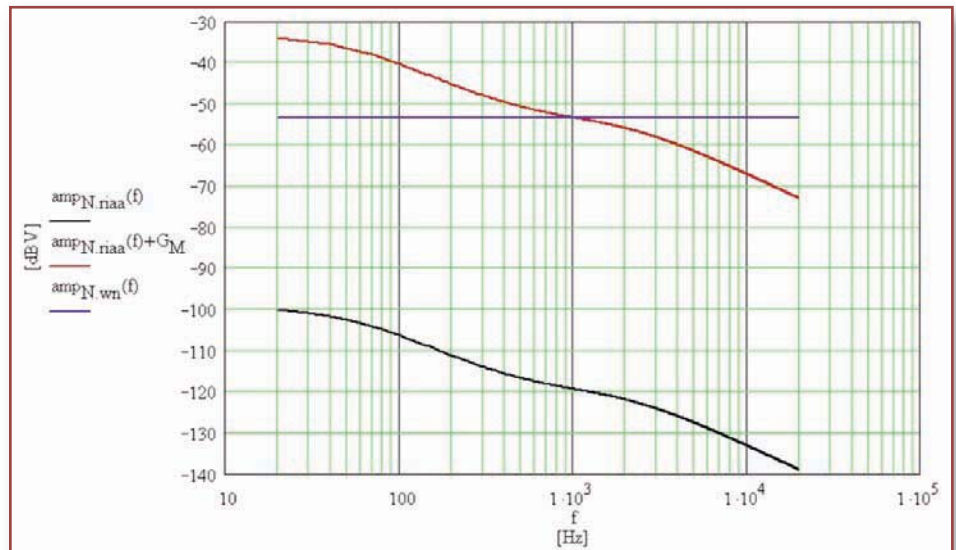


Figure 6: Mathematical-graphical sequence from black via red to blue to get the non-equalized white-noise based signal-to-noise ratio $\text{SN}_{\text{ne.wn}}$

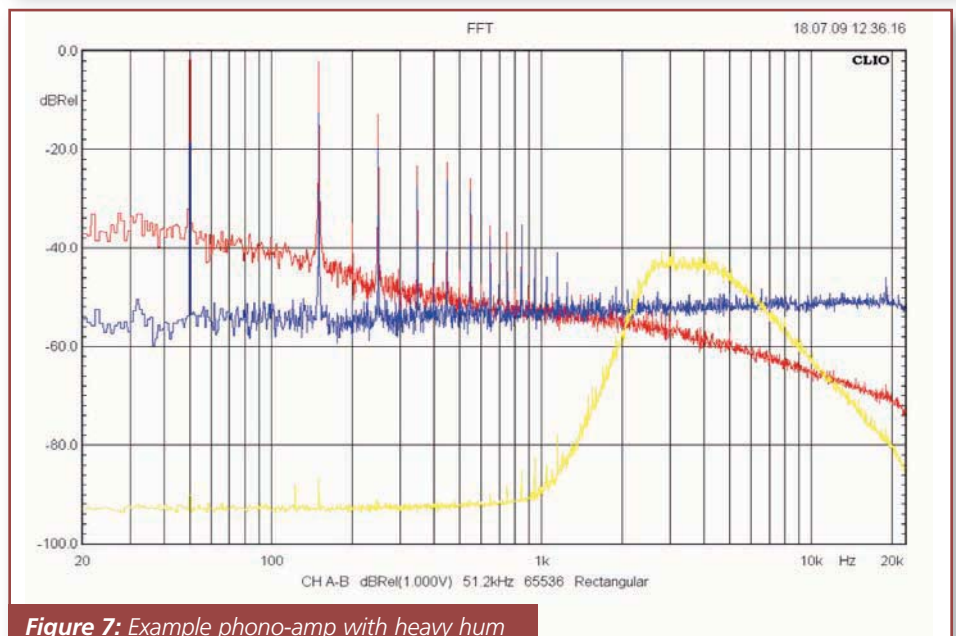


Figure 7: Example phono-amp with heavy hum impact ($G_M = +66\text{dB}$, 1kHz at -118.8dBV)

digit after the decimal point.

It is important to note that the A-weighting results in column D are not able to give a customer a good and exact answer to his

potential question on the amount of hum produced by a specific phono-amp (see also respective remarks and analysis at the beginning of the March 2009 article).

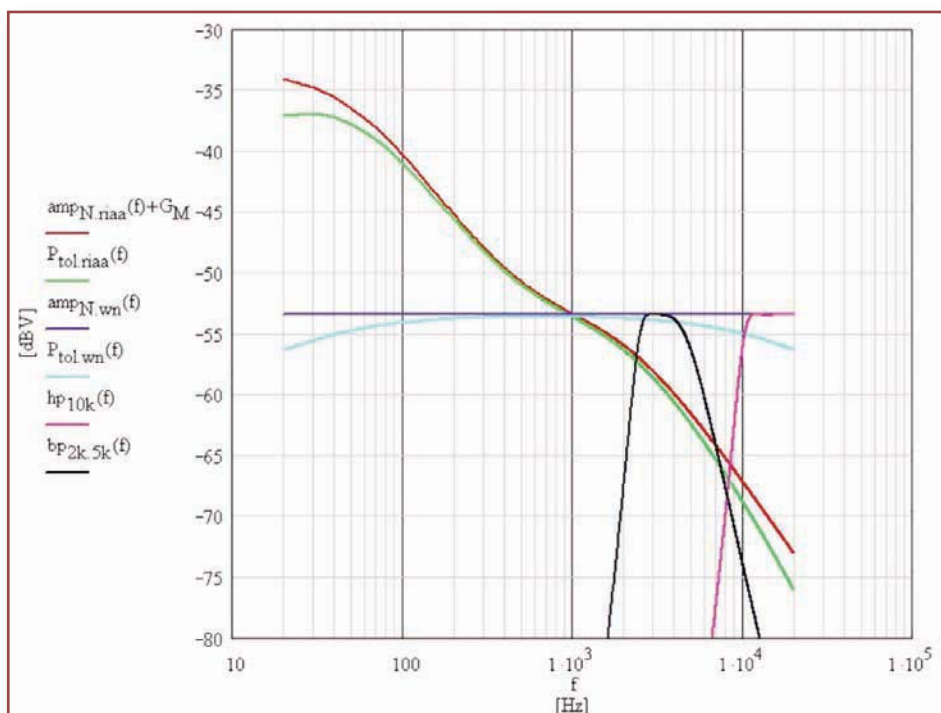


Figure 8: Mathematical graph showing all the relevant plots on a logarithmic frequency scale, after a $G_M = +66\text{dB}$ amplification by the measurement amplifier

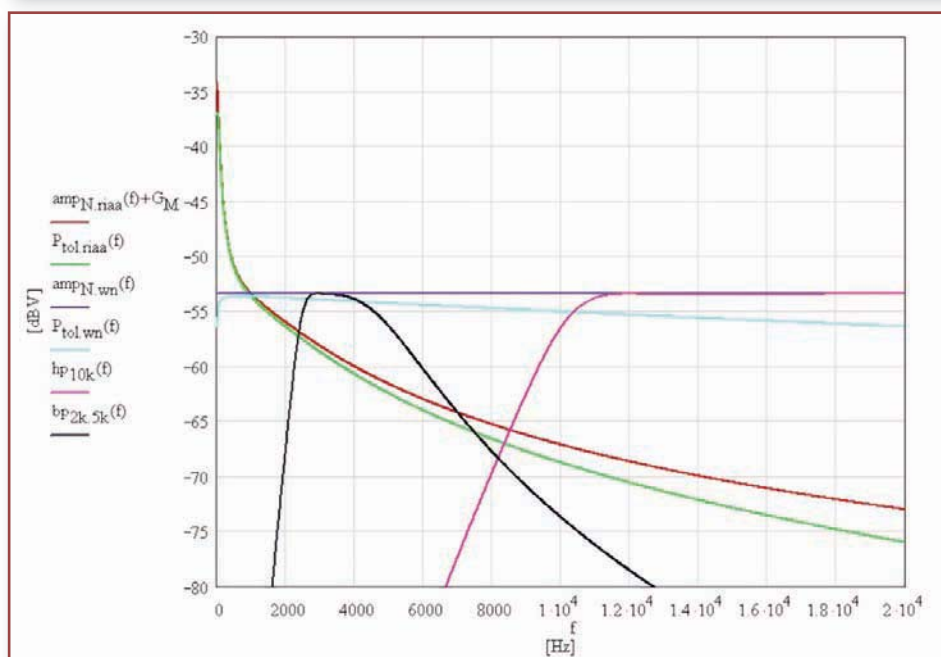


Figure 9: Mathematical graph showing all the relevant plots on a linear frequency scale, after a $G_M = +66\text{dB}$ amplification by the measurement amplifier

Line 7, column D leads us to believe in a wonderful phono-amp. Line 7, column C, however, signals that this is not the case. Because of the high sensitivity of the measurement approach I must also point out that rather low HFe values also indicate rather a

worsening of the respective SN_{riaa} values (for example see line 5).

For comparison reasons I add calculation results in line 9. They all lie within the 1.0dB boundaries that I found as part of my article on noise in MM cartridges, published in Electronics

World magazine, May 2005 ('Adventure: Noise') and, later on, in my 'The Sound of Silence' book.

The measurement instrument's circuitries are shown in Figures 10, 11. They contain nearly all of the relevant information. Fed with a broadband white noise signal and with S2 set to "Fi on", we have to trim the gain of the filter block of Figure 11 with P6 (approx +9dB). In B_{20k} OP7's o/p voltage must have the same value to the one in "Fi off" mode. The calculation rules for the ARIAA network look as follows (a detailed derivation is given on Worksheet X of my book 'The Sound of Silence', a free download of all Mathcad worksheets from the Springer Edition website is also ensured):

$$\begin{aligned} C4 &= 3.6 * C5 \\ R8 &= 11.77 * R9 \\ C5 * R9 &= 75\mu s \end{aligned} \quad (3)$$

Between test points TT1 and TT2, P4 trims the gain of the ARIAA transfer block to 0.00dB. The outputs are balanced via OP9/J03 and unbalanced via OP8/J02. They always produce the same output level. Together with the two different gain setting possibilities of the input amplifier OP1, they perform a total gain G_M of +40dB or +60dB. I use an FFT analyzer with a +6dB gain amp in front of it. That's why the gains always end up with an additional +6dB. A test wise insertion of R6 and/or C3 may prevent OP2 from negative impacts because of a heavy capacitive load.

Final Remarks

There is no need to discuss whether the H&N of a certain phono-amp, or any other audio amplifier, will be audible in a certain distance of a certain loudspeaker or not. Any amplifier internally generated signal that does not come from the program material that passes through that specific amp, adds negatively to the original program material.

I guess, the price of an audio product also dictates the amount of quality one can expect from the manufacturers. Unfortunately, for thermal noise there are boundaries that no one can cross. However, for hum such boundaries do not exist. That's why the following rule must become the main guideline for the amplifier designer: no hum is always better than any one! The design goal should be to get a zero hum figure.

By leaving aside any doubts of the industry's willingness to accept stronger quality goals, the proposed analogue solution could be turned into a digital one and commercially easier to handle. If the FFT analyzer producers (like Audio Precision

of the US, Rhode und Schwarz in Germany or Audiomatica from Italy) would start with corresponding developments as soon as possible, I guess, any such solution could mainly be found in the adaptation of their existing low-frequency FFT measurement instrument software. In addition, if the standardization organisations would set a positive signal as well, things could be moved towards the right direction rather fast.

H&N measurements within B_{20k} should always be performed with the adequate i/p load "IN" for phono-amps, hence, the manufacturers must be forced to indicate the information about the H&N situation of a specific phono-amp as follows:

$$\frac{SN_{riaa}}{HF_e / IN} = -x \text{ dB} + \text{reference level} / y \text{ dB} / z \text{ IN} \quad (4)$$

It makes no sense to measure HFe the analogue way, as long as the DUT's RIAA transfer does not hit the exact RIAA transfer within deviation boundaries of $\pm 0.5\text{dB}$ (better $\pm 0.25\text{dB}$). A digital FFT solution could bend the measurement instrument's ARIAA transfer function exactly inverse to the error-afflicted RIAA transfer of the phono-amp under test in a way that, after application of **Equation 1**, only hum (or no hum) will remain. ■

Figure 12 is shown on the next page.

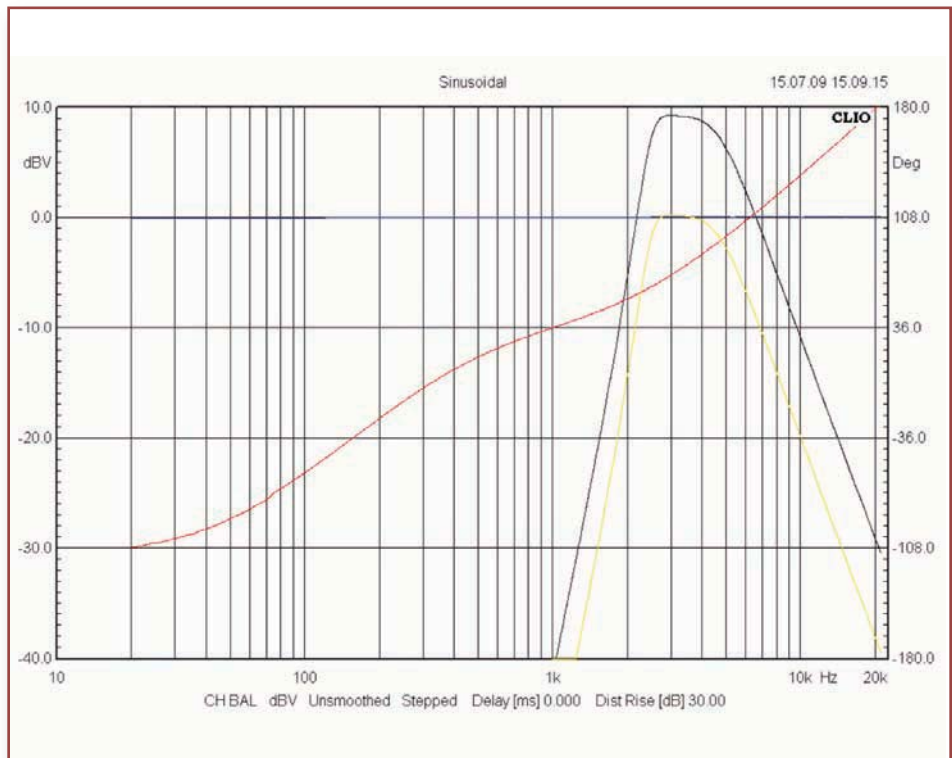


Figure 10: Measured performance of the phono-amp test instrument
blue: represents gains +46dB and +66dB and S2 plus S3 off
red: ARIAA transfer function (deviation: < $\pm 0.02\text{dB}$ > 1kHz)
yellow: 2.5...5.1kHz bp filter at the o/p of OP10
black: 2.5...5.1kHz bp filter at the o/p of OP7

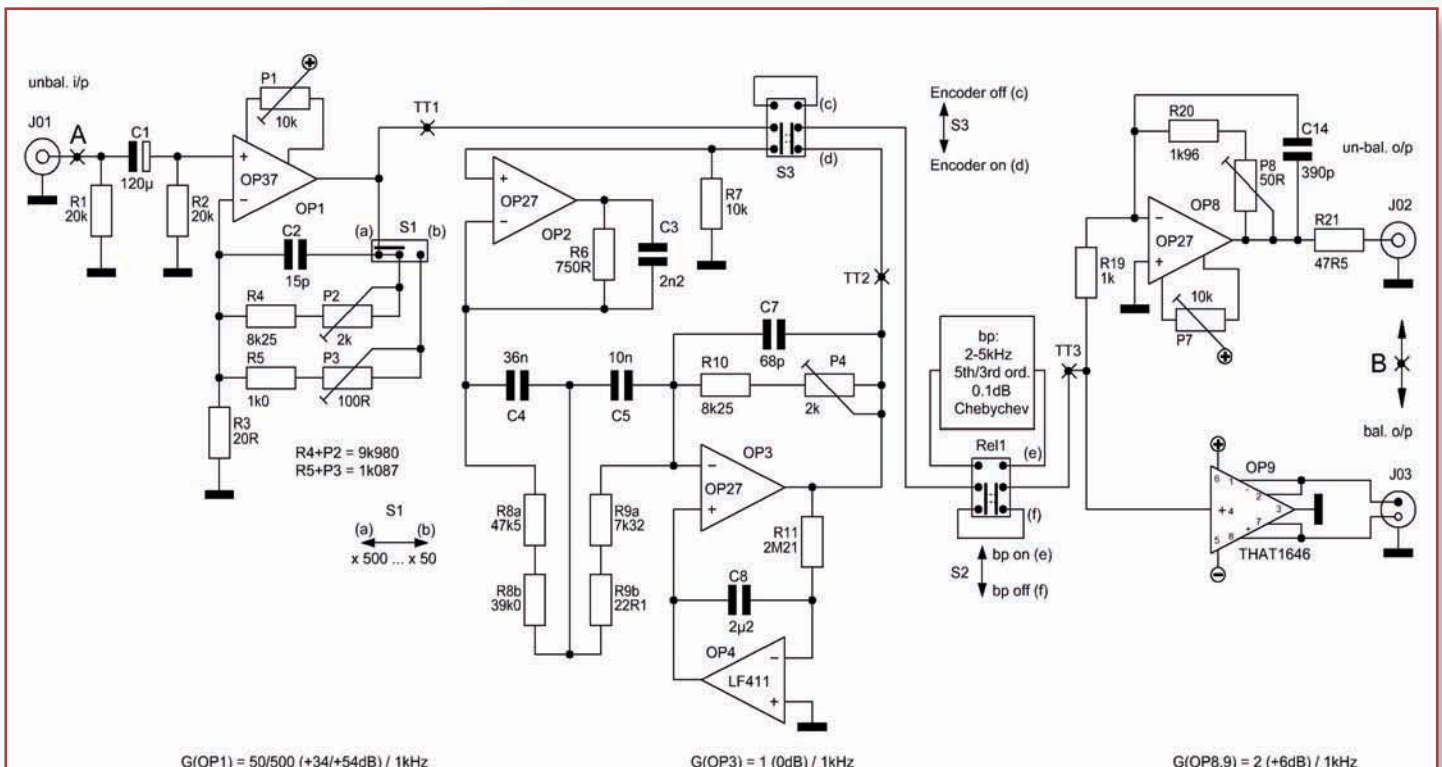


Figure 11: Circuitry of the measurement amp (OP1, OP8 and OP9) and ARIAA transfer function generator (OP2, 3, 4)

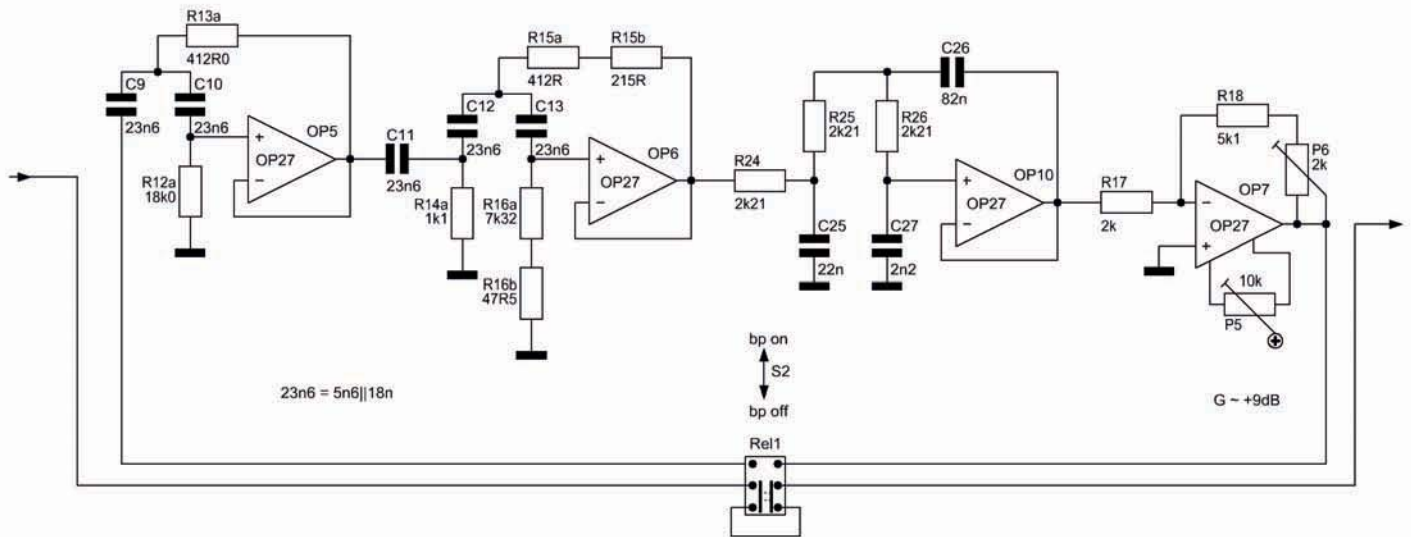


Figure 12: Filter section showing the 5th order 0.1dB Chebyshev 2.1kHz hp plus the 3rd order 0.1dB Chebyshev 5.1kHz lp that form the bp filter section

the little red book
Issue 9

flexible and specialist cables

CABLES
CONNECTING TODAY'S NEEDS

the little red book

- 128 pages of facts, figures, tables and technical specs
- Data, signal and control cables including many alternatives to Belden
- High temperature, robotics and rubber cables held in stock
- Next working-day delivery as standard, carriage paid on orders over £100
- Cut to length service on many products
- Commitment to service and delivery like no other cable company

Including Selected Tables From The 17th Edition Wiring Regulations

Call our sales team or email
littleredbook@fscables.com
for your free copy

• Tel: 01727 840 841
• www.fscables.com
• sales@fscables.com



PLC with PIC16F648A Microcontroller

Part 17

Macro	Symbol	Truth table																		
<pre>----- macro: decod_1_2 ----- decod_1_2 macro regs0,bits0, regd1,btd1,regd0,btd0 local L1,L2 btfss regs0,bits0 goto L2 bsf regd1,btd1 bcf regd0,btd0 goto L1 L2 bsf regd0,btd0 bcf regd1,btd1 L1 endm -----</pre>	<div><div>1x2 DECODER</div><div><div>A</div><div>d₀</div><div>d₁</div></div></div> <table><tr><td>A =</td><td>regs0,bits0</td></tr><tr><td>d0 =</td><td>regd0,btd0</td></tr><tr><td>d1 =</td><td>regd1,btd1</td></tr></table>	A =	regs0,bits0	d0 =	regd0,btd0	d1 =	regd1,btd1	<table><tr><th>input</th><th colspan="2">outputs</th></tr><tr><th>A</th><th>d0</th><th>d1</th></tr><tr><td>0</td><td>1</td><td>0</td></tr><tr><td>1</td><td>0</td><td>1</td></tr></table>	input	outputs		A	d0	d1	0	1	0	1	0	1
A =	regs0,bits0																			
d0 =	regd0,btd0																			
d1 =	regd1,btd1																			
input	outputs																			
A	d0	d1																		
0	1	0																		
1	0	1																		

Table 1: The macro "decod_1_2" together with its symbol and truth table

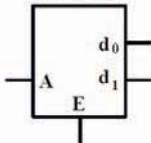
Macro	Symbol	Truth table																												
<pre>----- macro: decod_1_2_E ----- decod_1_2_E macro regs0,bits0, regd1,btd1,regd0,btd0 local L1,L2,L3 movwf Temp_1 btfss Temp_1,0 goto L2 btfss regs0,bits0 goto L3 bsf regd1,btd1 bcf regd0,btd0 goto L1 L3 bsf regd0,btd0 bcf regd1,btd1 goto L1 L2 bcf regd1,btd1 bcf regd0,btd0 L1 endm -----</pre>	<div><div>1x2 DECODER</div><div></div></div> <table><tr><td>W</td><td>E</td></tr><tr><td>A =</td><td>regs0,bits0</td></tr><tr><td>d0 =</td><td>regd0,btd0</td></tr><tr><td>d1 =</td><td>regd1,btd1</td></tr></table>	W	E	A =	regs0,bits0	d0 =	regd0,btd0	d1 =	regd1,btd1	<table><tr><th colspan="2">inputs</th><th colspan="2">outputs</th></tr><tr><th>E</th><th>A</th><th>d0</th><th>d1</th></tr><tr><td>0</td><td>×</td><td>0</td><td>0</td></tr><tr><td>1</td><td>0</td><td>1</td><td>0</td></tr><tr><td>1</td><td>1</td><td>0</td><td>1</td></tr></table> <p>×: don't care</p>	inputs		outputs		E	A	d0	d1	0	×	0	0	1	0	1	0	1	1	0	1
W	E																													
A =	regs0,bits0																													
d0 =	regd0,btd0																													
d1 =	regd1,btd1																													
inputs		outputs																												
E	A	d0	d1																											
0	×	0	0																											
1	0	1	0																											
1	1	0	1																											

Table 2: The macro "decod_1_2_E" together with its symbol and truth table

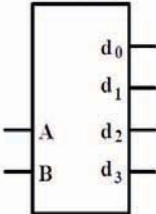
Macro	Symbol	Truth table																																																
<pre>----- macro: decod 2 4 ----- decod 2 4 macro regsl,bits1, regs0,bits0,regd3,btd3, regd2,btd2,regd1,btd1,regd0,btd0 local L1,L2,L3,L4 btfss regsl,bits1 goto L4 bcf regd1,btd1 bcf regd0,btd0 btfss regs0,bits0 goto L3 bsf regd3,btd3 bcf regd2,btd2 goto L1 L4 bcf regd3,btd3 bcf regd2,btd2 btfss regs0,bits0 goto L2 bsf regd1,btd1 bcf regd0,btd0 goto L1 L3 bcf regd3,btd3 bsf regd2,btd2 goto L1 L2 bcf regd1,btd1 bsf regd0,btd0 endm -----</pre>	<p>2x4 DECODER</p>  <table><tr><td>A =</td><td>regsl,bits1</td></tr><tr><td>B =</td><td>regs0,bits0</td></tr><tr><td>d3 =</td><td>regd3,btd3</td></tr><tr><td>d2 =</td><td>regd2,btd2</td></tr><tr><td>d1 =</td><td>regd1,btd1</td></tr><tr><td>d0 =</td><td>regd0,btd0</td></tr></table>	A =	regsl,bits1	B =	regs0,bits0	d3 =	regd3,btd3	d2 =	regd2,btd2	d1 =	regd1,btd1	d0 =	regd0,btd0	<table><tr><th colspan="2">inputs</th><th colspan="4">outputs</th></tr><tr><th>A</th><th>B</th><th>d0</th><th>d1</th><th>d2</th><th>d3</th></tr><tr><td>0</td><td>0</td><td>1</td><td>0</td><td>0</td><td>0</td></tr><tr><td>0</td><td>1</td><td>0</td><td>1</td><td>0</td><td>0</td></tr><tr><td>1</td><td>0</td><td>0</td><td>0</td><td>1</td><td>0</td></tr><tr><td>1</td><td>1</td><td>0</td><td>0</td><td>0</td><td>1</td></tr></table>	inputs		outputs				A	B	d0	d1	d2	d3	0	0	1	0	0	0	0	1	0	1	0	0	1	0	0	0	1	0	1	1	0	0	0	1
A =	regsl,bits1																																																	
B =	regs0,bits0																																																	
d3 =	regd3,btd3																																																	
d2 =	regd2,btd2																																																	
d1 =	regd1,btd1																																																	
d0 =	regd0,btd0																																																	
inputs		outputs																																																
A	B	d0	d1	d2	d3																																													
0	0	1	0	0	0																																													
0	1	0	1	0	0																																													
1	0	0	0	1	0																																													
1	1	0	0	0	1																																													

Table 3: The macro "decod_2_4" together with its symbol and truth table

Professor Dr Murat

Uzam from Nigde

University in Turkey

presents a series of articles on a project that focuses on a microcontroller-based PLC. This article describes decoder macros

IN THIS ARTICLE the following decoder macros are described: decod_1_2 (1x2 decoder), decod_1_2_E (1x2 decoder with Enable input), decod_2_4 (2x4 decoder), decod_2_4_E (2x4 decoder with Enable input), decod_3_8 (3x8 decoder), decod_3_8_E (3x8 decoder with Enable input). Four examples will be provided in the next article to show the applicability of these decoder macros.

Decoder Macros

A decoder is a circuit that changes a code into a set of signals. A common type of decoder is the line decoder which takes an m -bit binary input data and decodes it into 2^m data lines. As a standard combinational component a decoder asserts one out of n output lines, depending on the value of an m -bit binary input data. The general form of an m -to- n decoder can be seen in **Figure 1**.

In general, an m -to- n decoder has m input lines, $i_{m-1} \dots i_1, i_0$, and n output lines $d_{n-1} \dots d_1, d_0$, where $n = 2^m$. Although, not shown in Figure 1, in addition, it may have an enable line, E , for enabling the decoder. When the decoder is disabled with E set to 0 (for active-high enable input E), all the output lines are de-asserted. When the decoder is enabled, then the output line whose index is equal to the value of the input binary data is asserted (set to 1 for active-high), while the rest of the output lines are de-asserted (set to 0 for active-high). A decoder is used in a system having multiple components, and we want only one component to be selected or enabled at any one time.

In this article, there are six decoder macros, namely decod_1_2 (1x2 decoder), decod_1_2_E (1x2 decoder with Enable input), decod_2_4 (2x4 decoder), decod_2_4_E (2x4 decoder with Enable input), decod_3_8 (3x8 decoder), decod_3_8_E (3x8 decoder with Enable input), described for UZAM_PLC as shown in **Tables 1, 2...6**.

Let us now consider these macros.

The macro "decod_1_2" is shown in Table 1, together with its symbol and truth table. In this macro, A is a Boolean input variable taken into the macro through "regs0.bits0" and it represents the selected input; "d₀" and "d₁" are Boolean output variables produced as outputs through "regd0.bitd0" and "regd1.bitd1" respectively, and they represent two output signals. In this decoder, when the select input is A = 0, the output line, d₀, is asserted (set to 1 for active-high) and output line, d₁ is de-asserted (set to 0 for active-high). Similarly, when the select input is A = 1, the output line, d₁, is asserted (set to 1 for active-high) and output line, d₀, is de-asserted (set to 0 for active-high).

The macro "decod_1_2_E" is shown in Table 2, together with its symbol and truth table. In addition to the "decod_1_2", this decoder macro has an active-high enable line, E, for enabling it. In this macro, E is a Boolean input variable taken into the macro through W. When this decoder is disabled with E set to 0, all output lines are de-asserted (set to 0 for active-high). When this decoder is enabled with E set to 1, it functions as described for "decod_1_2".

The macro "decod_2_4" is shown in Table 3, together with its symbol and truth table. In this macro, A (MSB – most significant bit) and B are Boolean input variables taken into the macro through "regs1.bits1" and "regs0.bits0" respectively and they represent the select inputs; "d₀", "d₁", "d₂" and "d₃" are Boolean output variables produced as outputs through "regd0.bitd0", "regd1.bitd1", "regd2.bitd2" and "regd3.bitd3" respectively, and they represent four output signals. In this decoder, when the select inputs are AB = 00 (respectively 01, 10, 11), the output line, d₀ (respectively d₁, d₂, d₃), is asserted (set to 1 for active-high) and all other output lines are de-asserted (set to 0 for active-high).

The macro "decod_2_4_E" is shown in Table 4, together with its symbol and truth table. In addition to the "decod_2_4", this decoder macro has an active-high enable line, E, for enabling it. In this macro, E is a Boolean input variable taken into the macro through W. When this decoder is disabled with E set to 0, all output lines are de-asserted (set to 0 for active-high). When this decoder is enabled with E set to 1, it functions as described for "decod_2_4".

Macro	Symbol	Truth table																																																															
<pre>----- macro: decod_2_4_E ----- decod_2_4_E macro regs1.bits1, regs0.bitd0,regd3.bitd3,regd2.bitd2, regd1.bitd1,regd0.bitd0 local L1,L2,L3,L4,L5 movwf Temp_1 btfss Temp_1,0 goto L2 btfss regs1.bits1 goto L5 bcf regd1.bitd1 bcf regd0.bitd0 btfss regs0.bitd0 goto L4 bsf regd3.bitd3 bcf regd2.bitd2 goto L1 L5: bcf regd3.bitd3 bcf regd2.bitd2 btfss regs0.bitd0 goto L3 bsf regd1.bitd1 bcf regd0.bitd0 goto L1 L4: bcf regd3.bitd3 bsf regd2.bitd2 goto L1 L3: bcf regd1.bitd1 bsf regd0.bitd0 goto L1 L2: bcf regd3.bitd3 bcf regd2.bitd2 bcf regd1.bitd1 bcf regd0.bitd0 L1: endm -----</pre>	<p>2x4 DECODER</p> <table><tr><th>W</th><th>E</th></tr><tr><td>A =</td><td>regs1.bits1</td></tr><tr><td>B =</td><td>regs0.bitd0</td></tr><tr><td>d3 =</td><td>regd3.bitd3</td></tr><tr><td>d2 =</td><td>regd2.bitd2</td></tr><tr><td>d1 =</td><td>regd1.bitd1</td></tr><tr><td>d0 =</td><td>regd0.bitd0</td></tr></table>	W	E	A =	regs1.bits1	B =	regs0.bitd0	d3 =	regd3.bitd3	d2 =	regd2.bitd2	d1 =	regd1.bitd1	d0 =	regd0.bitd0	<table><tr><th colspan="3">inputs</th><th colspan="4">outputs</th></tr><tr><th>E</th><th>A</th><th>B</th><th>d0</th><th>d1</th><th>d2</th><th>d3</th></tr><tr><td>0</td><td>x</td><td>x</td><td>0</td><td>0</td><td>0</td><td>0</td></tr><tr><td>1</td><td>0</td><td>0</td><td>1</td><td>0</td><td>0</td><td>0</td></tr><tr><td>1</td><td>0</td><td>1</td><td>0</td><td>1</td><td>0</td><td>0</td></tr><tr><td>1</td><td>1</td><td>0</td><td>0</td><td>0</td><td>1</td><td>0</td></tr><tr><td>1</td><td>1</td><td>1</td><td>0</td><td>0</td><td>0</td><td>1</td></tr></table> <p>x: don't care</p>	inputs			outputs				E	A	B	d0	d1	d2	d3	0	x	x	0	0	0	0	1	0	0	1	0	0	0	1	0	1	0	1	0	0	1	1	0	0	0	1	0	1	1	1	0	0	0	1
W	E																																																																
A =	regs1.bits1																																																																
B =	regs0.bitd0																																																																
d3 =	regd3.bitd3																																																																
d2 =	regd2.bitd2																																																																
d1 =	regd1.bitd1																																																																
d0 =	regd0.bitd0																																																																
inputs			outputs																																																														
E	A	B	d0	d1	d2	d3																																																											
0	x	x	0	0	0	0																																																											
1	0	0	1	0	0	0																																																											
1	0	1	0	1	0	0																																																											
1	1	0	0	0	1	0																																																											
1	1	1	0	0	0	1																																																											

Table 4: The macro "decod_2_4_E" together with its symbol and truth table

Macro	Symbol	Truth table																																																																																																														
<pre>----- macro: decod_3_8 ----- decod_3_8 macro regs2.bits2,regs1.bits1, regs0.bits0,regd7.bitd7,regd6.bitd6, regd5.bitd5,regd4.bitd4,regd3.bitd3, regd2.bitd2,regd1.bitd1,regd0.bitd0 local L1,L2,L3,L4,L5,L6,L7,L8 btfss regs2.bits2 goto L8 bcf regd3.bitd3 bcf regd2.bitd2 bcf regd1.bitd1 bcf regd0.bitd0 btfss regs1.bits1 goto L7 bcf regd5.bitd5 bcf regd4.bitd4 btfss regs0.bits0 goto L6 bcf regd7.bitd7 bcf regd6.bitd6 goto L1 L8 bcf regd7.bitd7 bcf regd6.bitd6 bcf regd5.bitd5 bcf regd4.bitd4 btfss regs1.bits1 goto L4 bcf regd1.bitd1 bcf regd0.bitd0 btfss regs0.bits0 goto L3 bcf regd3.bitd3 bcf regd2.bitd2 goto L1 L7 bcf regd7.bitd7 bcf regd6.bitd6 btfss regs0.bits0 goto L5 bsf regd5.bitd5 bcf regd4.bitd4 goto L1 L6 bcf regd7.bitd7 bcf regd6.bitd6 goto L1 L5 bcf regd5.bitd5 bcf regd4.bitd4 goto L1 L4 bcf regd3.bitd3 bcf regd2.bitd2 btfss regs0.bits0 goto L2 bsf regd1.bitd1 bcf regd0.bitd0 goto L1 L3 bcf regd3.bitd3 bcf regd2.bitd2 goto L1 L2 bcf regd1.bitd1 bcf regd0.bitd0 L1 endm -----</pre>	<p>3x8 DECODER</p> <p>A = regs2.bits2 B = regs1.bits1 C = regs0.bits0 d7 = rego7.bitd7 d6 = rego6.bitd6 d5 = rego5.bitd5 d4 = rego4.bitd4 d3 = rego3.bitd3 d2 = rego2.bitd2 d1 = rego1.bitd1 d0 = rego0.bitd0</p>	<table><tr><th colspan="3">inputs</th><th colspan="8">outputs</th></tr><tr><th>A</th><th>B</th><th>C</th><th>d0</th><th>d1</th><th>d2</th><th>d3</th><th>d4</th><th>d5</th><th>d6</th><th>d7</th></tr><tr><td>0</td><td>0</td><td>0</td><td>1</td><td>0</td><td>0</td><td>0</td><td>0</td><td>0</td><td>0</td><td>0</td></tr><tr><td>0</td><td>0</td><td>1</td><td>0</td><td>1</td><td>0</td><td>0</td><td>0</td><td>0</td><td>0</td><td>0</td></tr><tr><td>0</td><td>1</td><td>0</td><td>0</td><td>0</td><td>1</td><td>0</td><td>0</td><td>0</td><td>0</td><td>0</td></tr><tr><td>0</td><td>1</td><td>1</td><td>0</td><td>0</td><td>0</td><td>1</td><td>0</td><td>0</td><td>0</td><td>0</td></tr><tr><td>1</td><td>0</td><td>0</td><td>0</td><td>0</td><td>0</td><td>0</td><td>1</td><td>0</td><td>0</td><td>0</td></tr><tr><td>1</td><td>0</td><td>1</td><td>0</td><td>0</td><td>0</td><td>0</td><td>0</td><td>1</td><td>0</td><td>0</td></tr><tr><td>1</td><td>1</td><td>0</td><td>0</td><td>0</td><td>0</td><td>0</td><td>0</td><td>0</td><td>1</td><td>0</td></tr><tr><td>1</td><td>1</td><td>1</td><td>0</td><td>0</td><td>0</td><td>0</td><td>0</td><td>0</td><td>0</td><td>1</td></tr></table>	inputs			outputs								A	B	C	d0	d1	d2	d3	d4	d5	d6	d7	0	0	0	1	0	0	0	0	0	0	0	0	0	1	0	1	0	0	0	0	0	0	0	1	0	0	0	1	0	0	0	0	0	0	1	1	0	0	0	1	0	0	0	0	1	0	0	0	0	0	0	1	0	0	0	1	0	1	0	0	0	0	0	1	0	0	1	1	0	0	0	0	0	0	0	1	0	1	1	1	0	0	0	0	0	0	0	1
inputs			outputs																																																																																																													
A	B	C	d0	d1	d2	d3	d4	d5	d6	d7																																																																																																						
0	0	0	1	0	0	0	0	0	0	0																																																																																																						
0	0	1	0	1	0	0	0	0	0	0																																																																																																						
0	1	0	0	0	1	0	0	0	0	0																																																																																																						
0	1	1	0	0	0	1	0	0	0	0																																																																																																						
1	0	0	0	0	0	0	1	0	0	0																																																																																																						
1	0	1	0	0	0	0	0	1	0	0																																																																																																						
1	1	0	0	0	0	0	0	0	1	0																																																																																																						
1	1	1	0	0	0	0	0	0	0	1																																																																																																						

Table 5: The macro "decod_3_8" together with its symbol and truth table

The macro "decod_3_8" is shown in Table 5, together with its symbol and truth table. In this macro, A (MSB), B and C (LSB – least significant bit) are Boolean input variables taken into the macro through "regs2, bits2", "regs1, bits1" and "regs0, bits0" respectively and they represent the select inputs; "d₀", "d₁", "d₂", "d₃", "d₄", "d₅", "d₆" and "d₇" are Boolean output variables produced as outputs through "regd0, bitd0", "regd1, bitd1", "regd2, bitd2", "regd3, bitd3", "regd4, bitd4", "regd5, bitd5", "regd6, bitd6" and "regd7, bitd7" respectively, and they represent eight output signals. In this decoder, when the select inputs are ABC = 000 (respectively 001, 010, 011, 100, 101, 110, 111), the output line, d₀ (respectively d₁, d₂, d₃, d₄, d₅, d₆, d₇), is asserted (set to 1 for active-high) and all other output lines are de-asserted (set to 0 for active-high).

The macro "decod_3_8_E" is shown in Table 6, together with its symbol and truth table. In addition to the "decod_3_8", this decoder macro has an active-high enable line, E, for enabling it. In this macro, E is a Boolean input variable taken into the macro through W. When this decoder is disabled with E set to 0, all output lines are de-asserted (set to 0 for active-high). When this decoder is enabled with E set to 1, it functions as described for "decod_3_8".

The file "dcd_r_mcr_def.inc" including the six decoder macros shown in Tables 1, 2...6 can be downloaded from <http://host.nigde.edu.tr/muzam/>.

Macro	Symbol	Truth table																																																																																																																																																												
<pre>----- macro: decod_3_8_E ----- decod_3_8_E macro regs2, bits2, regs1, bits1, regs0, bits0, regd7, bitd7, regd6, bitd6, regd5, bitd5, regd4, bitd4, regd3, bitd3, regd2, bitd2, regd1, bitd1, regd0, bitd0 local L1, L2, L3, L4, L5, L6, L7, L8, L9 movwf Temp_1 btfss Temp_1, 0 goto L2 btfss regs2, bits2 goto L9 bcf regd3, bitd3 bcf regd2, bitd2 bcf regd1, bitd1 bcf regd0, bitd0 btfss regs1, bits1 goto L8 bcf regd5, bitd5 bcf regd4, bitd4 btfss regs0, bits0 goto L7 bsf regd7, bitd7 bcf regd6, bitd6 goto L1 L9 bcf regd7, bitd7 bcf regd6, bitd6 bcf regd5, bitd5 bcf regd4, bitd4 btfss regs1, bits1 goto L5 bcf regd1, bitd1 bcf regd0, bitd0 btfss regs0, bits0 goto L4 bsf regd3, bitd3 bcf regd2, bitd2 goto L1 L8 bcf regd7, bitd7 bcf regd6, bitd6 btfss regs0, bits0 goto L6 bsf regd5, bitd5 bcf regd4, bitd4 goto L1 L7 bcf regd7, bitd7 bsf regd6, bitd6 goto L1 L6 bcf regd5, bitd5 bsf regd4, bitd4 goto L1 L5 bcf regd3, bitd3 bcf regd2, bitd2 btfss regs0, bits0 goto L3 bsf regd1, bitd1 bcf regd0, bitd0 goto L1 L4 bcf regd3, bitd3 bsf regd2, bitd2 goto L1 L3 bcf regd1, bitd1 bsf regd0, bitd0 goto L1 L2 bcf regd7, bitd7 bcf regd6, bitd6 bcf regd5, bitd5 bcf regd4, bitd4 bcf regd3, bitd3 bcf regd2, bitd2 bcf regd1, bitd1 bcf regd0, bitd0 L1 endm -----</pre>	<div>3x8 DECODER</div>	<table><tr><th colspan="4">inputs</th><th colspan="8">outputs</th></tr><tr><th>E</th><th>A</th><th>B</th><th>C</th><th>d0</th><th>d1</th><th>d2</th><th>d3</th><th>d4</th><th>d5</th><th>d6</th><th>d7</th></tr><tr><td>0</td><td>0</td><td>0</td><td>0</td><td>0</td><td>0</td><td>0</td><td>0</td><td>0</td><td>0</td><td>0</td><td>0</td></tr><tr><td>1</td><td>0</td><td>0</td><td>0</td><td>1</td><td>0</td><td>0</td><td>0</td><td>0</td><td>0</td><td>0</td><td>0</td></tr><tr><td>1</td><td>0</td><td>0</td><td>1</td><td>0</td><td>1</td><td>0</td><td>0</td><td>0</td><td>0</td><td>0</td><td>0</td></tr><tr><td>1</td><td>0</td><td>1</td><td>0</td><td>0</td><td>0</td><td>1</td><td>0</td><td>0</td><td>0</td><td>0</td><td>0</td></tr><tr><td>1</td><td>0</td><td>1</td><td>1</td><td>0</td><td>0</td><td>0</td><td>1</td><td>0</td><td>0</td><td>0</td><td>0</td></tr><tr><td>1</td><td>1</td><td>0</td><td>0</td><td>0</td><td>0</td><td>0</td><td>0</td><td>1</td><td>0</td><td>0</td><td>0</td></tr><tr><td>1</td><td>1</td><td>0</td><td>1</td><td>0</td><td>0</td><td>0</td><td>0</td><td>0</td><td>1</td><td>0</td><td>0</td></tr><tr><td>1</td><td>1</td><td>1</td><td>0</td><td>0</td><td>0</td><td>0</td><td>0</td><td>0</td><td>0</td><td>1</td><td>0</td></tr><tr><td>1</td><td>1</td><td>1</td><td>1</td><td>0</td><td>0</td><td>0</td><td>0</td><td>0</td><td>0</td><td>0</td><td>1</td></tr></table> <p>0 = don't care</p> <table><tr><th>W</th><th>E</th></tr><tr><td>A =</td><td>regs2, bits2</td></tr><tr><td>B =</td><td>regs1, bits1</td></tr><tr><td>C =</td><td>regs0, bits0</td></tr><tr><td>d7 =</td><td>regd7, bitd7</td></tr><tr><td>d6 =</td><td>regd6, bitd6</td></tr><tr><td>d5 =</td><td>regd5, bitd5</td></tr><tr><td>d4 =</td><td>regd4, bitd4</td></tr><tr><td>d3 =</td><td>regd3, bitd3</td></tr><tr><td>d2 =</td><td>regd2, bitd2</td></tr><tr><td>d1 =</td><td>regd1, bitd1</td></tr><tr><td>d0 =</td><td>regd0, bitd0</td></tr></table>	inputs				outputs								E	A	B	C	d0	d1	d2	d3	d4	d5	d6	d7	0	0	0	0	0	0	0	0	0	0	0	0	1	0	0	0	1	0	0	0	0	0	0	0	1	0	0	1	0	1	0	0	0	0	0	0	1	0	1	0	0	0	1	0	0	0	0	0	1	0	1	1	0	0	0	1	0	0	0	0	1	1	0	0	0	0	0	0	1	0	0	0	1	1	0	1	0	0	0	0	0	1	0	0	1	1	1	0	0	0	0	0	0	0	1	0	1	1	1	1	0	0	0	0	0	0	0	1	W	E	A =	regs2, bits2	B =	regs1, bits1	C =	regs0, bits0	d7 =	regd7, bitd7	d6 =	regd6, bitd6	d5 =	regd5, bitd5	d4 =	regd4, bitd4	d3 =	regd3, bitd3	d2 =	regd2, bitd2	d1 =	regd1, bitd1	d0 =	regd0, bitd0
inputs				outputs																																																																																																																																																										
E	A	B	C	d0	d1	d2	d3	d4	d5	d6	d7																																																																																																																																																			
0	0	0	0	0	0	0	0	0	0	0	0																																																																																																																																																			
1	0	0	0	1	0	0	0	0	0	0	0																																																																																																																																																			
1	0	0	1	0	1	0	0	0	0	0	0																																																																																																																																																			
1	0	1	0	0	0	1	0	0	0	0	0																																																																																																																																																			
1	0	1	1	0	0	0	1	0	0	0	0																																																																																																																																																			
1	1	0	0	0	0	0	0	1	0	0	0																																																																																																																																																			
1	1	0	1	0	0	0	0	0	1	0	0																																																																																																																																																			
1	1	1	0	0	0	0	0	0	0	1	0																																																																																																																																																			
1	1	1	1	0	0	0	0	0	0	0	1																																																																																																																																																			
W	E																																																																																																																																																													
A =	regs2, bits2																																																																																																																																																													
B =	regs1, bits1																																																																																																																																																													
C =	regs0, bits0																																																																																																																																																													
d7 =	regd7, bitd7																																																																																																																																																													
d6 =	regd6, bitd6																																																																																																																																																													
d5 =	regd5, bitd5																																																																																																																																																													
d4 =	regd4, bitd4																																																																																																																																																													
d3 =	regd3, bitd3																																																																																																																																																													
d2 =	regd2, bitd2																																																																																																																																																													
d1 =	regd1, bitd1																																																																																																																																																													
d0 =	regd0, bitd0																																																																																																																																																													

Table 6: The macro "decod_3_8_E" together with its symbol and truth table

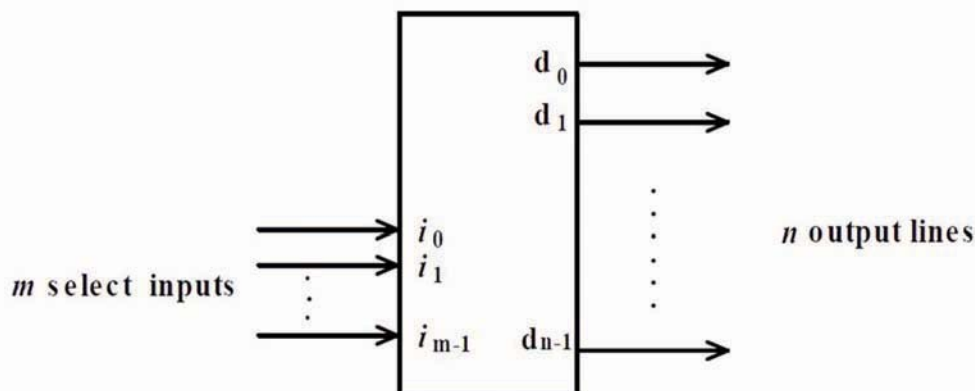


Figure 1: The general form of an m -to- n decoder, where $n = 2^m$

LOG DOMAIN HYBRID DESIGN: BLOCK MODEL AND STATE SPACE SYNTHESIS

THE CLASS OF log domain filters is a new member of current mode active continuous time filters, also known as ELIN (Externally Linear Internally Nonlinear) filters, ESS (Exponential State Space) filters and translinear filters.

Log domain filters are suitable for low voltage/low power applications. The filters are highly linear, have low distortion and are electronically tunable; advantages that make log domain filters so interesting. Only transistors, capacitors and current sources are required to design this type of filters. General block diagrams of log domain filters are shown in **Figure 1**.

Essentially, this class of circuits, based on the principles of translinear circuits, run in nonlinear fashion whilst keeping the transfer function linear.

Log domain filters use the idea of *companding* (Compressing and Expanding) signal processing. The input current is first compressed using a logarithmic function while it is forced to drive a BJT transistor, since the emitter-base voltage of the device is logarithmic of the current.

The output circuitry has an expanding block, which means that the output voltage is applied to a BJT's base-emitter junction in order to obtain a current that is an exponential of the voltage. Since the output function is a reverse function of the input function, the overall transfer function remains linear without using any element to linearize it. Therefore, there is no need for additional components to operate the circuit in the linear region. As such, the dynamic range is increased by using a companding signal processing strategy. A comparison of the classical signal processing procedure and log domain signal processing are depicted in **Figure 2**.

Let us focus on hybrid synthesis method of log domain filters. Detailed synthesis steps are given in **Table 1**. This table describes how to realize the blocks with circuits and what terminal equation the blocks have.

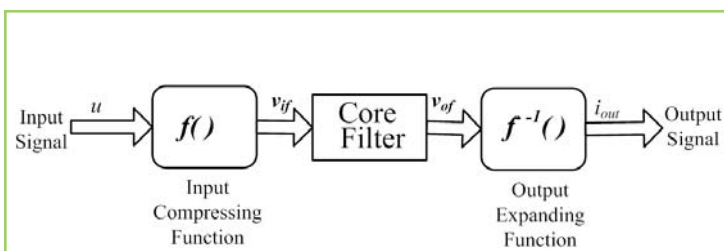


Figure 1: General functional structure

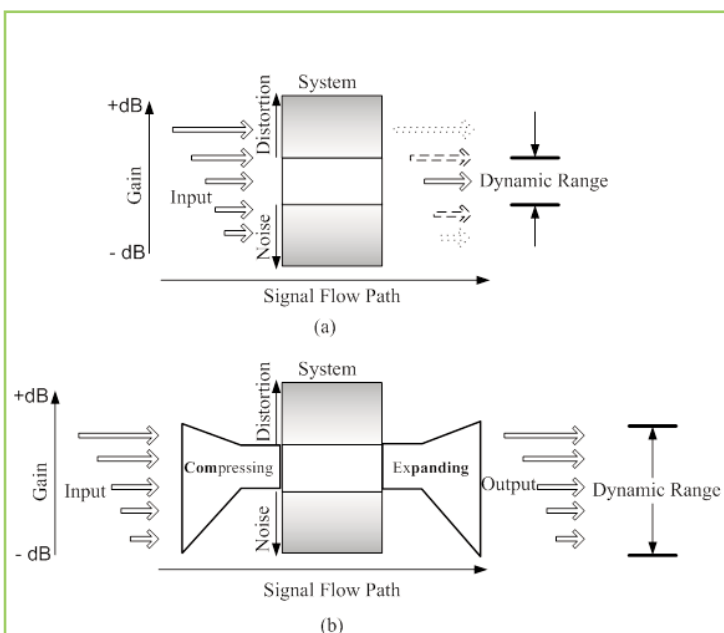


Figure 2: (a) Classical signal processing procedure
(b) Log domain signal processing procedure

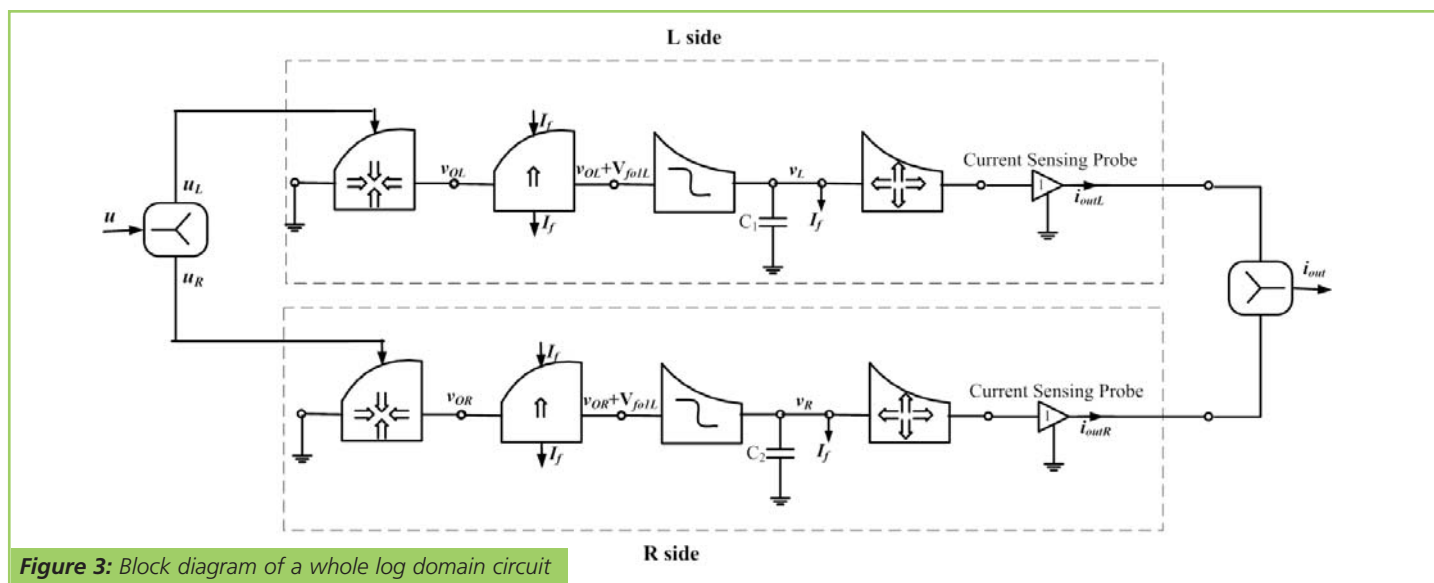


Figure 3: Block diagram of a whole log domain circuit

Classification	Mathematical Equation	Block	BJT Circuit	Function
Logarithmic Converter	$ V_a - V_b = V_T \ln \frac{I_f}{I_s}$			Increasing Level $v_b > v_a$
				Decreasing Level $v_a > v_b$
	$ v_a - v_b = V_T \ln \frac{U}{I_s}$			Pressing
Exponential Converter	$i = I_s e^{\frac{v_a - v_b}{V_T}}$			Nonlinear Converting
	$i_{out} = I_s e^{\frac{v_a - v_b}{V_T}}$			Expanding

Table 1: Detailed block investigation

Design of A First Order Low Pass Filter

First order low pass filter transfer function can be written as:

$$H(s) = \frac{Y(s)}{U(s)} = \frac{\omega_o}{s + \omega_o} \quad (1)$$

where ω_o is the cutoff frequency.

According to class AB circuit design, we process the signal in two parts which are named as "L" side and "R" side. Both sides have same architecture blocks. The relationship of L, R and the original signals is shown in **Equation 2**. The input signal is split into two pieces by using a current splitter. The outputs of both sides are also collected in summery blocks to obtain the general output of the low pass filter.

$$\begin{aligned} X &= X_L - X_R \\ U &= U_L - U_R \end{aligned} \quad (2)$$

Since the equations of both sides are similar, only the equations of the L side will be given from now on. State space representation of the transfer function is given in the following equations:

$$\dot{x}_{1L} = -\omega_o x_{1L} + \omega_o u_L \quad (3)$$

$$y_L = x_{1L} \quad (4)$$

A nonlinear mapping transformation is applied to the state space variables and the input signal of each side is as following:

$$\begin{aligned} x_L &= I_s e^{\frac{v_L}{V_T}} \\ u_L &= I_s e^{\frac{v_{OL}}{V_T}} \end{aligned} \quad (5)$$

After some basic manipulation, **Equation 6** is obtained. This equation is written for a node that a grounded capacitor is tied to.

$$\begin{aligned} C \dot{v}_L &= I_s e^{\frac{v_{OL} + V_f - v_L}{V_T}} - I_s e^{\frac{v_R}{V_T}} \\ y_L &= I_s e^{\frac{v_L}{V_T}} \end{aligned} \quad (6)$$

Here:

$$\begin{aligned} V_f &= V_T \ln \frac{I_f}{I_s} \\ I_f &= \omega_o C V_T \end{aligned}$$

I_f is a constant value; it can be represented by a current source. The natural frequency of the filter can be tuned electronically by varying the values of the current sources of the circuit.

By using this nodal equation, block diagram of whole circuit can be obtained as shown in **Figure 3**.

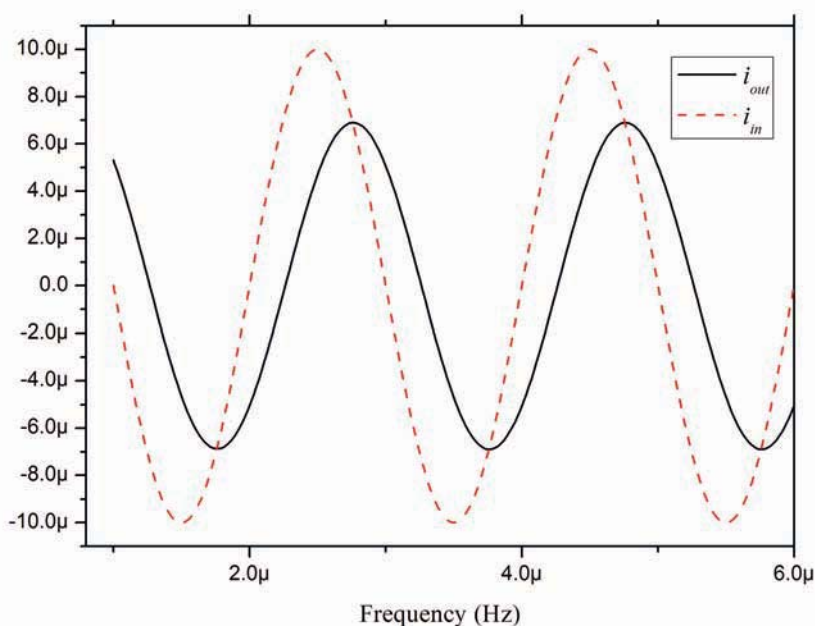
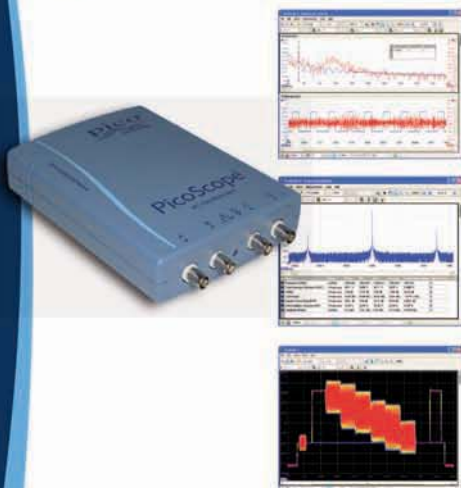


Figure 4: Time response of the filter



The new PicoScope 4000 Series high-resolution oscilloscopes

PicoScope 4000 Series



The PicoScope 4224 and 4424 High Resolution Oscilloscopes have true 12-bit resolution inputs with a vertical accuracy of 1%. This latest generation of PicoScopes features a deep memory of 32 M samples. When combined with rapid trigger mode, this can capture up to 1000 trigger events at a rate of thousands of waveforms per second.

- **PC-based** - capture, view and use the acquired waveform on your PC, right where you need it
- **Software updates** - free software updates for the life of the product
- **USB powered and connected** - perfect for use in the field or the lab
- **Programmable** - supplied with drivers and example code

Resolution	12 bits (up to 16 bits with resolution enhancement)
Bandwidth	20 MHz (for oscilloscope and spectrum modes)
Buffer Size	32 M samples shared between active channels
Sample Rate	80 MS/s maximum
Channels	PicoScope 4224: 2 channels PicoScope 4424: 4 channels
Connection	USB 2.0
Trigger Types	Rising edge, falling edge, edge with hysteresis, pulse width, runt pulse, drop out, windowed

www.picotech.com/scope1058
01480 396395

Simulation Result

The designed first order low-pass filter is simulated in PSpice using the CBIC-R transistor model. The circuit supply voltage is selected to be 3V. The value for capacitances of the integrators is chosen to be 123pF. DC current sources are swept from 0.5μA to 80μA to tune the cutoff frequencies. Time domain and frequency domain analysis are performed. The obtained results are given in **Figures 4, 5 and 6**.

Remzi Arslanalp, Saziye Surav Yilmaz and Abdullah T. Tola
Pamukkale University
Turkey

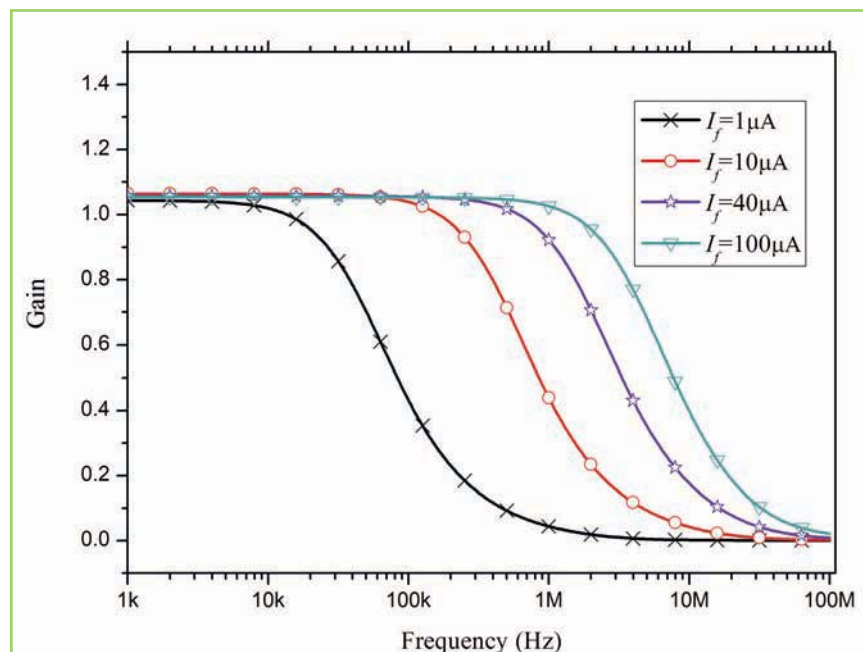


Figure 5: Frequency response of the filter

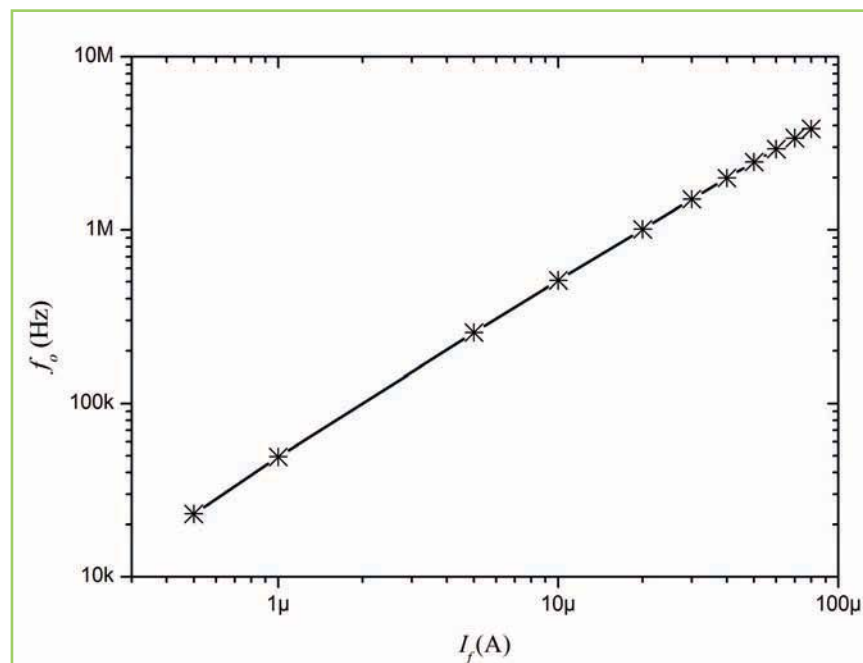
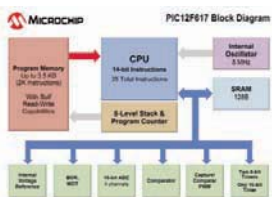


Figure 6: Varying I_f to tune f_o

MICROCHIP ADDS SELF-PROGRAMMABLE FLASH MEMORY TO 8-BIT FAMILY

Microchip has announced a new member of its popular 8- and 14-pin PIC16F61X 8-bit PIC microcontroller (MCU) family, targeting cost-effective general-purpose applications.

The PIC12F617 MCU features 3.5kbyte of self-programmable Flash program memory and



peripherals such as a 10-bit Analogue-to-Digital Converter (ADC), comparator, Pulse-Width Modulator (PWM) and VREF for closed-loop-control

applications, all in a miniature 3mm x 3mm DFN package. The memory offers a self read-write capability, which serves as a low-cost alternative to data EEPROM and is useful when an application requires remote updates, or the ability to store system data or look-up tables.

The microcontroller features an 8MHz internal oscillator, an on-chip 4-channel 10-bit ADC, a comparator with hysteresis and a PWM with complementary outputs that provide a framework for applications such as LED lighting control, motor control, capacitive touch keys and system monitors.

Microchip also announced a price reduction on the rest of the PIC16F61X family members.

www.microchip.com

LASER-BASED SENSING IN M18 HOUSING

Panasonic Electric Works UK Ltd now offers a range of M18 style Photo Electric Sensors using visible laser light as its light source.

The highly visible laser light (class 1) allows the sensor to be easily aligned and, due to the small beam size, can detect objects accurately. Housed in the industry standard M18 package, the sensors are available in two formats, axial and radial. The radial versions allow the sensor to be mounted at 90° to the sensing plane.

Plastic and Metal versions are available with either a 2m cable or M12 connector and offer the following sensing types are available:

Thru-beam	Range	Radial: 50m	Axial: 60m
Retroreflective	Range	Radial: 9m	Axial: 16m
Reflective	Range	Radial: 250mm	Axial: 350mm

The supply voltage range is 10-30VDC and both PNP and NPN outputs are available, capable of switching up to 100mA. Environmental protection is to IP67 with an operating temperature range of -10° to 50°C.

www.panasonic.com



AVX EXPANDS MINIATURE SINGLE-SIDED SSL CONNECTOR SERIES

AVX Corporation, a leading manufacturer of advanced passive components and interconnect solutions, has expanded its 9159 Series solid-state lighting connector offering to include a miniature, single-sided SMT connector for PCB strip lighting applications.

The robust 5A connectors provide reliable board-to-board connection for end-to-end board mating, also known as "butt mating", which optimizes LED spacing for maximum optical performance. The 9159



Series LED connectors feature a slide-top receptacle that enables quick and easy in-field repair and replacement once the lighting fixture has been installed. The connectors also include a shorting socket and locking mechanism to ensure positive attachment and to meet emerging harsh environment SSL system requirements. Optional wire-to-board plug connectors are also available with the standard receptacle to get power and signals onto the board.

The two-piece wire-to-board connector is typically surface mounted to the top side of the PCB.

www.avx.com

NEW 19-WAY COMMERCIAL POGO PIN CONNECTOR FROM ITT INTERCONNECT SOLUTIONS

The new 19-way commercial pogo pin connector from ITT Interconnect Solutions ensures 100% effective EMI shielding in high cycle count applications. They meet the stringent electrical and mechanical specifications required in demanding environments including medical test and diagnostic equipment such as diagnostic imaging systems.



Rated to IP 55, this new interconnect solution also suits other harsh environment applications including commercial aircraft electronics, instrumentation, and industrial equipment.

ITT ICS's 19-way Pogo pin interconnect features the company's proprietary pogo pin technology which achieves low contact resistance of under 10mΩ and ensures reliable and robust performance of over 5,000 mating cycles. The commercial pogo cable assembly (including bulkhead, front mount, receptacle cable assembly, plug with RJ45 and in-line plug to jack assembly) also provides exceptional EMI shielding with 100% effectiveness through the entire assembly.

www.ittcannon.com

RITTAL GUIDE RAILS CAN BE VARIED IN LENGTH

Rittal has introduced two ranges of guide rails for Printed Circuit Boards which can be made to suit any depth of PCB insertion.

Utilising plastic end pieces which include a funnel entry to ease PCB insertion, the new guides can be equipped with clips to discharge static charges from the board prior to full insertion. The end pieces are simply pushed into a central aluminium section which can be varied in length to suit any application.

One family of guide rails has 2HP (approximately 10mm) wide ends, are designed for snap-fastening to the horizontal rails of the Ripac subrack range and can be further screw fastened for additional rigidity.

The plastic end parts of the other range are 4HP (20mm) and are equipped with cavities to enable coding of the slot to prevent an incorrect PCB being fully inserted.

www.rittal.co.uk



MULTI-FIELD TESTER FAMILY FOR OPTICAL LOSS MEASUREMENTS

The new Yokogawa AQ1100 Series is a family of multi-field testers for carrying out optical loss measurements in the installation, commissioning and maintenance of fibre-optic infrastructure including FTtx systems.

Designed to complement Yokogawa's existing range of portable optical time-domain reflectometry (OTDR) instruments, the AQ1100 Series consists of three models, each incorporating a light source and an optical power meter in a single compact package.

The three models are differentiated by the wavelength of the light source used: the AQ1100A is single-mode 1310/1550nm; the AQ1100B is single-mode 1310/1550/1625nm; and the AQ1100D is multimode 850/1300nm or single-mode 1310/1550nm. All models feature a choice of built-in optical power-meter options: standard (+10 to -70dBm), high power (+27 to -50dBm) or PON (1490/1550nm parallel measurement).

The AQ1100A and AQ1100C are available now; the AQ1100B is scheduled to be available in March.

www.yokogawa.com



HAMEG OFFERS HMS SERIES OF FOUR NEW COMPACT TFT SPECTRUM ANALYZERS

Hameg offers the HMS series of 4 new compact TFT spectrum analyzers with or without a tracking generator with bandwidths of 1 and 3GHz. They are ideally suited for pre-compliance EMI measurements and for checking the signal quality during maintenance work.

The HMS100 and HMS3000 operate over a frequency range of 100kHz to 1 resp. 3GHz. For four-terminal (two-port) measurements the HMS1010 and the HMS3010 are available with tracking generators. The amplitude ranges extend from -114dBm to +20dBm (1kHz RBW); with the optional preamplifier the HMS3000 and HMS3010 ranges can be increased to -135dBm (100Hz). The spectral purity exceeds -100dBc/Hz at 100kHz carrier frequency spacing.

The HMS3000 covers the range of 100Hz to 1MHz (-3dB) in a 1-3 sequence and also offers the bandwidths 200Hz, 9kHz, 120kHz and 1MHz (-6dB) for pre-compliance measurements.

www.hameg.com



KONTRON EXTENDS PERFORMANCE AND SCALABILITY OF COM EXPRESS COMPUTER-ON-MODULES

Kontron's COM Express Computer-on-Modules family ETXexpress now includes three new Kontron ETXexpress-PC SKUs, adding support for the Mobile Intel GM45 Express and Mobile Intel GL40 Express chipsets. Customers benefit from a greater performance range and scalability in Kontron's extensive COM Express compliant (Basic Form Factor, pin-out Type 2) ETXexpress product line.

Equipped with the Mobile Intel GM45 Express chipset and Intel Core2 Duo T9400 processor, this new version of the Kontron ETXexpress-PC brings the highest processing power to Kontron's COM Express Basic Form Factor offering. Kontron's COM Express module equipped with the Intel Core 2 Duo P8400 processor pairs processing power with cost-efficiency. The third new Kontron ETXexpress-PC module SKU, based on the Mobile Intel GL40 Express chipset and 2.0GHz Intel Celeron M Processor M575, is ideal for very cost-sensitive applications.

www.kontron.com



HARWIN'S EZ-BOARDWARE SMT COMPONENTS PROVIDE COST-SAVING SOLUTIONS

Harwin, a hi-rel connector and SMT board hardware manufacturer, is launching a whole new brand – EZ BoardWare – comprising surface mount products that improve manufacturing flexibility, reduce manufacturing costs and improve in field maintenance.

Considering EMC, shielding cans are usually soldered to the board as a secondary operation after the main automated assembly process. However, EZ-Shield Clips can be surface-mounted, allowing a shielding can to be simply pushed into place during final assembly. Also part of the EZ BoardWare range, EZ-RFI Fingers are very versatile, allowing for a sliding or wiping contact and simply facilitating electrical contact between PCB and metal cases etc, yet save manufacturing costs when compared to using grounding finger strips.

For cable management, EZ-Cable Clips are much smaller and lower profile than equivalent plastic devices; they are placed directly onto solder pads.

www.harwin.com



SPACE SAVING DUAL CONCENTRIC ENCODERS

Specialist Emech distributor Foremost Electronics announces the availability of the Elma E37 range of dual concentric encoders. Offering two independent control functions in just one panel space, these new encoders offer space savings and increased control panel functionality.

The E37 encoders are available with a standard resolution of 16 or 32 detents and may be specified with an integrated push button for menu selection. They feature the Swiss Click Indexing System and an indexing feel with 0.5, 1.5, 2.0 or 2.5Ncm switching torque, and have an operational life of up to 1,000,000 revolutions.

Available for vertical or horizontal mounting with threaded or non-threaded bushing, the E37 encoders have a robust 11.5 x 12.3 x 9.1mm metal housing with a metal, shaft, gold-plated contacts; have an operating temperature range of -40 to +85°C; are MIL-STD-202G compliant and have optional IP60 or IP68 front panel sealing.

www.4most.co.uk



ROBOTBITS LAUNCHES NEW ARDUINO BASED ROBOT KIT

RobotBits launches a new robot kit based around Arduino, the open-source electronics prototyping platform.

Arduino, the popular open-source electronics platform, has found a place in a wide variety of fields from art to home automation. With this new kit from RobotBits, Arduino can now add robotics to its ever-expanding list of applications.

The new Arduino based robot kit includes an Arduino Duemilanove 328, motor driver "shield" and all the electrical and mechanical components needed to build a complete mobile robotics platform for fun, research and education.

The kit is available in three build levels including a "no-solder" kit and "fully assembled" forms. The robot is also complemented by a new selection of sensor options and mounting hardware designed for applications such as line following, room mapping and obstacle avoidance.

Prices start at just £76.59 +VAT for the basic kit (without sensors).

www.robotbits.co.uk



KONTRON AM4020 ADVANCEDMC PROCESSOR BOARD WITH INTEL CORE I7 PROCESSOR

Kontron introduced one of market's most powerful single-width AdvancedMC processor modules, designed with the new Intel Mobile Core i7 processor: the Kontron AM4020. With up to 2 x 2.53GHz, the new Kontron AMC module offers the ultimate in computing power and integrated graphics when utilized in MicroTCA and AdvancedTCA integrated platforms.

The single-width

Kontron

AM4020

AdvancedMC

processor board

integrates for the

first time the memory

controller, PCI Express

and the graphics processor

within the multi-core

processor. Equipped with the

highly-integrated Intel QM 57

Platform Controller Hub, it offers high

power-density and performance on an extremely

compact footprint. With its outstanding overall

performance it is ideal for MicroTCA and

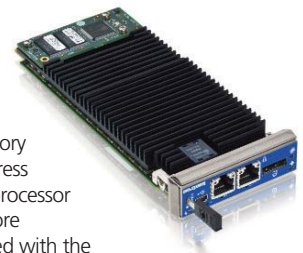
AdvancedTCA telecommunications applications such

as IPTV, media servers and media gateways,

conference systems, and in test systems for wireline

networks.

www.kontron.com





LECROY CHOOSES KEITHLEY RF SWITCH

LeCroy Corporation has chosen Keithley's System 46 (S46) RF/Microwave Switch as part of the original equipment for its new USB 3.0 Test Suite product family. Keithley's S46 switch is engineered to simplify the automated switching needed to test a wide range of telecommunications products and devices, including Bluetooth devices.

The USB 3.0 Test Suite represents the industry's first single-source lineup of test instruments that can comprehensively support the Universal Serial Bus (USB) 3.0 standard, also known as SuperSpeed USB.

The standard S46 system is specified for a bandwidth of 18GHz; custom S46 systems can support bandwidths up to 40GHz. As test requirements change, relays can be easily added to the system to create a new switch configuration.

www.lecroy.com

www.keithley.com

HCD HELPS UK FILM COMPANY WIN FOUR 'TECH OSCARS'

HCD, the contract electronics manufacturer, PCB design house, cable assembler and box build specialist, has made a significant contribution to film processing company, FilmLight, winning four Science and Technology Awards from The Academy of Motion Picture Arts and Sciences – commonly referred to as 'Tech Oscars'. HCD provided PCB layout and assembly services to the Soho-based company.

FilmLight produces film finishing equipment and systems which have been used on many films including Casino Royale, The Chronicles of Narnia: The Lion, the Witch and the Wardrobe, and the Harry Potter series, as well popular TV programs and advertisements for the world's leading brands. In a separate ceremony shortly after the main Oscars celebrity-fest, FilmLight's key personnel will receive: Technical Achievement and Scientific and Engineering Awards for the company's Truelight colour management system; and Scientific and Engineering Awards for the Northlight film scanner and Baselight colour correction system.

www.hcduk.com



FAIRCHILD LIGHTS THE WAY AT OSRAM

Fairchild Semiconductor has been selected by lighting manufacturer Osram to supply LED driver solutions. The FSEZ1016A was developed by Fairchild to meet and exceed the stringent performance benchmarks set by Osram.

"We worked closely with Osram's engineers, based at the company's LED R&D facilities in China, and frequently discussed the technical details with Osram in our efforts to ensure that the FSEZ1016A was the industry's leading LED driver solution," said Benjamin Tan, Fairchild's regional vice president of sales, China and South East Asia.

Fairchild's FSEZ1016A fits Osram's 1W-4W LED products. Lighting applications consume nearly 22 percent of electrical energy generated worldwide. Reducing wasted energy in these applications can have a significant impact on energy conservation. As the industry moves from standard incandescent light bulbs to CFL, LFL and LED lighting, a 75 percent energy saving can be realized.

www.fairchildsemi.com

TRANSFORMER MANUFACTURE



AUTOMATIC windings Ltd.



NEW



Our new East European production plant for medium to high volume production is now fully operational.

We are pleased to offer an end to end solution for wire wound components Via a UK based company

D2, 4 Nimrod Way, East Dorset Trade Park,
Wimborne Dorset. BH21 7SH.

Tel: 01 202 87 21 01 Fax: 01 202 87 20 87

E-Mail: sales@automatic-windings.co.uk

Web: www.automatic-windings.co.uk



WEBSITE DIRECTORY

Sky systems ltd

www.sky-pcb.com

Sky Systems Ltd. was established with the vision and promise of providing manufacturing high quality, cost effective solution and one-stop service to meet the most demanding of our customers' requirements.

We offer the followings:

- 1-12 Layers • Fr-4 / Cem-3 • HAL(Lead Free),Flash Gold, Electroless Gold Plating, OSP ,Immersion Silver, Immersion Tin • Gold Finger • Soldermask • Silkscreen • Routing / Punching / V-Cut • Online quotation • FREE PCB Prototype with quantity orders • Short



lead time • Fast worldwide delivery • Flexible quantity • CHINA Factory
For more information or request a quote today from our web site.

Robot Bits

www.RobotBits.co.uk

Robot kits and components for fun and learning!

Whether you're just getting started or looking for parts for your next robot; RobotBits has everything you need to power your next creation: Motors, gearboxes, chassis, wheels, controllers, motor drivers and more!

RobotBits stock kits and components from many of the well known brands including: POB Technologies, Pololu, Arduino, Dimension Engineering, Devantech and Solarbotics.



THOR – STRIKING TECHNOLOGIES FOR POWER

The THOR project aims at developing highly efficient, integrated and reliable power electronics technologies for automotive, aeronautics and healthcare applications (Magnetic Resonance Imaging systems) in the effort to combat CO2 emissions. Key part of this project is the development of high power switches (transistors and diodes) based on innovative silicon process, silicon on insulator or wide band gap materials (Silicon Carbide – SiC or Gallium Nitride – GaN) targeting the voltages from 200V to 3000V. The project covers the development of new technologies for discrete power components (IGBTs, JFET, diodes, based on wide band gap semiconductors), power cores, storage elements (super-capacitors). In addition, the aim is to also develop innovative and affordable packaging for high temperature, thermal and EMC management solutions. The THOR project is part of CATRENE (Cluster for Application and Technology Research in Europe on NanoElectronics), a EUREKA programme which aims to make the European ICT industry a technological leader.

Our panel of commentators says the following on this development:

MAURIZIO DI PAOLO EMILIO, TELECOMMUNICATIONS ENGINEER, INFN – LABORATORI NAZIONALI DEL GRAN SASSO, ITALY:

CO2 emissions are an undeniable consequence of energy development. In the transport field it is a fundamental issue as one-third of CO2 emissions are caused by transportation; this will become worse as the number of vehicles on the road is expected to increase to 40% by 2030.

Therefore, increasing energy efficiency will be definitely required, as well as for clean energy but also for more reliable energy sources. However, the solutions nowadays are too expensive, and overcoming the cost issue is essential.

The THOR project is a great solution to resolve the energy and CO2 emission problems. Moreover, it can also be a starting point for developing new technologies in the telecommunications, sensor, computer and control system fields where applications are various and wide. Preserving resources and creating highly efficient reliable power are an absolute must for developments in the future.

PROFESSOR DR DOGAN IBRAHIM FROM THE NEAR EAST UNIVERSITY IN NICOSIA, CYPRUS:

Energy saving has become one of the most important topics in everyday life. The THOR project will certainly play an important role in energy saving in most fields of electronics applications, especially in the field of power electronics. The development of energy-efficient, high-power switches, power components and storage elements will enable more energy-saving products to be developed and marketed with the possible results of lowering the overall demand on energy and using the energy more efficiently. The CATRENE project seems to provide the necessary prerequisite for a successful development of new power-efficient semiconductor products.

BARRY MCKEOWN, RF AND MICROWAVE ENGINEER IN THE DEFENCE INDUSTRY, AND DIRECTOR OF DATOD LTD, UK:

The CATRENE website lists 297 partners but only one British company is identified: the refrigeration company STS. The THOR website lists 39 participating partners; none from Britain. Sadly that says it all about

the nature of British involvement in European collaborative ventures and the existence of a viable material science industry; due primarily to the funding priorities given to chemistry in UK universities. Given the short timelines involved, it would be instructive to compare and contrast the improvement in Silicon Carbide semiconductor performance, eventually attained with the last step-change in this technology – circa 1995 in the US.

ASNAOUI OTHMAN, ASSOCIATE PROFESSOR, UNIVERSITY OF TUNIS, TUNISIA:

The conventional resources of energy are objects of controversies on an international scale, particularly lately. Indeed, the rate of demand and supply becomes increasingly ambiguous, which also affects the manageability of short and long-term forecasts. Moreover what complicates the situation is the dilemma between the increased energy demand of the new industrialized countries (China, India....) and the limited oil layer.

The other shutter of the international debate on conventional energies resides in the emission of CO2 which contributes to the climatic reheating of the planet. Especially since 1/3 of the CO2 emission comes from transport (terrestrial, maritime and aeronautical etc). Power electronics is one of the very promising solutions to reduce CO2 emissions with the use of electric processes ordered by static converters based on power electronics. These techniques make it possible to reduce energy consumption by means of recovery in the car itself, for example, with electric traction.

There's a move towards a technology that'll integrate the power electronic modules with their control systems. The necessary performances of these modules lie in reliability, their low cost and efficient electromagnetic radiation reduction. These objectives will be achieved with increase in the commutation frequency and suitable solutions that'll combat parasitics.

In addition, the standardization of these electronic power modules will contribute towards simplifying the implementation processes and reduction of the prices. With them we will achieve high efficiency solutions but without the polluting gas-emissions.



GO FASTER WITH PROTEUS PCB DESIGN

The latest version of the Proteus Design Suite harnesses the power of your computer's graphics card to provide lightning fast performance. Together with unique transparency options it's now easier than ever to navigate and understand large, multi-layer boards.

PROTEUS DESIGN SUITE **Features:**

- Hardware Accelerated Performance.
- Unique Thru-View™ Board Transparency.
- Over 35k Schematic & PCB library parts.
- Integrated Shape Based Auto-router.
- Flexible Design Rule Management.
- Polygonal and Split Power Plane Support.
- Board Autoplacement & Gateswap Optimiser.
- Direct CAD/CAM, ODB++ & PDF Output.
- Integrated 3D Viewer with 3DS and DXF export.
- Mixed Mode SPICE Simulation Engine.
- Co-Simulation of PIC, AVR, 8051 and ARM7.
- Direct Technical Support at no additional cost.

All levels of the **Proteus Design Suite** include a world class, fully integrated shape-based autorouter at no additional cost - prices start from just £150 exc. VAT & delivery

labcenter  www.labcenter.com
Electronics

Labcenter Electronics Ltd, 53-55 Main Street, Grassington, North Yorks. BD23 5AA.
Registered in England 4692454 Tel: +44 (0)1756 753440, Email: info@labcenter.com

Visit our website or
phone 01756 753440
for more details

ENABLING PERFORMANCE BASED OPERATIONS

avionics

europe



Incorporating Defence Electronics

Conference and Exhibition

24th–25th March 2010

Passenger Terminal (City Centre)

Amsterdam, The Netherlands

www.avionics-event.com

PLEASE USE THIS PROMOTIONAL
CODE WHEN REGISTERING:
EW-0210

www.avionics-event.com

Learn and discover more at the leading conference and exhibition for global avionics and defence electronics

International competition has intensified during a challenging economic atmosphere as companies and governments look to keep pace with next-generation avionics, air traffic management capabilities and defence electronics developments.

Avionics conference track includes:

- Avionics With ATM
- Performance Based Operations
- Regulatory Frameworks for Avionics
- Next Generation Military Avionics

Defence Electronics conference track includes:

- COTS Integration Challenge
- Thermal Management
- Trusted COTS
- Software Defined Radio In Defence Applications

Exhibition Times

Wednesday 24th March: 10:00am – 6:00pm

Thursday 25th March: 10:00am – 4:30pm

Opening Keynote

Open and FREE of charge to all

Wednesday 24th March: 9:00am – 10:00am

Networking Reception

Wednesday 24th March: 5:30pm – 7:30pm

Exhibitor Presentations

Open and FREE of charge to all throughout the exhibition
opening hours

For full conference programme or to register online visit www.avionics-event.com

Co-located with:



Flagship Media Sponsors:



Owned & Produced by:



Sponsors: WIND RIVER



Supporting Organisation:

